

Håkon Engan Myrstad

Ignition probability of hydrogen facilities

Master's thesis in Energy & Environmental Engineering

Supervisor: Nicola Paltrinieri

Co-supervisor: Ingar Fossan

June 2023

Håkon Engan Myrstad

Ignition probability of hydrogen facilities

Master's thesis in Energy & Environmental Engineering
Supervisor: Nicola Paltrinieri
Co-supervisor: Ingar Fossan
June 2023

Norwegian University of Science and Technology
Faculty of Information Technology and Electrical Engineering
Department of Energy and Process Engineering



Norwegian University of
Science and Technology

Abstract

For hydrogen to grow as an energy carrier, safety is highly important. In risk consultant businesses, the goal of a risk assessment is often to find an ignition probability. This can in turn be used with other parameters to make up an overall risk level of a certain facility, and whether or not the facility meets regulatory demands. To ensure accuracy of the final result, a proper ignition probability model is required. This is one of the goals of the SAFEN project, and will be the focus of this master thesis. In the present thesis, hydrogen leaks are simulated with the CFD software KFX RBM, and the ignition probability for a hydrogen refueling station and hydrogen storage container are obtained. In addition, the results are used to describe the behaviour of hydrogen leaks when simulated with CFD software, and construct key design points for hydrogen facilities to lower the risk of accidents. When using leak rates of 0.1, 1 and 10 kg/s to empty a 13 kg vessel of hydrogen, the ignition probability obtained was 1.7%, 12.0% and 8.6% respectively. Design details such as fencing surrounding leak sources, and using equipment rated for use in explosive atmospheres were found to be key to ensure a low ignition probability. The thesis will provide a detailed picture of what contributes to an ignition probability, and a wide perspective of ignition probability modelling.

Sammendrag

Sikkerhet er et viktig aspekt for at hydrogen skal vokse som energibærer. I sikkerhetsrådgivning er ofte målet med en risikoanalyse å finne en tennsannsynlighet. Hvis man kombinerer tennsannsynligheten med andre parametre, kan dette brukes til å avgjøre om et anlegg er trygt, og om det tilfredsstillende krav fra myndigheter. For å oppnå et resultat som er mest mulig nøyaktig, er det viktig å bruke en passende tennsannsynlighetsmodell. Dette er et av målene i SAFEN-prosjektet, og vil være fokusområdet i denne masteroppgaven. I oppgaven simuleres hydrogenlekkasjer med CFD-verktøyet KFX RBM. Dette gjøres for å finne en tennsannsynlighet for en hydrogenfyllstasjon og en fraktcontainer for hydrogen. I tillegg brukes resultatene til å beskrive hydrogenets oppførsel når man simulerer utslipp med CFD, og beskrive viktige designdetaljer når man skal konstruere et hydrogenanlegg som har lav risiko for ulykke. Når det ble brukt utslippsrater på 0.1, 1 og 10 kg/s for å tømme en hydrogentank på 13 kg, ble det funnet tennsannsynligheter på 1.7%, 12.0% og 8.6% respektivt. Det ble også konkludert med at det er viktig med vegger rundt utslippspunkter for å hindre stor gassspredning, og å bruke utstyr som er godkjent for bruk i brennbare atmosfærer for å forebygge en høy tennsannsynlighet. Denne masteroppgaven gir et detaljert bilde over hva som bidrar til en tennsannsynlighet, og et bredt perspektiv på modellering av tennsannsynlighet.

List of symbols

P	Probability
I	Ignition
E	Exposure
f	Frequency
P_C	Continuous ignition probability
P_D	Discrete ignition probability
P_I	Immediate ignition probability
P_T	Total ignition probability
λ_C	Expected number of ignitions per m^3
λ_D	Expected number of ignitions per second $\cdot \text{m}^3$

List of abbreviations

<i>CFD</i>	Computational fluid dynamics
<i>LFL</i>	Lower flammability limit
<i>UFL</i>	Upper flammability limit
<i>LPG</i>	Liquefied petroleum gas
<i>CNG</i>	Compressed natural gas
<i>CH₂</i>	Compressed hydrogen gas
<i>LH₂</i>	Liquid hydrogen
<i>BOG</i>	Boil off gas
<i>CAPEX</i>	Capital expenditures
<i>OPEX</i>	Operational expenditures
<i>MISOF</i>	Modelling of ignition sources on offshore oil and gas facilities
<i>QRA</i>	Quantitative risk analysis
<i>KFX</i>	Kameleon FireEx
<i>RBM</i>	Risk barrier management
<i>IP</i>	Ingress protection

Table of Contents

List of Figures	v
List of Tables	vii
1 Introduction	1
1.1 Avoiding hydrogen accidents	1
1.2 Current hydrogen risk modelling tools	2
1.3 Scope	4
2 Theory	5
2.1 Hydrogen	5
2.2 Hydrogen refueling stations	6
2.3 Hydrogen in ISO-containers	7
2.4 Ignition probability modelling	8
2.5 KFX	8
2.6 KFX RBM	9
2.7 Input to KFX RBM	10
2.8 IP code	10
2.9 Output of KFX RBM	11
2.10 Understanding cars as ignition sources	13
3 Method	16
3.1 Simulating a basic hydrogen leak	16
3.2 Simulating the hydrogen refueling station	17
3.2.1 3D model	17
3.2.2 Parameters	18
3.2.3 Ignition sources	20
3.2.4 Detectors	22
3.2.5 Switching hydrogen with methane	22
3.2.6 The final SAFEN parameters	22
3.3 Simulating the container storage	23
3.3.1 3D model	23
3.3.2 Parameters, ignition sources and detectors	24
3.4 Creating a post processing tool in Python	24
4 Results	26

4.1	Basic hydrogen leak	26
4.2	The hydrogen refueling station	30
4.2.1	Gas dispersion	30
4.2.2	Non-ATEX equipment	34
4.2.3	Standard MISOF model	34
4.2.4	Offshore MISOF model	36
4.2.5	Onshore MISOF model	38
4.2.6	SAFEN ₁₀ model	39
4.2.7	SAFEN ₁₀₀ model	40
4.2.8	Ignition probability summary	41
4.2.9	Comparison with methane	42
4.2.10	The final SAFEN parameters	44
4.2.11	Grid sensitivity	44
4.3	The container storage	46
4.3.1	Gas dispersion	46
4.3.2	Ignition probability	48
5	Verification and validation	51
5.1	Verification	51
5.1.1	Grid sensitivity	51
5.1.2	Hand calculations	51
5.2	Validation	53
6	Discussion	54
6.1	Basic hydrogen leak	54
6.2	The hydrogen refueling station	54
6.2.1	Gas dispersion	54
6.2.2	Ignition probability	55
6.2.3	Comparison with methane	57
6.2.4	The final SAFEN parameters	57
6.3	The container storage	57
7	Conclusion	59
8	Additional content	60
8.1	Workflow and complications	60
8.2	Further work	60

8.3	Acknowledgement	60
Bibliography		61
Appendix		63
A	Container storage detailed ignition probabilities	63
A.1	Standard MISOF model	63
A.2	SAFEN ₁₀ model	63
A.3	SAFEN ₁₀₀ model	64
B	Sandvika accident description from HIAD [16]	65
C	Radar Python code	65
D	Unignite Python code	67
List of Figures		
1	The Sandvika hydrogen refueling station [35]	1
2	Initial ignition probability VS flow rate ranges [2]	2
3	HyRAM's total ignition probability	4
4	Stages in a refueling station	6
5	40 ft. ISO-container [29]	7
6	The setup menu in KFX	9
7	IP components	10
8	An example of an ignition source	14
9	Gas cloud exposing road	15
10	3D-model of the ferry at the jetty	16
11	Radar plot example	17
12	3D-model of the refueling station	18
13	Dimensions of the refueling station	18
14	Ignition sources at the refueling station	22
15	3D model of the container	23
16	3D model of the container at the refueling station	24
17	Ignition sources inside the container	24
18	Concentration plot of flat geometry	26
19	Concentration plot of geometry with terrain	27
20	Wind sensitivity on flat geometry	28
21	Wind sensitivity on geometry with terrain	28

22	Pressure sensitivity on flat geometry	28
23	Pressure sensitivity on geometry with terrain	29
24	Mass flow sensitivity on flat geometry	29
25	Mass flow sensitivity on geometry with terrain	29
26	Release direction sensitivity on flat geometry	30
27	Release profile of 0.1 kg/s downward release	30
28	Surface plot of 4% H ₂ concentration for 0.1 kg/s downward release	31
29	Release profile of 1 kg/s downward release	31
30	Surface plot of 4% H ₂ concentration for 1 kg/s downward release	31
31	Release profile of 10 kg/s downward release	32
32	Surface plot of 4% H ₂ concentration for 10 kg/s downward release	32
33	Surface plot of 4% H ₂ concentration for 1 kg/s releases at 15 seconds	32
34	X-plane plot of H ₂ concentration for 1 kg/s downward release at 20 seconds	33
35	X-plane plot of temperature for 1 kg/s downward release at 20 seconds	33
36	X-plane plot of velocity for 1 kg/s downward release at 3 seconds	33
37	Surface plot of 1% H ₂ concentration for 0.1 kg/s releases at 20 seconds	34
38	Surface plot of 1% H ₂ concentration for 0.1 kg/s releases at 20 seconds	34
39	Total ignition probability for the standard MISOF model	36
40	Ignition probabilities for 1 kg/s release in different directions	36
41	Total ignition probability for the offshore MISOF model	37
42	Total ignition probability for the onshore MISOF model	38
43	Total ignition probability for the SAFEN ₁₀ model	39
44	Total ignition probability for the SAFEN ₁₀₀ model	40
45	Plot of total ignition probability for the refueling station with IP44 equipment	41
46	Plot of total ignition probability for the refueling station with IP64 equipment	42
47	Surface plot of 4% CH ₄ concentration for 1 kg/s downward release	42
48	Transient flammable cloud volume for downward releases with methane and hydrogen	43
49	Transient ignition probability for downward releases with methane and hydrogen	43
50	Grid sensitivity for 0.1 kg/s leak rate	44
51	Grid sensitivity for 1 kg/s leak rate	45
52	Grid sensitivity for 10 kg/s leak rate	45
53	Surface plot of 4% H ₂ concentration for 0.1 kg/s downward release	46
54	Surface plot of 4% H ₂ concentration for 1 kg/s downward release	46
55	Surface plot of 4% H ₂ concentration for 10 kg/s downward release	47
56	Surface plot of 4% H ₂ concentration for 1 kg/s releases at 5 seconds	47

57	Absolute velocity inside the container for downward releases at 3 seconds	47
58	Transient volume of flammable cloud for downward releases	48
59	Concentration of H ₂ inside the container	48
60	Total ignition probability for the container storage with IP44 equipment	49
61	Total ignition probability for the container storage with IP64 equipment	50

List of Tables

1	Basis of HyRAM's ignition probability	2
2	Initial ignition probability VS flow rate ranges for methane	3
3	HyRAM's first modification to find an ignition probability	3
4	HyRAM's second modification to find an ignition probability	3
5	HyRAM's third modification to find an ignition probability	3
6	First digit of IP-code	11
7	Second digit of IP-code	11
8	IP code lambdas	11
9	Ignition probability file setup	12
10	Sensitivity parameters for basic hydrogen simulations	16
11	Constant parameters for basic hydrogen simulations	16
12	Parameters constant for the hydrogen refueling station simulations	19
13	Parameters varied for the hydrogen refueling station simulations	20
14	Ignition source parameters kept constant for the hydrogen refueling station	21
15	Ignition source parameters varied for the hydrogen refueling station	21
16	Ignition source parameters in the final SAFEN model	23
17	Ignition probability results constant for all models	34
18	Ignition probability results for electrical, rotating and other equipment	35
19	Total ignition probability contribution from the sources in table 18	35
20	Total ignition probability results for the standard MISOF model	35
21	Ignition probability contribution from the volumetric source	37
22	Total ignition probability results for the offshore MISOF model	37
23	Ignition probability contribution from the volumetric source	38
24	Total ignition probability results for the onshore MISOF model	38
25	Ignition probability contribution from the volumetric source	39
26	Total ignition probability results for the SAFEN ₁₀ model	39
27	Ignition probability contribution from the volumetric source	40

28	Total ignition probability results for the SAFEN ₁₀₀ model	40
29	Total ignition probability results for IP44 equipment summarized	41
30	Total ignition probability results for IP64 equipment summarized	41
31	Total ignition probability for hydrogen and methane with standard MISOF model and IP44 equipment	43
32	Total ignition probabilities in the final SAFEN model	44
33	Grid sensitivity ignition probability for 0.1 kg/s release	45
34	Grid sensitivity ignition probability for 1 kg/s release	46
35	Grid sensitivity ignition probability for 10 kg/s release	46
36	Ignition probability results constant for all models	48
37	Total ignition probability results for the standard MISOF model	49
38	Parameters used for hand calculations	52
39	Total ignition probability contribution from the volumetric sources in the standard MISOF model	63
40	Total ignition probability contribution from the volumetric sources in the SAFEN ₁₀ model	63
41	Total ignition probability results for the SAFEN ₁₀ model	63
42	Total ignition probability contribution from the volumetric sources in the SAFEN ₁₀₀ model	64
43	Total ignition probability results for the SAFEN ₁₀₀ model	64

1 Introduction

1.1 Avoiding hydrogen accidents

On May 6th 1937, the airship Hindenburg caught on fire when hydrogen leaked and ignited. In less than a minute after ignition, there was little less than the aluminium skeleton left. 35 people making the trans-Atlantic flight lost their lives [32]. Since then, knowledge and safety regulations regarding use of hydrogen has increased substantially. In recent years, hydrogen has gotten much attention for its excellent potential as an energy carrier. It can be produced from a wide range of sources, including by using surplus electricity during low demand hours in the power grid. Although it can be used for a wide range of applications, it is believed it has much potential in replacing fossil fuels in the transportation industry. This is especially true for automotive industry, aviation and ferry services. For this revolution to take place, it is necessary to build hydrogen production facilities and refueling stations, as well as find better and safer solutions for transport of hydrogen.

It has been many hydrogen accidents throughout the last decades. Although the Hindenburg fire is one of the most famous, there are also relevant accidents from more recent time. A hydrogen refueling station in Sandvika was opened in 2016. It was a joint venture between Uno-X, NEL and Nippon Gases. Three years later, on the 10th of June 2019, there was a major explosion and fire at the facility. The windows in office buildings 65 meters away shattered. Knowing at which pressure glass shatters, it is possible to calculate the initial blast parameters. The investigation after the accident suggested between 1.5-3 kg of hydrogen was released. The wall surrounding the process equipment mostly served its purpose, preventing the gas cloud from reaching the nearby road. Only a section of the fence towards the road failed, although this could have sent projectiles flying towards bypassing cars [23]. The cause of the leak was untightened bolts between the high pressure tank and pipeline [16]. Investigation also uncovered that electrical equipment not rated for use in explosive atmospheres was used [35]. Manufacturer NEL immediately shut down similar facilities around the world to inspect bolts. The accident significantly slowed the process of developing a hydrogen refueling network in Norway, and raised scepticism concerning the safety of hydrogen. More information about the accident can be found in appendix B. If hydrogen is to be met with as little opposition as possible, it is important to keep such accidents to a minimum. Although there were no casualties in the Sandvika accident [23], it was a warning shot towards the hydrogen industry worldwide.



Figure 1: The Sandvika hydrogen refueling station [35]

Most of what is known about leak and ignition accidents comes from the oil and gas industry. The progress done regarding safety, especially on the Norwegian continental shelf, have made the

harsh environment offshore a relatively safe place to work. This statement can be supported by the declining number of offshore leaks [18]. The honour is shared among the production companies, third party safety companies and the Norwegian government for demanding strict safety procedures. Much of the knowledge gathered in the petroleum industry can also be applied to renewable energy carriers such as ammonia and hydrogen, but not without proper research and testing. Although similar, there are many ways hydrogen is different from light hydrocarbons. A problem in the risk consultant business, is that models are not as developed and tested for hydrogen as it is for hydrocarbons. In a risk assessment, hydrocarbon models are often extended beyond their intended area anyway, or done using questionable hydrogen modelling tools. To avoid future accidents, it is essential to build models as correctly as possible. A part of this includes developing better ignition probability models for accidents with hydrogen, which will be the focus of this thesis.

1.2 Current hydrogen risk modelling tools

One widely used model for determining risk levels for hydrogen facilities today is HyRAM, made by Sandia researchers. The scientists developing HyRAM had a very scarce database to determine an ignition probability model for hydrogen. The basis for their work is a SINTEF report from 1983 [8]. From the report, the scientists make up an initial ignition probability shown in table 1.

Blowout	No. blowouts	No. ignitions	Ignition probability
Gas	123	35	0.3
Oil	12	1	0.08

Table 1: Basis of HyRAM's ignition probability

It is somewhat unclear which sources Sandia has used to build their model other than the SINTEF report, but their procedure will be shown here. All information in the following subsection comes from their technical manual [5]. They use the two probabilities in table 1, and ignition probability data from small leaks shown as the leftmost point in figure 2. Lines are drawn between the points to construct the natural gas ignition probability seen in table 2. Note that this is still for natural gas, not hydrogen.

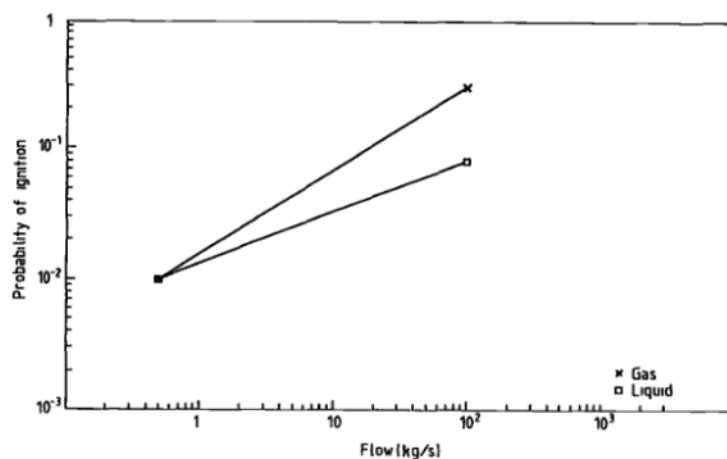


Figure 2: Initial ignition probability VS flow rate ranges [2]

Leak rate class	Leak rate	Ignition prob.
Small	<1 kg/s	0.01
Medium	1-50 kg/s	0.07
Large	>50 kg/s	0.30

Table 2: Initial ignition probability VS flow rate ranges for methane

The probabilities in table 2 are then changed to better fit hydrogen. This is done in three steps. The first step is to reduce the flow rates in table 2 with a factor of 8. This factor comes from the difference in molar mass between methane and hydrogen. By dividing the flow rates by 8, it will imply that a 1 kg/s leak of methane would produce a similar cloud volume as a hydrogen leak of 0.125 kg/s. One could raise questions to whether or not dividing by 8 is the correct number. Gas from an offshore rig contains other hydrocarbons than methane, which means the average molar mass of the mix would be greater than what of methane.

Leak rate class	Natural gas leak rate	Hydrogen leak rate
Small	<1 kg/s	<0.125 kg/s
Medium	1-50 kg/s	0.125-6.25 kg/s
Large	>50 kg/s	>6.25 kg/s

Table 3: HyRAM’s first modification to find an ignition probability

The second step is to increase the ignition probabilities by 16%. This is done because the flammability limits of hydrogen are much wider than what of hydrocarbons, and is explained in section 2.1. CFD simulations have shown that the cloud volume above methane’s UFL to hydrogen’s UFL is 16% larger for hydrogen releases than methane releases. For a natural gas leak of 1 kg/s, the ignition probability is 0.01, as seen in table 2. This means the corresponding 0.125 kg/s hydrogen leak will have a total ignition probability 16% higher, which is 0.012, shown in table 4.

Leak rate class	Natural gas ignition prob.	Hydrogen ignition prob.
Small	0.010	0.012
Medium	0.070	0.080
Large	0.300	0.350

Table 4: HyRAM’s second modification to find an ignition probability

The last step done by the Sandia team is to assume a 2:1 distribution between the immediate ignition and delayed ignition. The immediate ignition probability is the probability of ignition the moment the release starts, and the delayed ignition probability is the probability that it ignites later. The total ignition probability is their sum, and is shown in figure 3. Note that the ignition model which will be used in this thesis will use different probability classifications than HyRAM.

Leak rate class	Immediate ignition prob.	Delayed ignition prob.
Small	0.008	0.004
Medium	0.053	0.027
Large	0.230	0.120

Table 5: HyRAM’s third modification to find an ignition probability

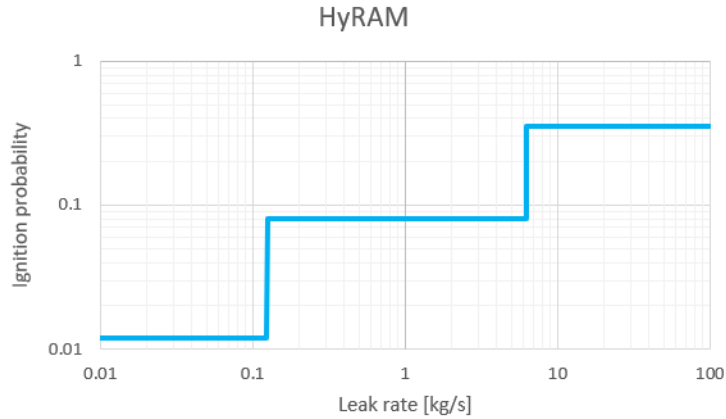


Figure 3: HyRAM's total ignition probability

1.3 Scope

This master thesis is part of the SAFEN project. SAFEN is a Safetec innovation project with several large industry partners, including Equinor, Yara, Vår Energi, Gassco, Aker Horizons, Gen2Energy, BW Offshore and others. The core of the project is to build knowledge and develop new and better models for hydrogen, ammonia and CO₂. The focus is mainly on loss of containment, ie. leaks of these gases or liquids, and ignition mechanisms [31]. This master thesis will only consider ignition, and ignition probability modeling in particular. With the development of the new risk based methodologies, cost effective and safe designs will be available for the growing renewable sector. When it comes to ignition probability modeling for hydrogen, SAFEN aims to establish a more up to date model than Sandia did in their HyRAM.

A problem with HyRAM that SAFEN wants to solve, is that the plant design does not affect the ignition probability. The ignition probability in HyRAM does only depend on the leak rate. In reality, it is a very crude approximation. In a flat geometry, it is true that the ignition probability increases with the leak rate, simply because the gas cloud will get bigger. The number of ignition sources, the protective equipment used and even the geometry of the facility has an effect on the ignition probability. By developing a model that considers this, old plants will be punished by getting a high ignition probability. On the other hand, the new model will motivate the industry to design plants that will have a low ignition probability.

The piece this master thesis will have in the greater picture, is to test ignition source parameters used in the SAFEN project. The ignition source parameters are inputs which will in turn determine the ignition probability. The ignition probability will be obtained through use of the CFD tool KFX RBM. This tool is unique in modelling ignition probabilities for gas releases in complex geometries. It will simulate the dispersion of the gas cloud, and whether or not the cloud will hit an ignition source placed in the 3D model. The result will be used in the SAFEN project. Multiple parameter models will be tested, all input data provided by Safetec. The reasoning behind the value of the parameters is outside the scope of this thesis, but is considered by others in the SAFEN project. The main goal of the thesis is to find the ignition probability of hydrogen facilities. However, it is also a goal to study the behaviour of hydrogen when released using the CFD software, determine what contributes to a high ignition probability, and formulate relevant design points for hydrogen facilities. These goals will be met by conducting simulations using three different geometries. First, a release at a jetty from a hydrogen ferry will be used to map the behaviour of released hydrogen in CFD software. No ignition probability calculations will be performed here. Second, the ignition probability for a hydrogen refueling station will be obtained using a variety of ignition models. Third, a hydrogen leak inside a shipping container will act as a comparison to the ignition probabilities obtained for the refueling station.

2 Theory

2.1 Hydrogen

Hydrogen is the smallest atom, and the lightest gas known when combined into an H_2 molecule. At standard temperature and pressure, 0°C and 1 atm, its density is only 0.089 g/m^3 [21]. Because of the extremely low density, storing hydrogen is trickier than storing light hydrocarbons, as higher pressures or lower temperatures is required to store the same amount of mass. Depending on the usage, hydrogen can be stored as either compressed hydrogen (CH_2) or liquefied hydrogen (LH_2). CH_2 production requires expensive and powerful compressors, and multiple compressor stages are usually required [4]. For instance, the hydrogen car Toyota Mirai uses hydrogen from vessels at 700 bar, much higher pressure levels than hydrocarbons would be stored at [14]. For comparison, CNG for automotive use is stored at around 200 bar [19]. On the other hand, storing LH_2 is no easy task either. Hydrogen has a boiling point of -252.87°C [21]. Reaching temperatures to produce LH_2 is an energy intensive process. After production, LH_2 must be stored in cryogenic vessels, and boil off gas (BOG) must be dealt with. It is difficult to store large quantities of compressed hydrogen, as it requires thicker and thicker walls. CH_2 is therefore preferred for small scale applications, such as automotive use. Liquid hydrogen requires more equipment surrounding the tank, and is also more expensive to produce. For small scale applications, using LH_2 does not make sense. For storing large quantities, LH_2 is preferred, as the tank doesn't need to be thicker to store a greater mass [30].

In the case of ignition, hydrogen will burn according to the following reaction if enough oxygen is present [21].



The lower and upper flammability limit of hydrogen are 4% and 75% respectively [9]. As hydrogen is cooled or compressed, the flammability range is known to get narrower [27]. Compared to light gaseous hydrocarbons, the flammability range of hydrogen is much wider. For example, propane has a range from 2.1% to 10.1%, while methane has a flammability range from 4.4% to 16.4% [34]. A narrower flammability range means the probability of an ignition source being exposed to a flammable cloud is smaller. Ignition sources will be presented later in this section. The auto ignition temperature of hydrogen is similar compared to other hydrocarbon gases, at approximately 550°C [21]. This is the temperature hydrogen can spontaneously ignite despite the absence of an external ignition source such as a spark. The minimum ignition energy of hydrogen is approximately 0.019 mJ, while other common gases such as methane and propane have a minimum ignition energy in the order of 0.1 mJ [3]. Therefore, a wider range of ignition sources can ignite a hydrogen-air mixture.

In addition to ignition by exposure to hot surfaces or sparks, there are more ways hydrogen can be ignited. Of course, ignition by flames is a highly effective way of igniting a gas cloud. Flames can reach very high temperatures, depending on what is being combusted. Flames can also travel through tight openings, meaning the flames from a smaller fire can ignite parts of a cloud still inside the flammable range [27].

Ignition by mechanical impact should be considered, especially when dealing with hydrogen. Such impacts can generate small, hot particles which can ignite a gas cloud. If the impact involves steel, the impact can create a hot spray of particles similar to when using an angle grinder. If CH_2 leaks from a vessel, the high velocity jet can hit small debris, gravel etc. When these small objects collide, they can cause sparks or hot particles leading to ignition [27].

There are many ways electricity can ignite an explosive atmosphere. Short circuits can increase temperatures of low resistance components above the auto ignition temperature [27]. Voltage spikes can cause components like electrolytic capacitors to blow up [22].

Static electricity can also ignite hydrogen, and is more relevant to consider than for hydrocarbon gases due to the low minimum ignition energy. When two points have a difference in electric

potential, this will pose a risk. Spark discharges occur when the voltage potential is equalized through a plasma channel. Corona discharges occur at sharp points with a voltage potential, resulting in a current, however no plasma channel. Lightning can of course ignite an explosive atmosphere [27].

LH₂ releases onto water pose a different risk than gaseous releases. This is especially relevant for the maritime sector. During experiments performed as part of the SH2IFT research projects, the researchers observed some astounding events. They did more than 80 releases of LH₂ onto and below a surface of water at rates between 0.25 kg/s and 0.8 kg/s. As the LH₂ at -253°C made contact with water, a phase transition occurred. The resulting hydrogen cloud ignited in nearly all experiments. The source of ignition is debatable. It is suggested that the cold hydrogen causes ice crystals to form. These ice crystals are then lifted with the evaporating hydrogen. Rubbing against each other, they might create discharges strong enough to ignite the hydrogen cloud [27].

2.2 Hydrogen refueling stations

To support the coming fleet of fuel cell electric vehicles (FCEV), commonly known as hydrogen cars, a network of hydrogen refueling stations is needed. Many stations have already been built around the world, but the technology is still at an early stage. There is currently great uncertainty about how to optimize the regulatory framework to guide station designs that are both safe and financially sustainable. In this subsection, the basic design of a hydrogen refuelling station will be explained, and specs for the refuelling station used in the simulations introduced.

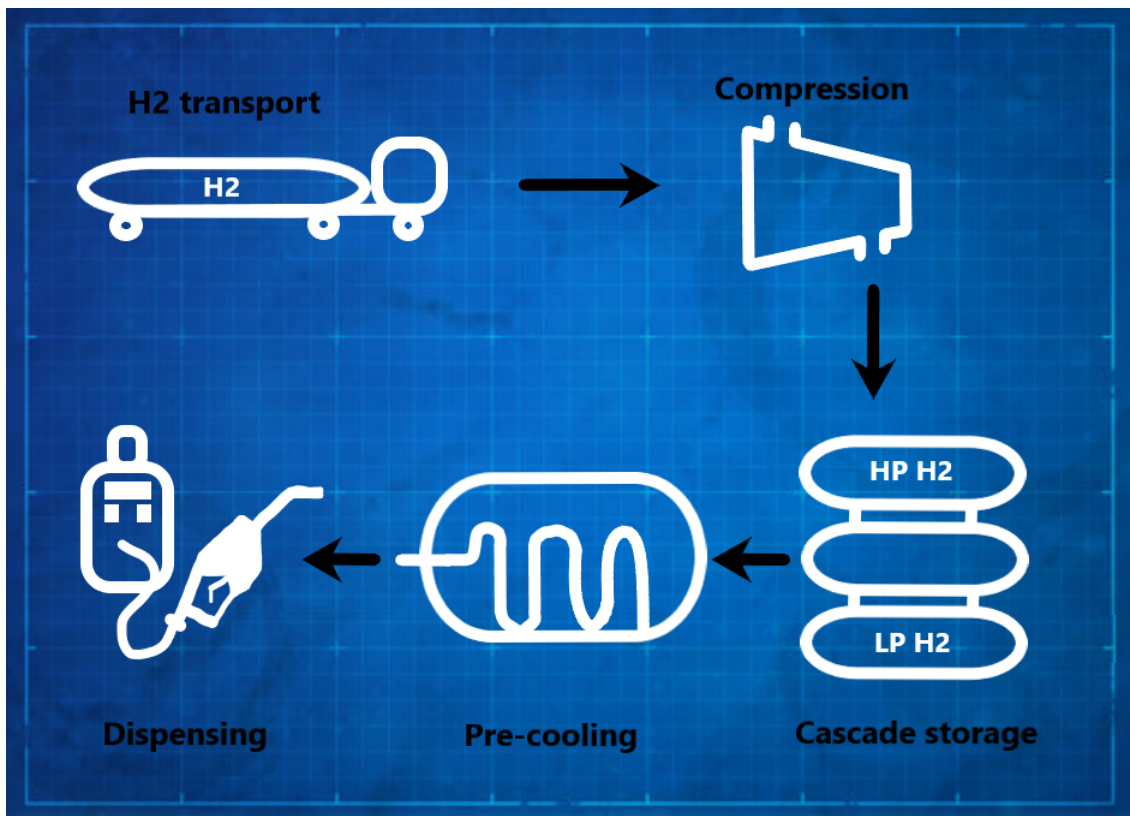


Figure 4: Stages in a refueling station

The basic components of a hydrogen refueling station are shown in figure 4. Sandia National Laboratories along with some partners suggests a few station designs that are financially plausible to be built in large numbers in the coming years [20]. The first stage in a refueling station is the source of hydrogen. The source can be on-site production with electrolyzer units, such as the former station in Sandvika, which was discussed in section 1.1 [23]. However, an option more

suitable for the early years of FCEV's is transport of hydrogen by trucks. A combination of both is possible for areas that need to meet a highly variable demand [20]. Delivery by pipeline is highly unlikely to be seen anytime soon due to high costs. The hydrogen is most likely to be delivered and stored as gaseous hydrogen. This is due to the low efficiency of producing LH₂ [26], and the demanding task of dealing with boil of gas. In addition to BOG in the storage tanks, hydrogen will evaporate every time it is pumped through piping and equipment which is hotter than -253°C. Expensive cryo coolers are required, adding extra capital expenditures (CAPEX) and operational expenditures (OPEX) to pay for the electricity needed [20].

Moving on with hydrogen from truck delivery, the pressure inside the tube trailer is 51- 252 bar. This is further compressed and stored in 3x13 kg tanks at three different pressure levels [20].

- Low pressure storage: 300-900 bar
- Medium pressure storage: 600-900 bar
- High pressure storage: 800 - 900 bar

To refuel a FCEV as fast as a fossil fueled car, the GH₂ must be cooled to approximately -40°C before dispensing [20]. This means in the case of a leak from the dispenser, the temperature of the compressed hydrogen will be -40°C already before expansion. The refueling time of hydrogen cars vary, but the Toyota Mirai refuels its 5 kg, 700 bar tank in approximately 3 minutes [14]. If filling an empty tank, the dispenser would initially draw hydrogen from the low pressure tank, and switch to the medium and high pressure as the pressure in the car's tank rise [20]. Some stations around the world have the possibility to choose between 350 bar pressure and 700 bar pressure, known as H350 and H700. For the Toyota Mirai, the cheaper H350 will result in approximately a half tank [13].

2.3 Hydrogen in ISO-containers

To unroll the use of hydrogen faster and cheaper, one way is to use modular hydrogen storages. An example of a modular storage is to use an ISO-container. Such containers are easy to transport with existing infrastructure, can be deployed fast, and produced in large quantities significantly cheaper than designing all hydrogen facilities uniquely. It is possible to store the hydrogen itself inside such containers, but also include compressors, pumps, piping and so on. An example of this is Engie's power unit. Their container based unit can convert excessive renewable power to hydrogen through electrolysis, and back to electricity when needed through a fuel cell [11].

This thesis will use a 40 ft. standard dry ISO-container in some of the simulations. Such a container is 2.3 meters wide, 2.3 meters tall, and 12.0 meters long, and shown in figure 5 [29].



Figure 5: 40 ft. ISO-container [29]

2.4 Ignition probability modelling

The HyRAM ignition probability model was introduced in section 1.2. Another model used much in the oil and gas industry, is MISOF [25]. The model will also be used much in this thesis.

In this thesis, the probability of ignition, $P(I)$, is modelled as the product of two probabilities [24].

1. The probability of an ignition source being exposed to a flammable cloud, $P(E)$
2. The probability of ignition when already exposed to a flammable cloud, $P(I \text{ given } E)$

$$P(I) = P(E) \cdot P(I \text{ given } E) \quad (2)$$

MISOF does only consider $P(I \text{ given } E)$. The model is made using data from offshore leak and ignition incidents. However, adaptations have been made to make the model adequate for land based facilities. The equipment density is usually higher on offshore installations where space is limited compared to land based facilities, where process volume is not as expensive [24].

MISOF divides ignition sources in two classes; continuous and discrete. A continuous ignition source can ignite a flammable cloud at any point in time. An example of this is a hot surface above the auto ignition temperature. A discrete ignition source can only ignite clouds in short time intervals [24].

2.5 KFX

Kameleon FireEx is a CFD tool owned and distributed by DNV GL, but made by ComputIT, SINTEF and NTNU. The main purpose of KFX is to simulate the transient behaviour of leaks of gas or liquid, cloud dispersion and fires [10]. A simulation is set up in the KFX Wizard shown in figure 6.

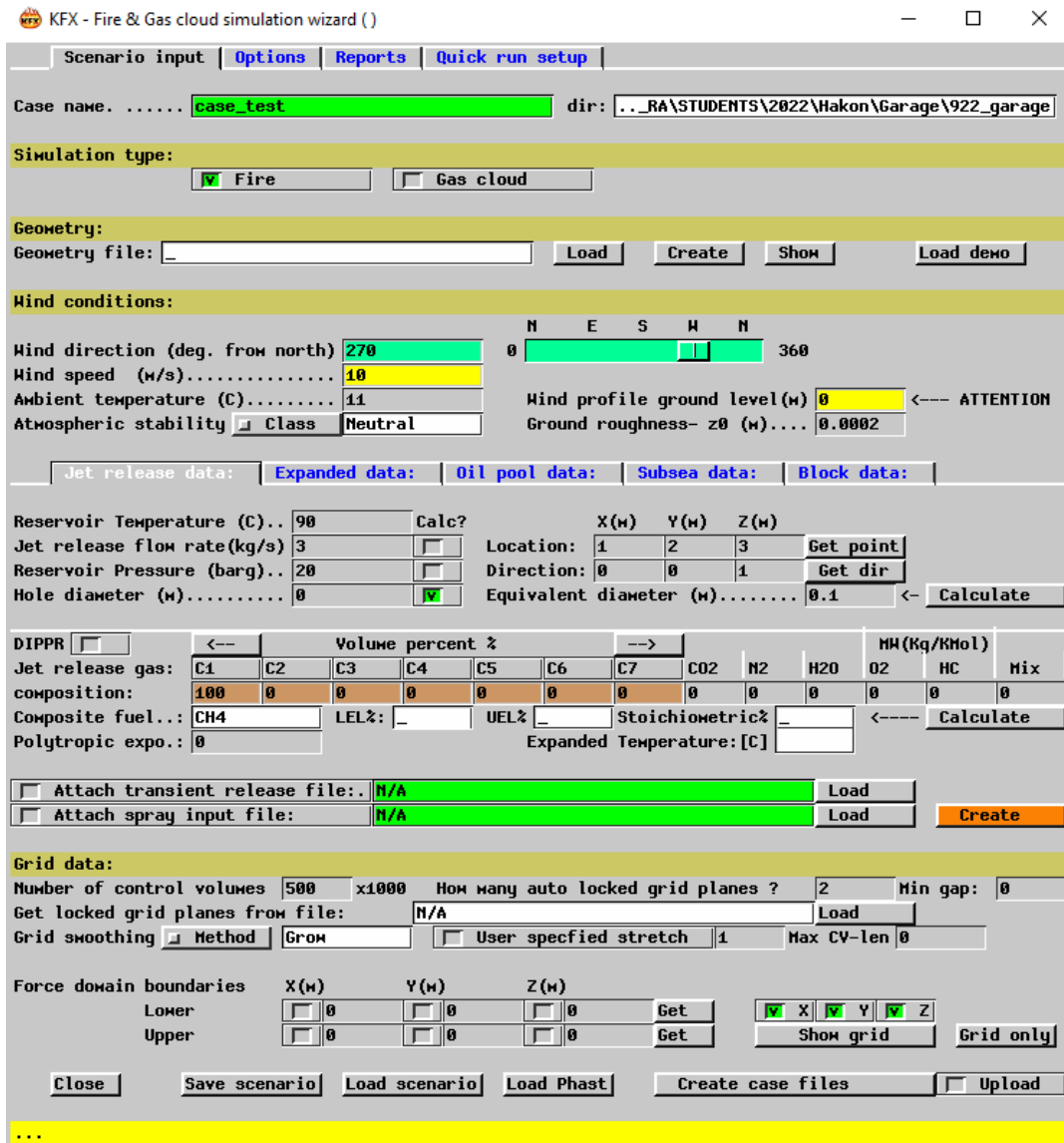


Figure 6: The setup menu in KFX

A simulation in KFX starts with a geometry. Then, the wizard is used to set up the case. This includes release substance, release location, release direction, wind conditions and reservoir parameters. The reservoir has four parameters. One must enter three of the four, and KFX calculates the last. The parameters are temperature, release mass flow rate, reservoir pressure and hole where substance leaks from. The mesh in KFX is made by blocks, and KFX does this automatically based on the total number of cells entered by the user. The grid is finer around the release [24].

2.6 KFX RBM

KFX Risk Barrier Management is an extension to KFX. It is an experimental software, and no manual has been made. All the features of KFX are found, but RBM includes a possibility to calculate ignition probabilities. The way this works, is that ignition sources are placed inside the geometry. The usual gas dispersion simulation of KFX will find out if ignition sources are hit by the gas cloud. If so, the ignition source will make a contribution to the ignition probability [24]. This is explained further in the next subsection.

2.7 Input to KFX RBM

The purpose of any model is to recreate a real world system. For the rest of this thesis, it is important to understand how KFX RBM models and calculates ignition, and how it actually happens in reality. This will be even more important when ignition from cars need to be modelled. As in any CFD software, the real world is discretized into a grid. A coarse grid will mean less accuracy, and as the number of grid cells approach infinity, it will be an exact replica of the real world. Inside this grid, KFX RBM can place ignition sources as boxes with parameters to calculate ignition probability. Note that this subsection only considers parameters used for the ignition probability modelling, not general CFD variables such as wind speed and courant number.

Each box ignition source in KFX RBM will be given the expected number of ignitions given exposure as input. This is a highly important parameter, and it is divided into a continuous and discrete contribution. The continuous expected number of ignitions is denoted λ_C , and its unit is $\frac{1}{m^3}$. Thus, it is the expected number of ignitions per meter cubed. The discrete expected number of ignitions is denoted λ_D , and its unit is $\frac{1}{s \cdot m^3}$. Thus, it is the expected number of ignitions per second per meter cubed.

The input variables are summarized below.

- λ_C : Expected number of ignitions due to continuous ignition mechanisms per volume.
- λ_D : Expected number of ignitions due to discrete ignition mechanisms per second per volume.

It is also possible to define detectors. Depending on the detector type, they can sense a gas leak before ignition, or sense an ignited leak, such as an IR-detector. In KFX RBM, any number of detectors can be added. When a given share of the detectors trigger, they turn off or disconnect a given share of the ignition sources. The share of ignition sources which is turned off is given through a parameter called p_{iso} , a number between 0 and 1. When p_{iso} is zero, the system will act as if there are no detectors present. When p_{iso} is 1, all ignition sources are turned off upon detection. Compared to other types of gas detectors, hydrogen detectors have longer response times [17].

2.8 IP code

The ingress protection (IP) code is an important parameter for ignition modeling. It gives a rating of how well equipment can handle dust and water without penetration. However, a high IP rating also means flammable gas will have a hard time getting inside equipment where sparks can occur. The IP-code used in this thesis only uses two digits, but generally up to four digits can be used. Each digit represent a different kind of equipment stress [6].



Figure 7: IP components

The first digit range runs from 0-6, and the maximum object size can enter the equipment is given in table 6 [6].

Level	Effective against
0	Nothing
1	>5 cm
2	>12.5 mm
3	>2.5 mm
4	>1 mm
5	Dust protected
6	Dust proof

Table 6: First digit of IP-code

The second digit range runs from 0-9, and the maximum liquid stress that can enter the equipment is given in table 7 [6].

Level	Effective against
0	Nothing
1	Dripping water
2	Dripping water when tilted at 15°
3	Spraying water
4	Splashing water
5	Water jet
6	Powerful water jet
7	Immersion up to 1 m depth
8	Immersion more than 1 m depth
9	Powerful, high temperature water jet

Table 7: Second digit of IP-code

MISOF suggests λ_C and λ_D values for different kinds of IP-ratings, summarized in table 8 [12].

IP-rating	λ_C [$1/m^3$]	λ_D [$1/s \cdot m^3$]
$\geq IP64$	$1.5 \cdot 10^{-4}$	$1.8 \cdot 10^{-6}$
$IP54$	$3.0 \cdot 10^{-4}$	$3.6 \cdot 10^{-6}$
$IP44$	$1.5 \cdot 10^{-3}$	$1.8 \cdot 10^{-5}$
$\leq IP44$	$1.5 \cdot 10^{-2}$	$1.8 \cdot 10^{-4}$

Table 8: IP code lambdas

In this thesis, the equipment which is not authorized for use in explosive atmospheres will be referred to as non-ATEX equipment [15]. This includes all equipment in table 8.

2.9 Output of KFX RBM

The result of a KFX RBM simulation is a discrete and continuous ignition probability for each source, as well as the total ignition probability. The contribution from each source is used to

make up the total ignition probability. Recall that the input variable for the discrete ignition probability was the expected number of ignitions per second per meter cubed. If an ignition source is exposed, the discrete ignition probability will increase as time passes, while the continuous ignition probability of a source is constant throughout the time of exposure. If the cloud covers an ignition source for a very long time, the discrete ignition probability would converge to 100%.

For each simulation, KFX will create an ignition probability file. Understanding how this file is constructed is important for understanding this thesis, as it will be manually tweaked later to overcome the limitations of the software. The csv file is organized as seen in table 9, with some example values.

i	P_T	P_I	P_C	P_D	$P_{T,n}$	$P_{C,n}$	$P_{D,n}$
0	0.01	0.01	0	0	0	0	0
0.005	0.01	0.01	0	0	0	0	0
0.115	0.01	0.01	0	0	0	0	0
0.126	0.010001	0.01	0	$1.1 \cdot 10^{-6}$	$1.1 \cdot 10^{-6}$	0	$1.1 \cdot 10^{-6}$
0.263	0.10002	0.01	0	$2.36 \cdot 10^{-6}$	$2.36 \cdot 10^{-6}$	0	$2.36 \cdot 10^{-6}$

Table 9: Ignition probability file setup

Each row in the file represents an iteration of the simulation. The columns are explained in the list below. Note that there can be any number of ignition sources in a system, which means the total, discrete and continuous ignition probability for source 1 to n will be found in the file.

- i: The time of the current iteration.
- n: Index of an ignition source, $n = 1, 2, 3 \dots N$.
- P_T : The total ignition probability of all sources.
- P_I : The probability of immediate ignition.
- P_C : The total contribution from continuous sources.
- P_D : The total contribution from discrete sources.
- $P_{T,n}$: The discrete and continuous contribution from ignition source n.
- $P_{C,n}$: The continuous contribution from ignition source n.
- $P_{D,n}$: The discrete contribution from ignition source n.

$P_{C,n}$ is the continuous ignition probability for one ignition source. In general, it is found using a Poisson distribution. λ_C is the input variable which was just explained in section 2.7, the expected number of ignitions per volume, and V_{new} is the new flammable volume in the time step.

$$P_{C,n} = P(1 \text{ or more ignitions}) = 1 - P(\text{Zero ignitions}) =$$

$$1 - e^{-E_C} \frac{E_C^0}{0!} = 1 - e^{-E_C} \quad (3)$$

E_C is the expected number of ignitions and given by

$$E_C = \lambda_C V_{New} \quad (4)$$

The total continuous ignition probability of all sources at a time step is found by

$$P_{C,i} = 1 - (1 - P_{C,1})(1 - P_{C,2})\dots(1 - P_{C,N}) \quad (5)$$

If a continuous source is not exposed to a cloud, there is of course no chance of ignition, and hence zero ignition probability for an unexposed ignition source. Therefore, V_{new} is treated like a true or false variable by KFX RBM.

$P_{D,n}$ is the discrete ignition probability for one ignition source. In general, the discrete ignition probability is also found using a Poisson distribution using λ_D and $V_{LFL:UFL}$, the cloud volume in the flammable range. Δt is the time since first exposure of the source.

$$P_{D,n} = 1 - e^{-\lambda_D V_{LFL:UFL} \Delta t} \quad (6)$$

The total discrete ignition probability of all sources at a time step is found by

$$P_{D,i} = 1 - (1 - P_{D,1})(1 - P_{D,2})\dots(1 - P_{D,N}) \quad (7)$$

In addition, for a single ignition source, $V_{LFL:UFL}$ will be a true or false variable in KFX RBM, whether the source is exposed to gas or not.

The total ignition probability at a time step is found by equation 8.

$$P_{T,i} = 1 - (1 - P_{continuous})(1 - P_{discrete})(1 - P_{Immediate}) \quad (8)$$

2.10 Understanding cars as ignition sources

A car has several potential ignition sources. The uncertainty related to ignition from cars is large, as few incidents are reported, and few experiments have been done. Some ignition sources found in cars are believed to be highly significant. First, brushed motors can ignite gas due to sparks. This is considered an effective ignition source, as sparks are generated at the brushes during normal operation. Such a fan is often found to be the coupe ventilation fan. In addition to generating sparks, it will also suck explosive gas through the duct, increasing the likelihood of exposure. Such fans are found in all vehicle types, both combustion and electric cars. The conditional ignition probability, $P(I \text{ given } E)$, is set to 90% in MISOF [12].

Another ignition source found in combustion engine cars is the air intake to the engine. This is either due to gas being exposed to hot surfaces above the auto ignition temperature, or gas getting into the combustion chamber [12]. For example, an engine was marked as a suspect ignition source of the Deepwater Horizon accident [28]. The conditional ignition probability is set to 50% by MISOF [12].

The rest of this section will consider how ignition from cars can be modelled in KFX RBM. If the ignition source KFX is trying to model is a point in space, a small box would be placed. For example, this could be a location where sparks occur. However, if the area of interest is not a fixed object, a large box with a given ignition probability can be placed to cover the area. Throughout this subsection, the goal is to describe how such a large box can be used to model multiple cars on a road.

To clarify how non-object ignition sources work, a simple example is given. First, assume a carpet on the floor is always charged with static electricity. The carpet is lying inside a chicken house, and chickens jump down from their boxes onto the carpet a few times a day when exiting the chicken house. When a chicken touches the carpet, a discharge happens and results in a spark. Right next to the chickens, there are cows such that the concentration of methane above the carpet is constantly within the flammable range. If it is unknown where on the carpet the spark occurs, but it is known how often a chicken lands there, the entire carpet can be modelled as thin plate with the same area as the carpet. In this case, there is no continuous ignition probability. The input

KFX RBM needs, the number of expected ignitions per second, would be the frequency of how often a chicken lands on the carpet, multiplied by the probability that a spark ignites the methane. Notice that in this simple example, the cloud is assumed static.

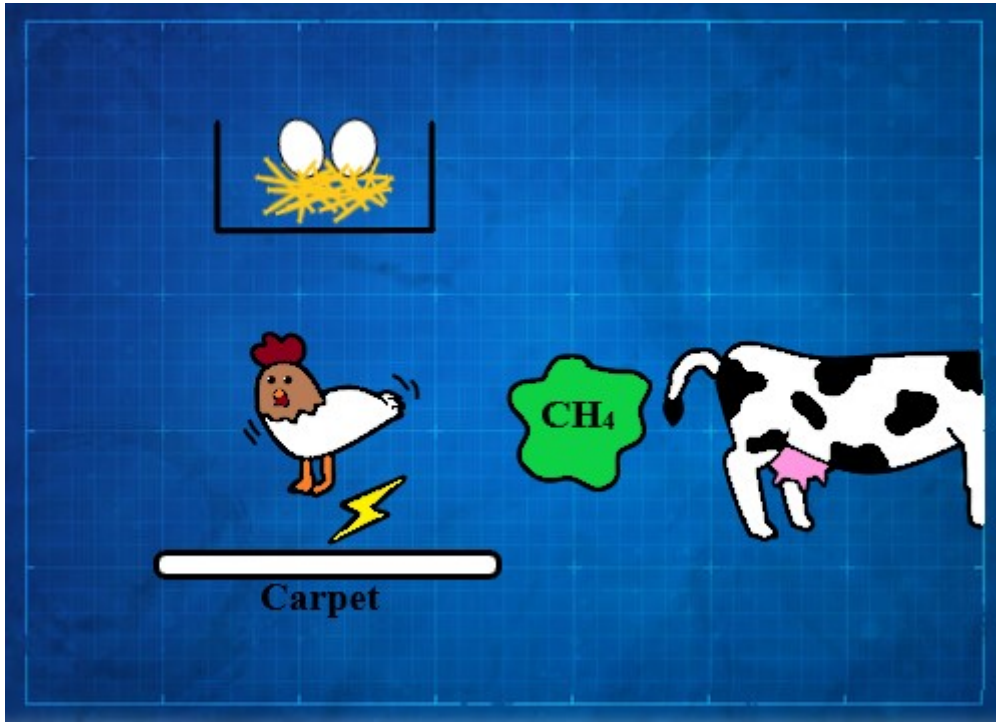


Figure 8: An example of an ignition source

Thinking the same way, it is possible to model ignition caused by cars exposed to a gas cloud. Using the same reasoning as for the chicken example, it is assumed that the frequency of cars passing by an area is known. In this case, it is no longer possible to assume a static gas cloud. To understand how to model ignition caused by moving cars in KFX RBM, imagine a birds eye view of a gas leak close to a road. The speed of the gas cloud is very small compared to that of moving cars. If one was to record and play the situation in fast speed, each car bypass would look like a blink compared to the slow cloud. Therefore, the position where a car makes contact with the cloud is irrelevant. If the cloud is not divided, the entire cloud will ignite no matter where the ignition happened. In the case of the chickens landing somewhere random on the carpet, it was possible to define the expected number of ignitions per second for the entire carpet based on how often a chicken would land. In the case of the cars on the road, it is possible to do the same based on how often cars pass by. This will be done in section 3.2.3.

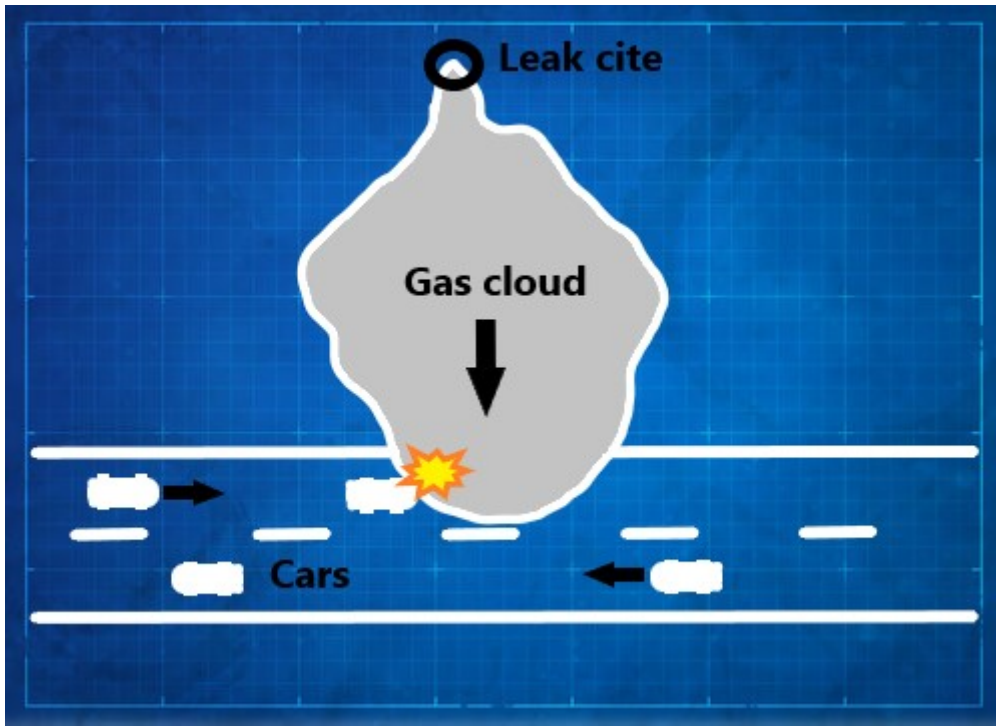


Figure 9: Gas cloud exposing road

KFX RBM is only able to model ignition sources as boxes. When modeling a bend in the road, one would need to place many boxes to make the bend. Another example of when one would need more boxes to model ignition from cars, is if cars spend more time in one area than another. This would happen if the speed limit changes on a stretch of road. In such a case, it is necessary to place boxes with different ignition probabilities along the road.

3 Method

3.1 Simulating a basic hydrogen leak

A basic geometry model of a jetty and a ferry are made using Autodesk Fusion 360, shown in figure 10. Behind the ferry, there are pipes for refueling the ship with gaseous hydrogen. There is also a parking lot, and the terrain slopes up from sea level. The leak occurs right behind the ferry. In addition, a base case with an empty, flay geometry is done as well.

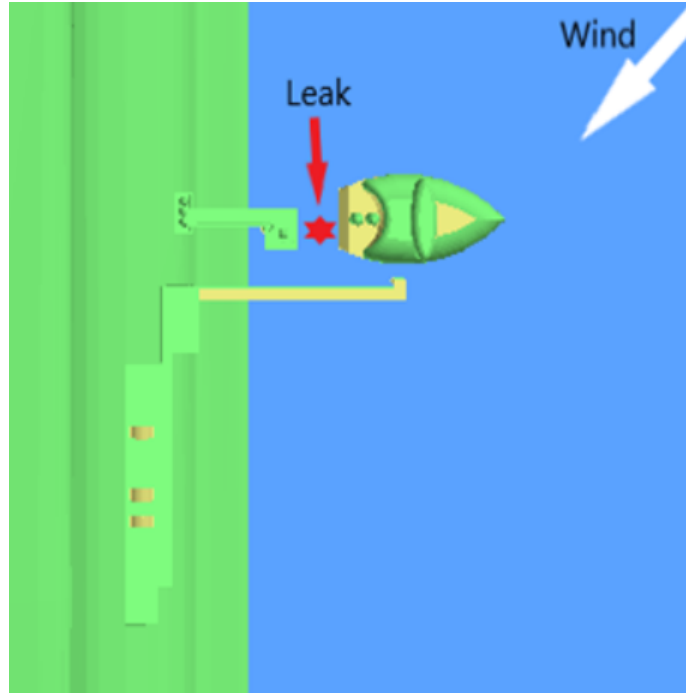


Figure 10: 3D-model of the ferry at the jetty

The parameters used for the sensitivity analysis of the basic hydrogen release are given in table 10. Note that the middle value in table 10 for 3/4 parameters is used while doing sensitivity on the last. To clarify with an example, this would mean all wind sensitivities would be done at 350 bar, 3 kg/s and a downward release direction.

Pressure [bar]	35	350	700
Mass flow rate [kg/s]	0.5	3	30
Wind speed [m/s]	0.5	5	15
Release direction	+z	-z	x

Table 10: Sensitivity parameters for basic hydrogen simulations

Wind direction	45°
Release duration	20 s
Ambient temperature	11°C
Substance	GH ₂
Grid cells	500 000

Table 11: Constant parameters for basic hydrogen simulations

To analyze each simulation, a Python script is written. This script divides the geometry seen from above into pizza slices. The code will check the maximum distance the cloud is found from the release center, at a certain concentration. The maximum distance for all elevations is projected onto the plot. As the LFL of hydrogen is 4%, this concentration is used for the radar plot. An example of this is shown in figure 11. The yellow blobs are a surface plot where the cloud is at 4% concentration. The maximum of all distances in one radar plot is saved to Excel. For the example in figure 11, this means 36 meters, the maximum of all the sectors, is saved to Excel. Parts of the code are found in appendix C. The code uses confidential libraries, and some source code is therefore not included.

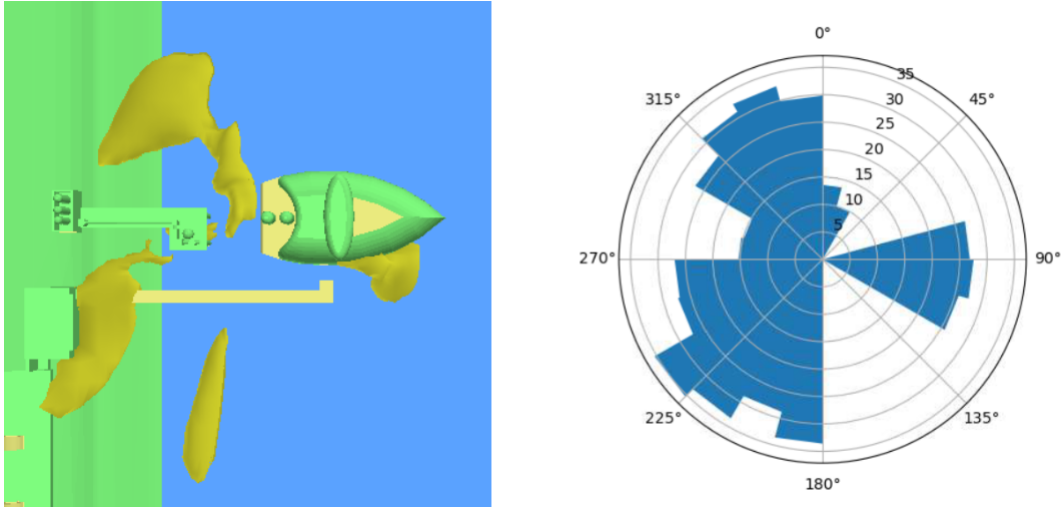


Figure 11: Radar plot example

3.2 Simulating the hydrogen refueling station

3.2.1 3D model

3D models of a generic hydrogen refueling station is shown in figure 12 and figure 13. The model is made in Autodesk Fusion 360. The design of the station is based on the theory in section 2.2, and partly by an example hydrogen refueling station found in ISO 19880's requirements for gaseous hydrogen refueling stations [1]. The fenced box to the upper left consists of process equipment where the hydrogen is compressed and stored. Hydrogen is delivered by trailer, and two tube trailers are present inside the process equipment area. Trailer delivery of GH_2 is chosen based on the theory in section 2.2. The fences are 5 meters tall, meaning the volume of the fenced area is 1300 m^3 . If the volume of the objects inside is subtracted, the open volume is 1170 m^3 . There is also a dispenser area and a shop.

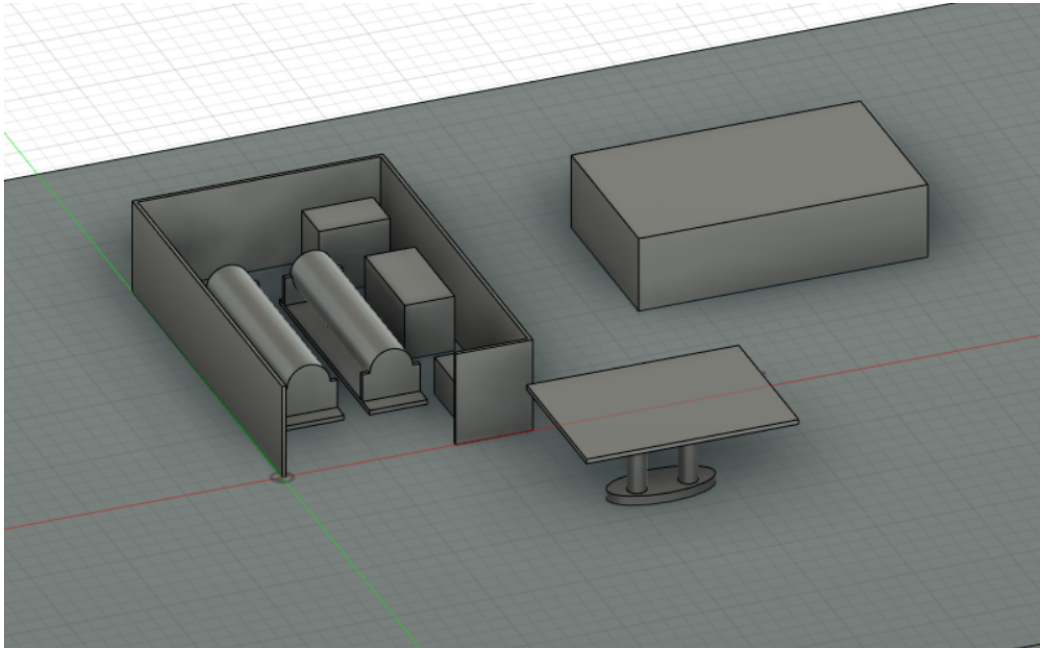


Figure 12: 3D-model of the refueling station

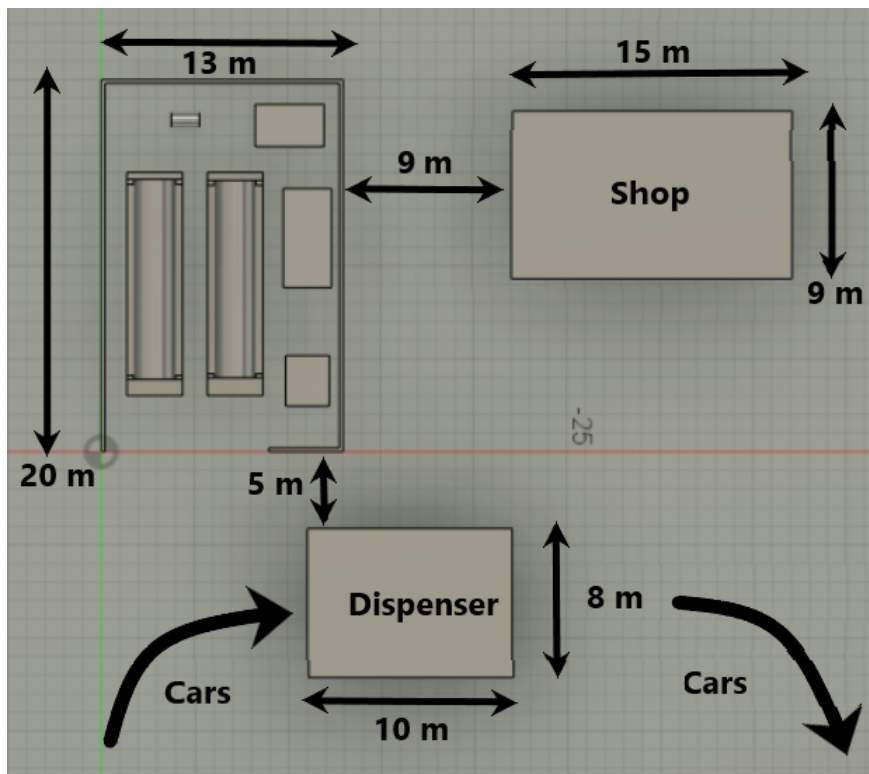


Figure 13: Dimensions of the refueling station

3.2.2 Parameters

A list of the main parameters needed to simulate a leak at a hydrogen refueling station are given below.

- Cylinder pressure

-
- Leak flow rate
 - λ_C and λ_D , described in 2.7
 - Placement and number of detectors and ignition sources

The theory about hydrogen refueling stations in section 2.2 gives some suggested values of pressure. To save simulation time, only one pressure level is chosen; 350 bar (H35). Even though the three tanks can have many different pressure levels, the system would mostly see 350 bar or 700 bar when filling. In addition, going to very high pressure levels requires time consuming simulations. This is because a high reservoir pressure gives a high jet velocity. The courant number dictates how far a particle can move in one iteration, and it should not move along multiple cells. Therefore, an extremely fine grid is needed near the release, giving a long simulation time.

The leak flow rate is determined through detailed conversations with experts at Safetec. The goal is not to have accurate numbers for a specific scenario, as it is difficult to predict where equipment would fail and what hole size it would lead to. Instead, leak rates covering a large span of severity should be chosen. The values chosen are 0.1 kg/s, 1 kg/s and 10 kg/s. Note that these are initial values. As the pressure in the system drops, the leak rate also drops. KFX calculates the transient release rate on its own. 0.1 kg/s would resemble a leak from a flange not tightened or a crack in a pipe. 1 kg/s would resemble a pipe breaking. 10 kg/s would resemble a tank rupture. Like simulating high pressure leaks are time consuming, low flow rate leaks are too. Therefore, the lower limit is set to 0.1 kg/s to save simulation time.

The tank volume is set to 0.55 m^3 . As discussed in section 2.2, 13 kg hydrogen tanks are suggested as a decent ballpark figure. To find the correct volume size, the density of hydrogen at 350 bar and 11°C is calculated to be 24.3 kg/m^3 [33]. Thus, a tank volume of approximately 0.55 m^3 is used.

The parameters which are kept constant in all sensitivities for the refueling station simulations are summarized in table 12.

Wind speed	3 m/s
Wind direction	West
Ambient temperature	11°C
Reservoir temperature	11°C
Reservoir pressure	350 bar
Substance	GH_2
Grid cells	300 000

Table 12: Parameters constant for the hydrogen refueling station simulations

Note that a grid sensitivity using leak rates of 0.1, 1 and 10 kg/s in domains with 100 000, 300 000 and 500 000 grid cells are conducted. The grid sensitivity simulations are only performed using a downward release direction. The parameters which are varied are summarized in table 13.

Case	Flow rate [kg/s]	Rel. direction
1	1	X
2	1	Y
3	1	-X
4	1	-Y
5	1	Z
6	1	-Z
7	10	X
8	10	Y
9	10	-X
10	10	-Y
11	10	Z
12	10	-Z
13	0.1	X
14	0.1	Y
15	0.1	-X
16	0.1	-Y
17	0.1	Z
18	0.1	-Z

Table 13: Parameters varied for the hydrogen refueling station simulations

3.2.3 Ignition sources

The expected number of ignitions per second per volume for the car area is not provided by Safetec. This is the λ_D introduced in section 2.7. Before other ignition sources used in the simulations are presented, the λ_D for the car area is calculated. To find this value, the number of fills per station per day is required. This will of course vary with demand. In this thesis, the hydrogen cars of Bærum will be used to get this estimate, as calculations of this were conducted in 2020 by a former master student [7]. This is only a rough figure, and is only performed to get the correct order of magnitude. Although the Sandvika accident described in section 1.1 slowed the progress of FCEV's in Norway, it is still a fair estimate of traffic for the refueling station which will be used for the simulations. It is assumed that the rapidly growing hydrogen car trend in Norway continued, and the Sandvika accident never happened. An overview of the calculations from the former master thesis [7] begins by finding the percentage of hydrogen cars in the future by regression of historical data.

$$share_{FCEV} = 0.0006e^{6931t} \quad (9)$$

where t is the number of years since 2016. Thus, in 2020, the share of FCEV's in the total vehicle fleet in Norway is approximately 1%. Using the total number of kilometers per year in Bærum in 2018, the road traffic volume was 2126.7 million km. Assuming the same traffic levels in 2020, the road traffic volume of FCEV's is

$$FCEV_{RTV} = 0.01 \cdot 2126700000 = 20.4 \text{ million km/year}$$

There were two hydrogen refueling stations in Bærum in 2020 assuming the Sandvika accident did not happen. The Toyota Mirai has a range of 500 km when completely filled with 5 kg hydrogen [14], so it is assumed that fills happen every 400 km driven, as the tank is usually never empty when refueling. Using this, the number of fills per station per day can be calculated [7].

$$fills = \frac{FCEV_{RTV}}{\frac{km}{fill} \cdot stations \cdot \frac{days}{year}} =$$

$$\frac{20400000}{400 \cdot 2 \cdot 365} = 70 \text{ fills/station} \cdot \text{day}$$

The Toyota Mirai has a fill time of 3 minutes [14]. It is also fair to assume one can add 2 minutes extra time for parking by the dispenser, exiting the car, paying and so on. However, assuming the car is turned off, it will not be a potential ignition source during filling. Thus, only 2 minutes per car per fill is considered.

Although a car has continuous ignition sources, problems emerge since there are not always cars at the filling station. To capture the fact that cars are not always present, a discrete ignition source must be used. The concept was introduced in section 2.10.

To find λ_D , the starting point is the number of fills at the station per day. If cars were to arrive evenly throughout the day, the time between each car would be as given in equation 10. Note that this is a period, as it is the inverse of the frequency. The station time is the time spent on the station with the car turned on.

$$t_{car} = \frac{\text{sec/day}}{\text{fills/day}} - \text{station time} = \frac{86400}{70} - 120 = 1114 \text{ s} \quad (10)$$

In section 2.10, the ignition probability of a car was set to 90%. The last calculation to find λ_D is shown in equation 11.

$$\lambda_D = \frac{P(I)_{car}}{t_{car}} = \frac{0.9}{1114} = 0.0008 \text{ (1/m}^3 \cdot \text{s)} \quad (11)$$

Thus, the λ_D for the car area is 0.0008 ($1/s \cdot m^3$), and λ_C is zero.

All the scenarios are run with some variations of ignition source parameters. The value of the lambdas which are varied are summarized in table 15. Note that the sources in table 15 are sources based on an expected equipment density per volume. Therefore, they cover the entire volume inside the fencing, and is referred to as volumetric sources. The lambdas which are kept constant, the non-ATEX equipment and car area are shown in table 14. Note that the immediate ignition probability contributes to the total ignition probability, and not the discrete or continuous. The placement of the ignition sources are shown in figure 14.

Ignition source	λ_C [$1/m^3$]	λ_D [$1/s \cdot m^3$]	p_{iso}
\leq IP44 Non-ATEX equipment	$1.5 \cdot 10^{-2}$	$1.8 \cdot 10^{-4}$	0.1
\geq IP64 Non-ATEX equipment	$1.5 \cdot 10^{-4}$	$1.8 \cdot 10^{-8}$	0.1
Car area	0.0	$7.3 \cdot 10^{-4}$	0
Immediate ignition prob.	$2.35 \cdot 10^{-4}$		

Table 14: Ignition source parameters kept constant for the hydrogen refueling station

Model name	Ignition source	λ_C [$1/m^3$]	λ_D [$1/s \cdot m^3$]	p_{iso}
Standard	Electrical equipment, MISOF	$1.8 \cdot 10^{-6}$	$1.5 \cdot 10^{-9}$	0.3
	Rotating equipment, MISOF	$3.7 \cdot 10^{-6}$	$1.5 \cdot 10^{-9}$	0.25
	Other equipment, MISOF	$6.0 \cdot 10^{-7}$	$1.2 \cdot 10^{-8}$	1
Offhore MISOF	Total volumetric	$2.8 \cdot 10^{-6}$	$1.5 \cdot 10^{-8}$	0.36
Onhore MISOF	Total volumetric	$2.8 \cdot 10^{-6}$	$1.5 \cdot 10^{-8}$	0.16
$SAFEN_{10}$	Total volumetric	$2.8 \cdot 10^{-5}$	$1.5 \cdot 10^{-7}$	0.36
$SAFEN_{100}$	Total volumetric	$2.8 \cdot 10^{-4}$	$1.5 \cdot 10^{-6}$	0.36

Table 15: Ignition source parameters varied for the hydrogen refueling station

Ten 10x10x10 cm boxes resembling non-ATEX equipment are placed 4 meters above the floor. This could for example be light armatures. It is done with different IP-ratings, equipment with rating less than IP44, and equipment with rating larger than IP64, which should be safer. The yellow box denoted as "other equipment" in figure 14 captures ignition from the volumetric sources.

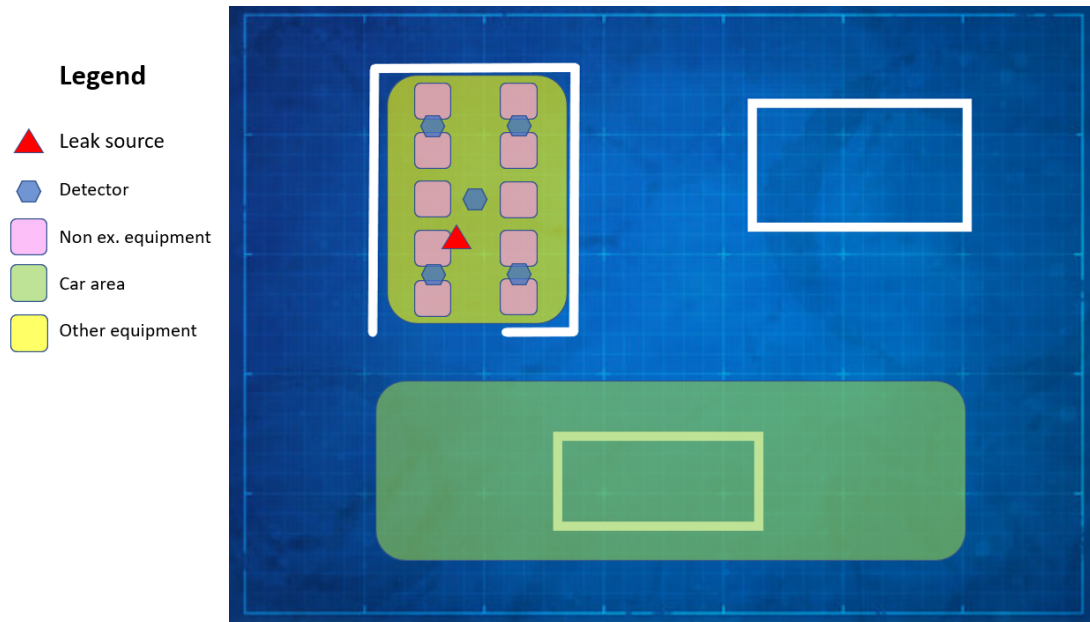


Figure 14: Ignition sources at the refueling station

3.2.4 Detectors

Detectors would most likely be placed in any facility handling large quantities of hydrogen [20]. Five IR detectors are placed at a height of 2 meters above the floor, as this covers the process equipment area evenly. The simulations are run with both disabled and enabled detectors, and given a response time of 5 seconds, suggested by experts at Safetec and relevant sources [17]. The position of the detectors are shown in figure 14. If one of five detectors sense gas, a fraction of the ignition sources given by P_{iso} will be turned off. As the consequences of a hydrogen ignition can be severe, it is unlikely that many detectors will need to sense gas to initiate a shutdown sequence, and is therefore set to one of five. The hydrogen detectors' sensing range is set to 1% to 5% volumetric concentration.

3.2.5 Switching hydrogen with methane

To compare the ignition probability of hydrogen against something already widely in use, a set of simulations with methane are conducted. The simulations with a release rate of 1 kg/s are done with methane, which are simulations 1-6 in table 13. The pressure is set to 200 bar, in line with pressures for CNG vehicles presented in section 2.1. The amount of methane inside the leak source is 13 kg, the same mass as in the hydrogen simulations. Only the standard MISOF model is used for the ignition sources.

3.2.6 The final SAFEN parameters

The input lambdas for the final SAFEN simulations are shown in table 16. Note that in the final SAFEN model, the immediate ignition probability is a function of leak rate. The immediate

ignition probability is higher than in any of the models above, because it considers topics like mechanical impact and electrostatic discharge ignition, which was introduced in section 2.1. The lambdas for non-ATEX equipment are also significantly higher. The simulations are done with 1 kg/s and 10 kg/s, and mirror case 6 and 12 in table 13 respectively. The open fenced refueling station geometry is used.

Ignition source	$\lambda_C [1/m^3]$	$\lambda_D [1/s \cdot m^3]$
Electrical equipment	$3.8 \cdot 10^{-5}$	$4.1 \cdot 10^{-7}$
Rotating equipment	$5.4 \cdot 10^{-6}$	$1.5 \cdot 10^{-9}$
Other equipment	$1.1 \cdot 10^{-5}$	$1.5 \cdot 10^{-9}$
\leq IP44 Non-ATEX equipment	$4.5 \cdot 10^{-2}$	$5.4 \cdot 10^{-3}$
\geq IP64 Non-ATEX equipment	$4.5 \cdot 10^{-3}$	$5.4 \cdot 10^{-5}$
Car area	0.0	$7.3 \cdot 10^{-4}$
Immediate ign. prob. 1 kg/s	$3.0 \cdot 10^{-2}$	
Immediate ign. prob. 10 kg/s	$4.3 \cdot 10^{-2}$	

Table 16: Ignition source parameters in the final SAFEN model

3.3 Simulating the container storage

3.3.1 3D model

A 3D-model of a 40 ft. ISO container is made in Autodesk Fusion 360, based on the dimensions given in section 2.3. The container is shown in figure 15. The white stripes along the sides is ventilation, which is added later in KFX. The ventilation is made of a custom porous material which is 50% open. This is mandatory, as KFX is unable to simulate a leak inside a closed volume. The front door of the container was opened later as the ventilation near the roof proved to be inadequate. The container replaces the volume containing the process equipment in the refueling station simulations. This is shown in figure 16.

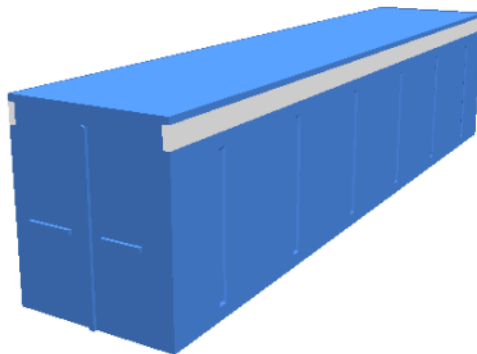


Figure 15: 3D model of the container

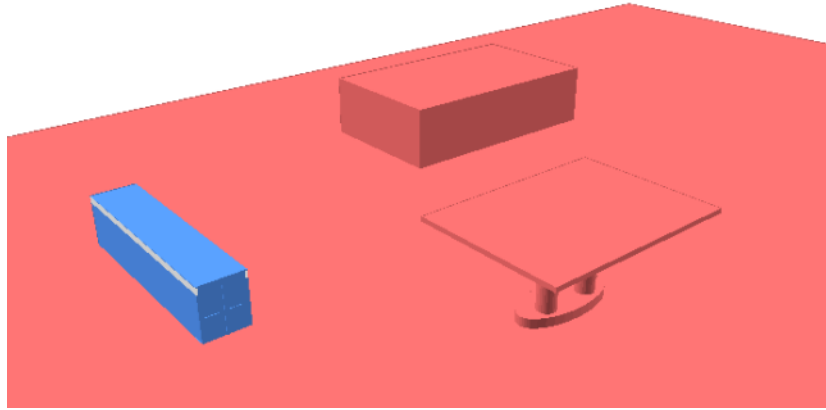


Figure 16: 3D model of the container at the refueling station

3.3.2 Parameters, ignition sources and detectors

All parameters and ignition sources are equal to that of the refueling station presented in section 3.2. However, the placement of ignition sources and detectors are changed to fit inside the container, shown in figure 17. The simulations are only run with detectors enabled. The offshore MISOF model and onshore MISOF model model are not tested due to reasons explained in section 6.2.2.

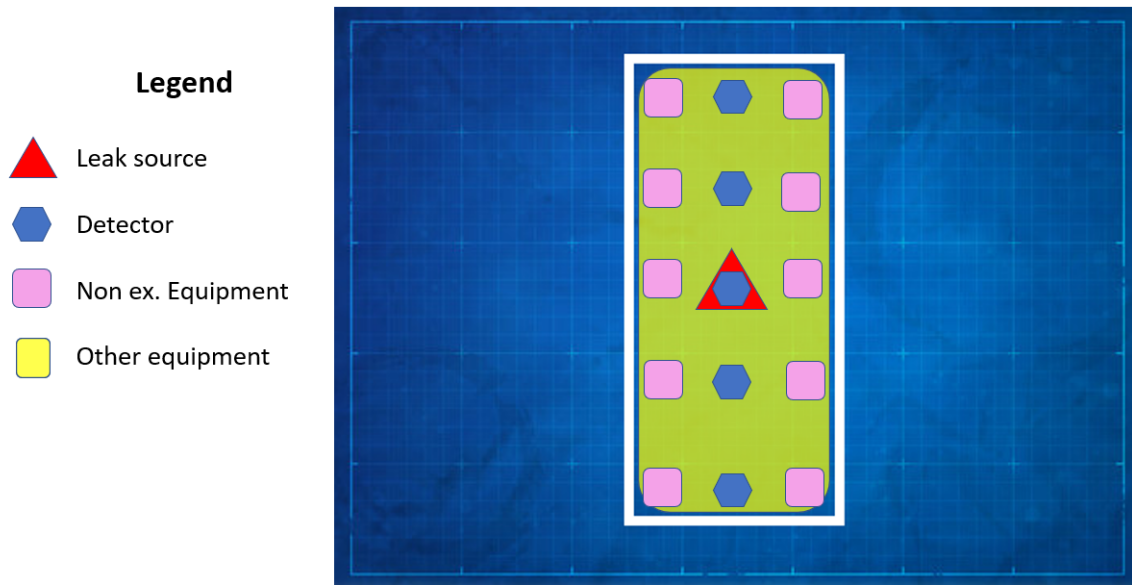


Figure 17: Ignition sources inside the container

3.4 Creating a post processing tool in Python

Doing a CFD simulation is often a time consuming process, and this is also the case in KFX. The software has two components, as described in section 2.6. The first is the usual CFD part, which simulates the dispersion of a gas cloud. The second component of KFX RBM is the calculation of ignition probability. While the first part can take days, the second part takes seconds. If one was to simulate the same case in terms of the release and geometry, and only change the ignition sources, the gas cloud dispersion would be equal, and only the ignition probability would change.

By default, one must do both parts when only the ignition sources is altered. However, it is possible to save time by only redoing the probability calculations. This means putting all ignition sources one would ever need into the original simulation, and turning on and off sources to create the different variations. Such a method was developed by DNV and Safetec years ago, but has not seen use in a long time. It was first attempted to get the old script working, but it was considered quicker to write a script in Python from scratch than dealing with the bugs.

The script starts by reading all columns from the ignition probability file created in the original simulation where all ignition sources are active. The format of the file is explained in section 2.9, which is necessary to read to understand how the script works. There are three parameters which are the output of the script. The total ignition probability, the total continuous ignition probability and the total discrete ignition probability. The user turns off some ignition sources, which means the discrete and continuous ignition probability of that source is set to zero. After this, the three parameters are calculated according to equation 5, 7 and 8. The last line of the new ignition probability file is written to Excel. In addition, the average values for each release rate is calculated. The code is found in appendix D.

4 Results

4.1 Basic hydrogen leak

Concentration plots in a y-plane at different simulation times are shown in figure 18 and 19.

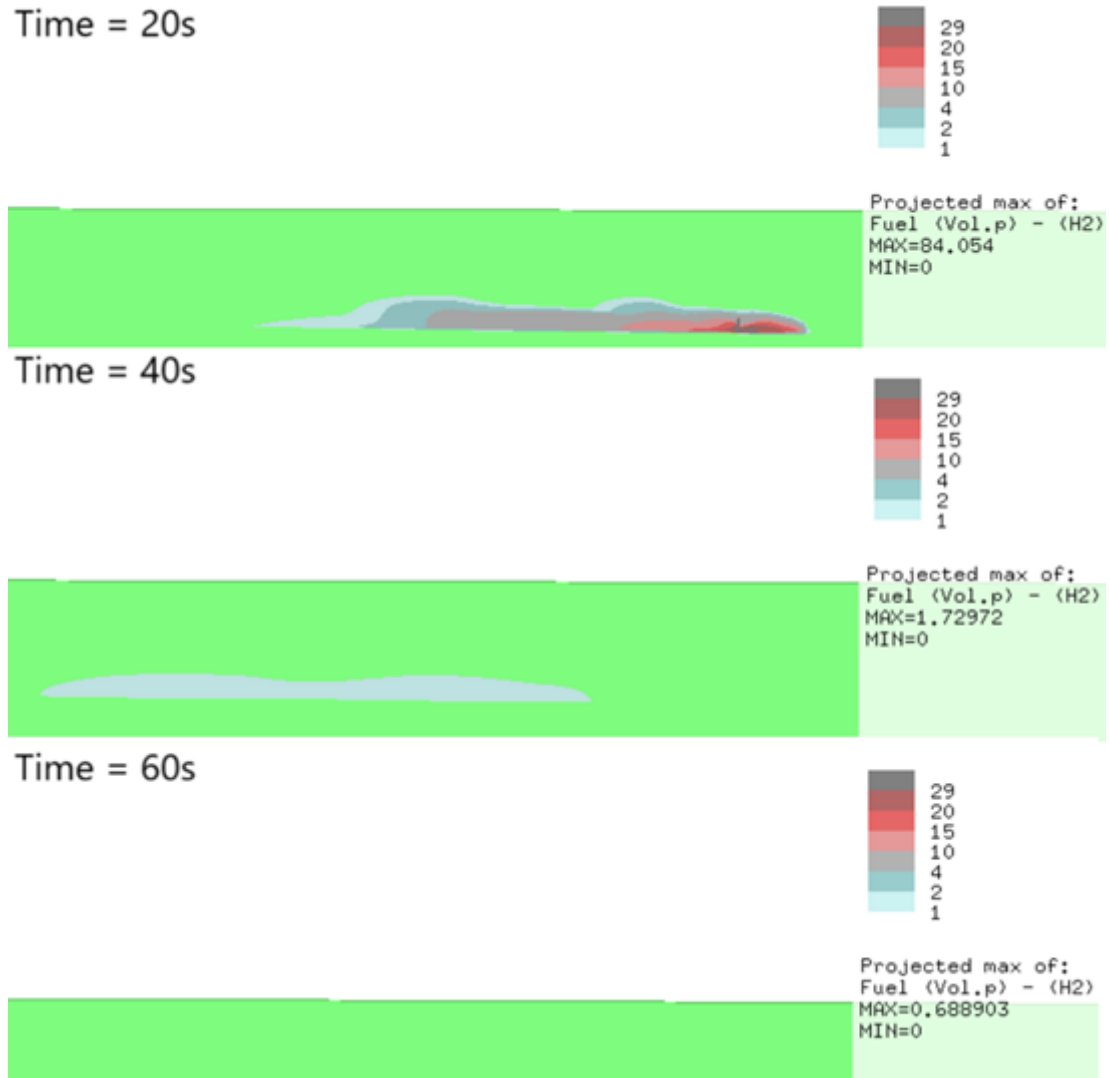


Figure 18: Concentration plot of flat geometry

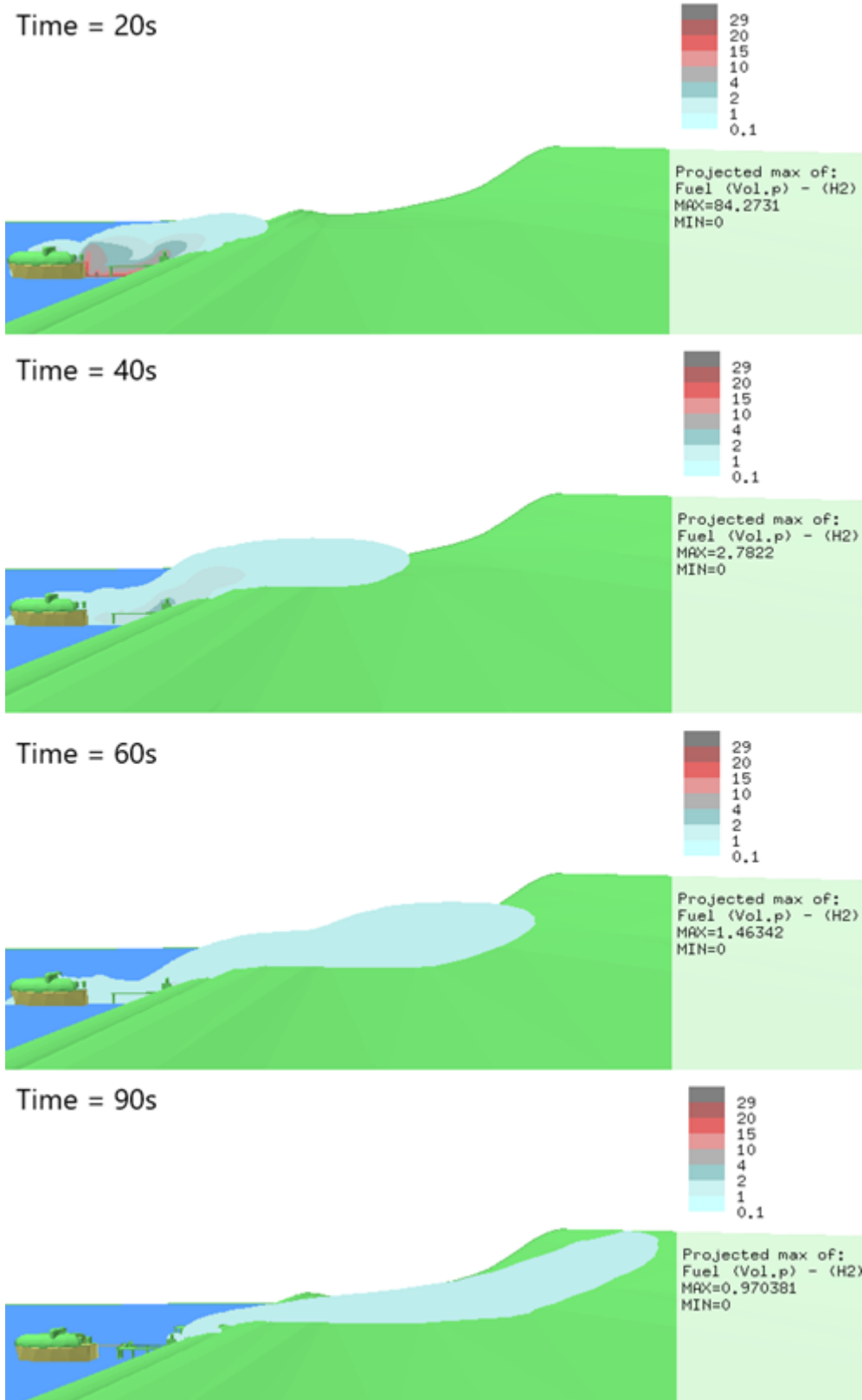


Figure 19: Concentration plot of geometry with terrain

The sensitivity results using the radar code are shown graphically in figure 20 to 26.

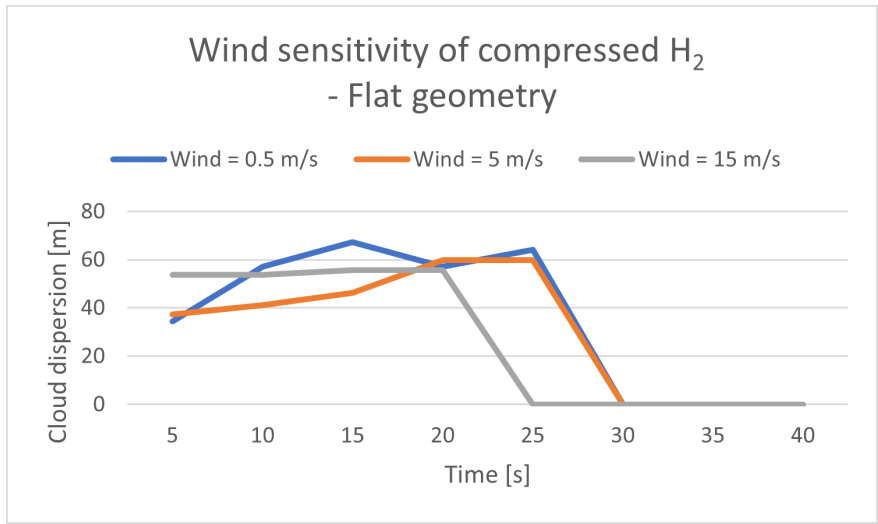


Figure 20: Wind sensitivity on flat geometry

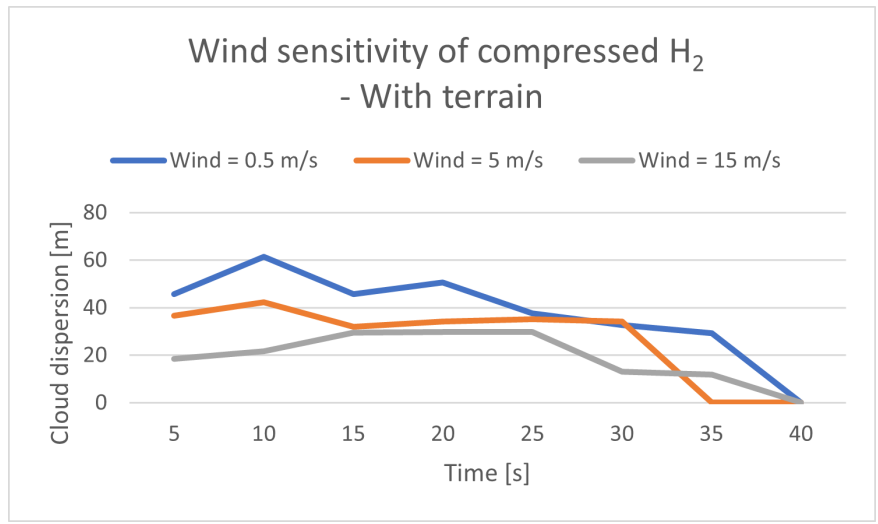


Figure 21: Wind sensitivity on geometry with terrain

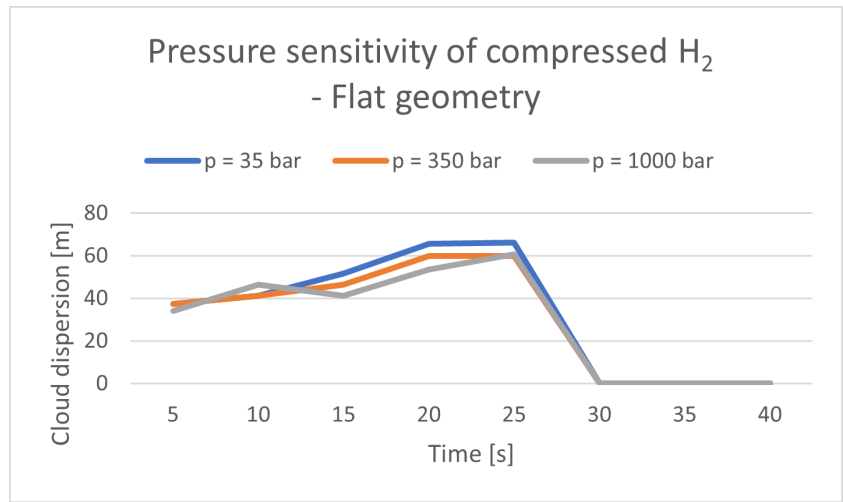


Figure 22: Pressure sensitivity on flat geometry

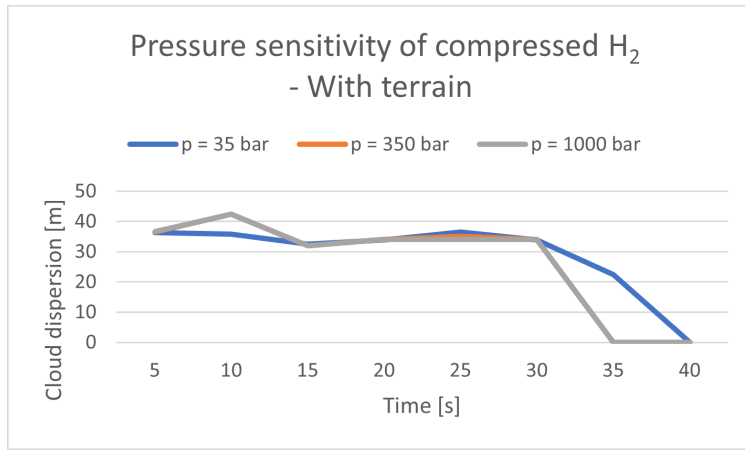


Figure 23: Pressure sensitivity on geometry with terrain

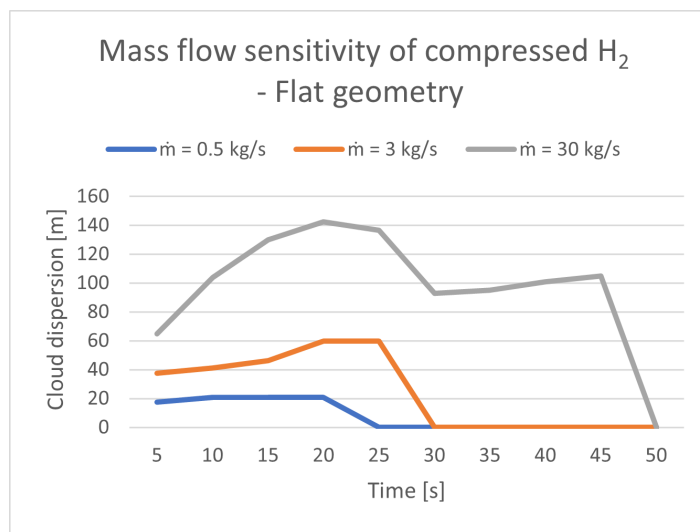


Figure 24: Mass flow sensitivity on flat geometry

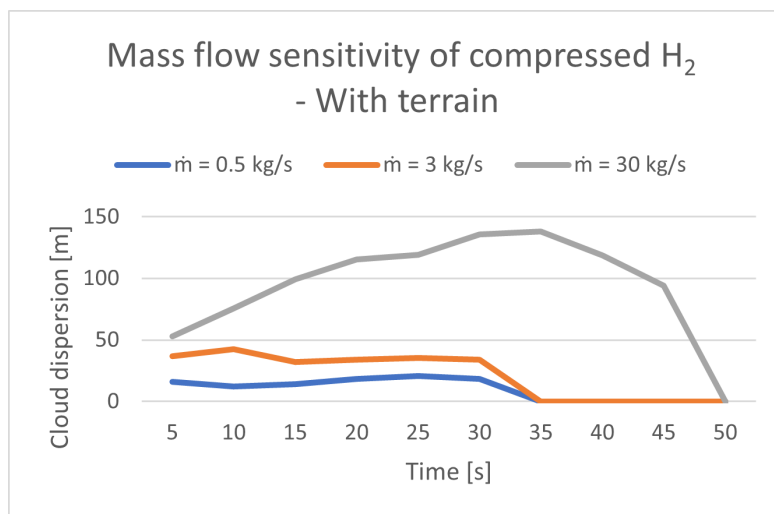


Figure 25: Mass flow sensitivity on geometry with terrain

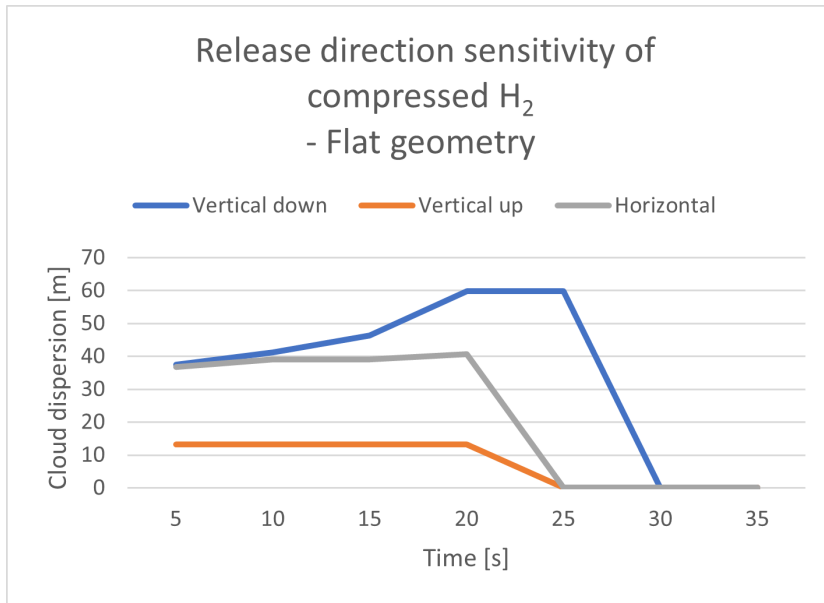


Figure 26: Release direction sensitivity on flat geometry

4.2 The hydrogen refueling station

4.2.1 Gas dispersion

To visualize the amount of gas in the domain, and the transient leak rate of a punctured vessel, three plots of the leak rate are shown in figure 27, 29 and 31. Figure 28, 30 and 32 show the 4% volumetric concentration cloud surface. All are shown for a release in a downward direction.

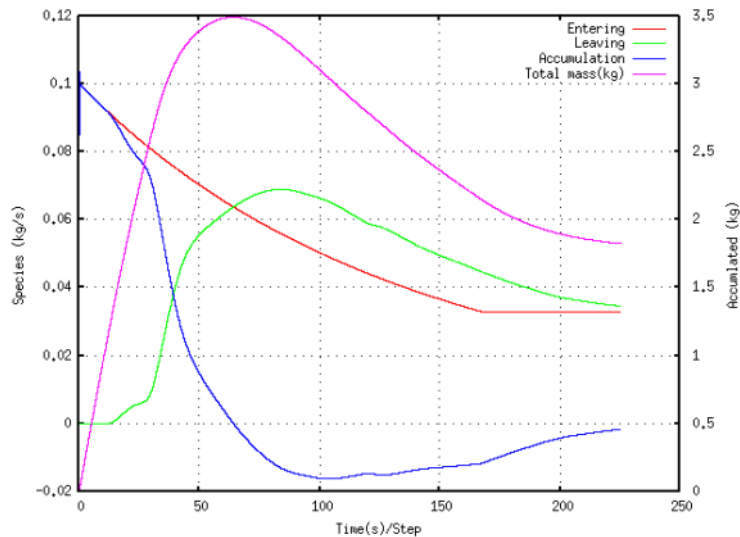


Figure 27: Release profile of 0.1 kg/s downward release

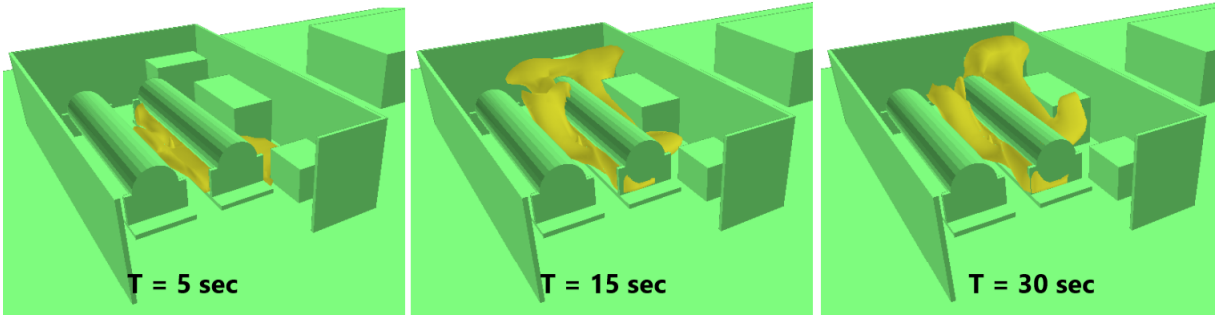


Figure 28: Surface plot of 4% H_2 concentration for 0.1 kg/s downward release

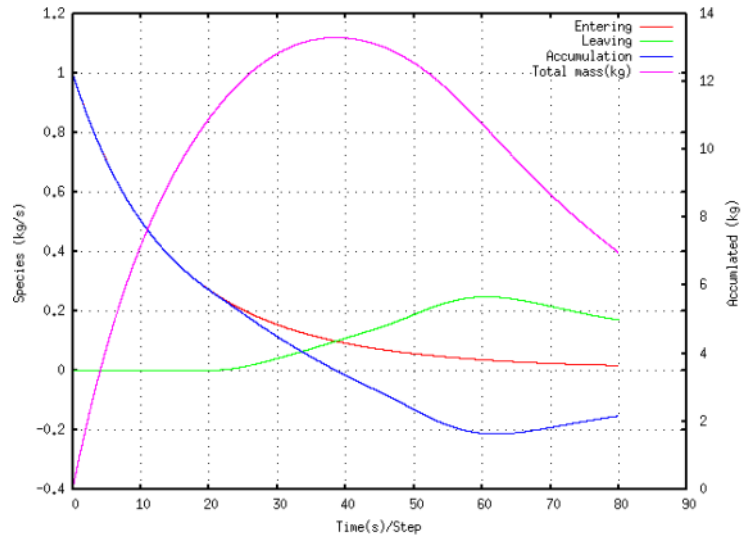


Figure 29: Release profile of 1 kg/s downward release

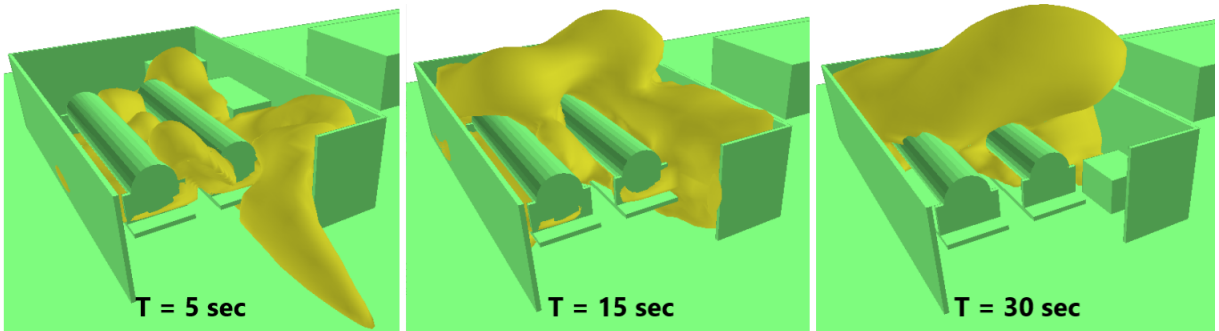


Figure 30: Surface plot of 4% H_2 concentration for 1 kg/s downward release

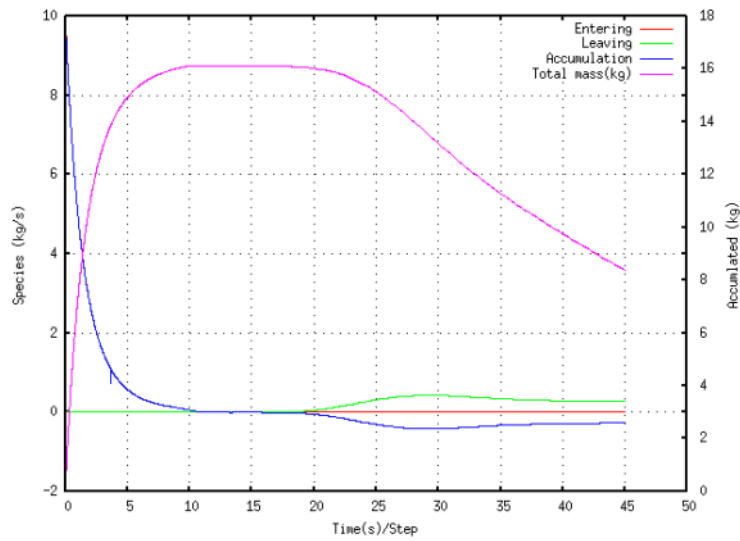


Figure 31: Release profile of 10 kg/s downward release

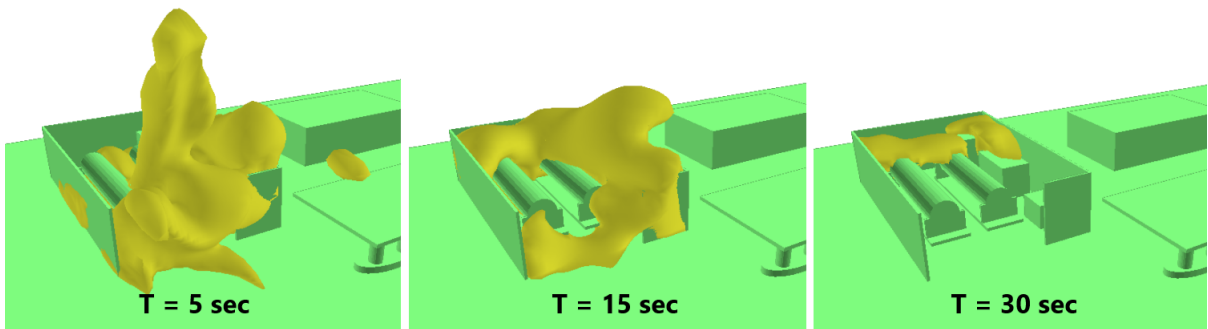


Figure 32: Surface plot of 4% H₂ concentration for 10 kg/s downward release

Figure 33 shows the cloud for different release directions, all for 1 kg/s releases. Figure 34 shows a vertical concentration plot of the 1 kg/s downward release, and figure 35 shows the temperature contours of the same release. Figure 36 shows the 1 kg/s jet hitting the ground and spreading.

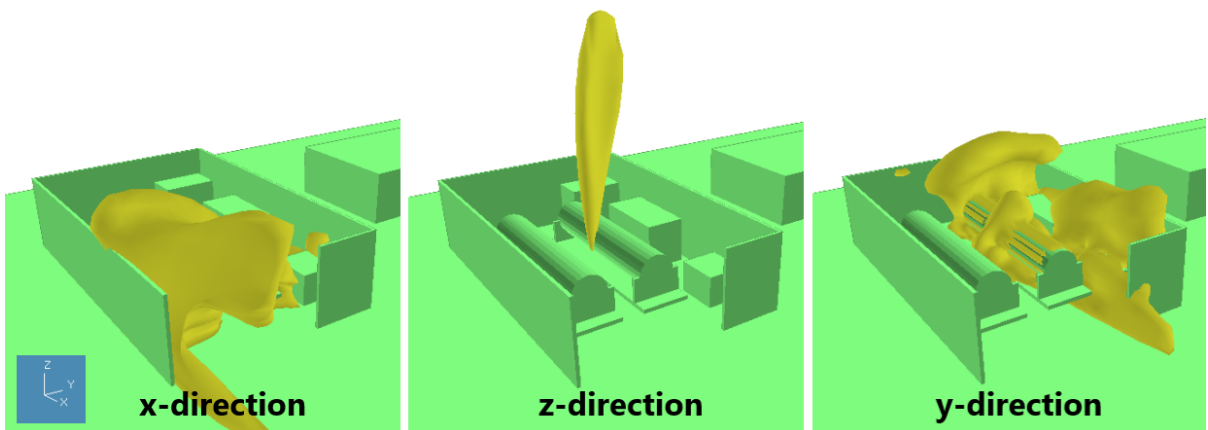


Figure 33: Surface plot of 4% H₂ concentration for 1 kg/s releases at 15 seconds

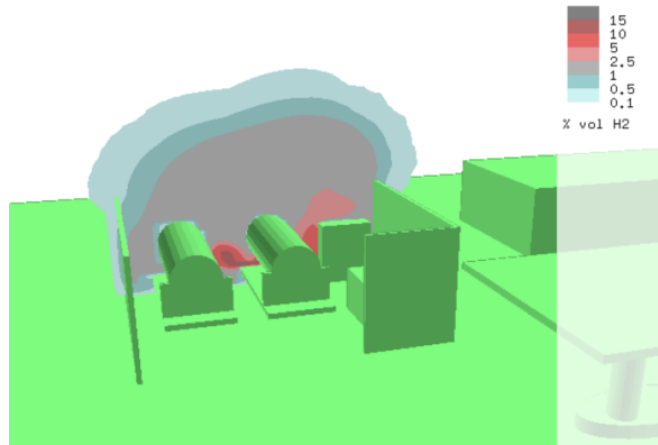


Figure 34: X-plane plot of H₂ concentration for 1 kg/s downward release at 20 seconds

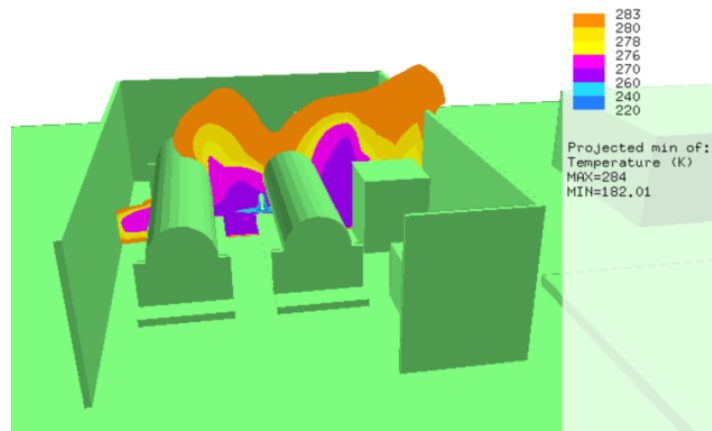


Figure 35: X-plane plot of temperature for 1 kg/s downward release at 20 seconds

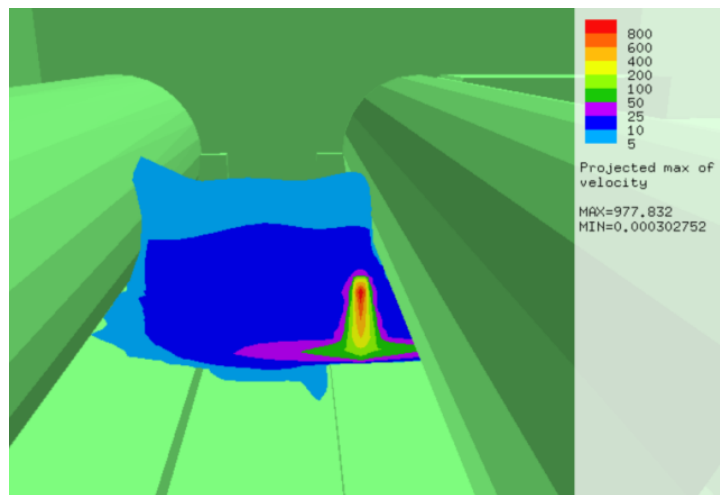


Figure 36: X-plane plot of velocity for 1 kg/s downward release at 3 seconds

Figure 37 and 38 show surface plots of 1% volumetric concentration. This is to analyze the effect of the detectors, which has their minimum trigger level at 1% H₂ concentration.

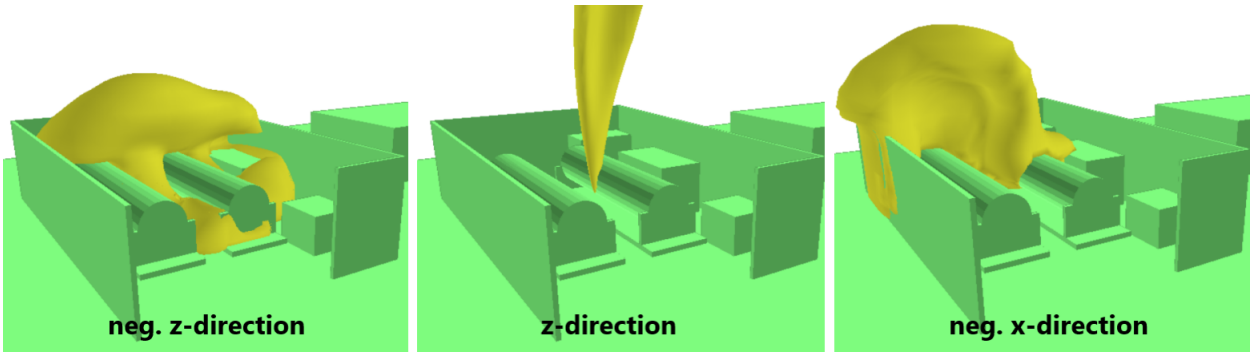


Figure 37: Surface plot of 1% H₂ concentration for 0.1 kg/s releases at 20 seconds

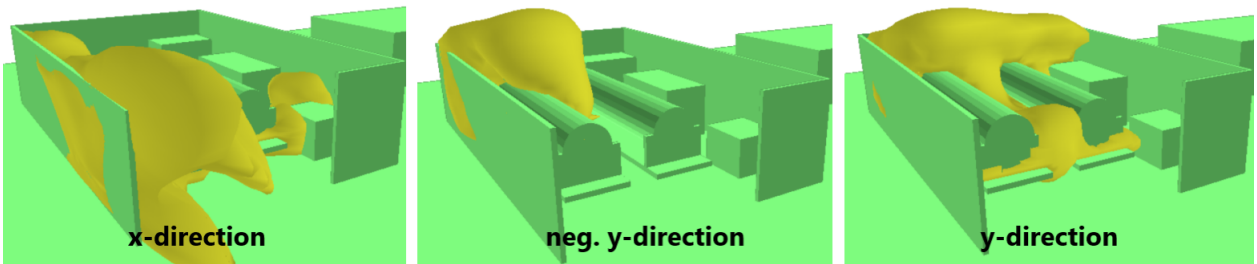


Figure 38: Surface plot of 1% H₂ concentration for 0.1 kg/s releases at 20 seconds

4.2.2 Non-ATEX equipment

The average ignition probabilities based on leak rate for the non-ATEX equipment and car area, including total, continuous and discrete probabilities, are shown in table 17. These sources' parameters are kept constant throughout the simulations, and therefore see no change when different models are used.

Detection	kg/s	$P_{T,IP44}$	$P_{C,IP44}$	$P_{D,IP44}$	$P_{T,IP64}$	$P_{C,IP64}$	$P_{D,IP64}$	$P_{D,Car}$
Off	0.1	$1.6 \cdot 10^{-2}$	$6.8 \cdot 10^{-3}$	$7.4 \cdot 10^{-3}$	$2.4 \cdot 10^{-3}$	$6.8 \cdot 10^{-5}$	$7.4 \cdot 10^{-7}$	0
	1	$1.1 \cdot 10^{-1}$	$8.0 \cdot 10^{-2}$	$3.2 \cdot 10^{-2}$	$3.2 \cdot 10^{-3}$	$8.4 \cdot 10^{-4}$	$3.3 \cdot 10^{-6}$	$2.2 \cdot 10^{-3}$
	10	$8.0 \cdot 10^{-2}$	$6.7 \cdot 10^{-2}$	$1.1 \cdot 10^{-2}$	$3.0 \cdot 10^{-3}$	$7.1 \cdot 10^{-4}$	$1.1 \cdot 10^{-6}$	$3.3 \cdot 10^{-3}$
On	0.1	$1.7 \cdot 10^{-2}$	$7.2 \cdot 10^{-3}$	$7.4 \cdot 10^{-3}$	$2.4 \cdot 10^{-3}$	$7.3 \cdot 10^{-5}$	$7.5 \cdot 10^{-7}$	0
	1	$1.2 \cdot 10^{-1}$	$8.4 \cdot 10^{-2}$	$3.3 \cdot 10^{-2}$	$3.2 \cdot 10^{-3}$	$8.8 \cdot 10^{-4}$	$3.4 \cdot 10^{-6}$	$2.2 \cdot 10^{-3}$
	10	$8.2 \cdot 10^{-2}$	$6.9 \cdot 10^{-2}$	$1.2 \cdot 10^{-2}$	$3.1 \cdot 10^{-3}$	$7.3 \cdot 10^{-4}$	$1.2 \cdot 10^{-6}$	$3.3 \cdot 10^{-3}$

Table 17: Ignition probability results constant for all models

4.2.3 Standard MISOF model

Table 18 shows the contribution from electrical equipment, rotating equipment and other equipment in the standard MISOF model.

Det.	kg/s	$P_{T,el}$	$P_{C,el}$	$P_{D,el}$	$P_{T,rot}$	$P_{C,rot}$	$P_{D,rot}$	$P_{T,other}$	$P_{C,other}$	$P_{D,other}$
Off	0.1	$9.9 \cdot 10^{-5}$	$5.3 \cdot 10^{-5}$	$4.6 \cdot 10^{-5}$	$1.3 \cdot 10^{-4}$	$1.2 \cdot 10^{-4}$	$6.1 \cdot 10^{-6}$	$1.7 \cdot 10^{-4}$	$1.7 \cdot 10^{-4}$	0
	1	$3.3 \cdot 10^{-4}$	$2.3 \cdot 10^{-4}$	$9.5 \cdot 10^{-5}$	$6.5 \cdot 10^{-4}$	$6.4 \cdot 10^{-4}$	$1.3 \cdot 10^{-5}$	$1.1 \cdot 10^{-3}$	$1.1 \cdot 10^{-3}$	0
	10	$2.8 \cdot 10^{-4}$	$2.1 \cdot 10^{-4}$	$7.5 \cdot 10^{-5}$	$6.2 \cdot 10^{-4}$	$6.1 \cdot 10^{-4}$	$1.0 \cdot 10^{-5}$	$1.2 \cdot 10^{-3}$	$1.2 \cdot 10^{-3}$	0
On	0.1	$9.7 \cdot 10^{-5}$	$5.6 \cdot 10^{-5}$	$4.1 \cdot 10^{-5}$	$1.5 \cdot 10^{-4}$	$1.4 \cdot 10^{-4}$	$5.4 \cdot 10^{-6}$	$2.4 \cdot 10^{-4}$	$2.4 \cdot 10^{-4}$	$6.9 \cdot 10^{-7}$
	1	$3.5 \cdot 10^{-4}$	$2.4 \cdot 10^{-4}$	$1.0 \cdot 10^{-4}$	$7.2 \cdot 10^{-4}$	$7.0 \cdot 10^{-4}$	$1.4 \cdot 10^{-5}$	$1.4 \cdot 10^{-3}$	$1.4 \cdot 10^{-3}$	$3.8 \cdot 10^{-6}$
	10	$3.2 \cdot 10^{-4}$	$2.1 \cdot 10^{-4}$	$1.1 \cdot 10^{-4}$	$6.5 \cdot 10^{-4}$	$6.4 \cdot 10^{-4}$	$1.4 \cdot 10^{-5}$	$1.3 \cdot 10^{-3}$	$1.3 \cdot 10^{-3}$	$1.2 \cdot 10^{-5}$

Table 18: Ignition probability results for electrical, rotating and other equipment

For the sake of comparison, all non-ATEX sources and the car area are turned off to better visualize the total contribution from the electrical, rotating and other equipment in table 18. These results are shown in table 19.

Detection	kg/s	P_T	P_C	P_D
Off	0.1	$2.3 \cdot 10^{-3}$	$3.5 \cdot 10^{-4}$	$5.2 \cdot 10^{-5}$
	1	$4.5 \cdot 10^{-3}$	$2.0 \cdot 10^{-3}$	$1.1 \cdot 10^{-4}$
	10	$4.5 \cdot 10^{-3}$	$2.0 \cdot 10^{-3}$	$8.5 \cdot 10^{-5}$
On	0.1	$2.8 \cdot 10^{-3}$	$4.4 \cdot 10^{-4}$	$4.7 \cdot 10^{-5}$
	1	$4.8 \cdot 10^{-3}$	$2.3 \cdot 10^{-3}$	$1.2 \cdot 10^{-4}$
	10	$4.6 \cdot 10^{-3}$	$2.2 \cdot 10^{-3}$	$1.4 \cdot 10^{-4}$

Table 19: Total ignition probability contribution from the sources in table 18

The total, continuous and discrete ignition probabilities for the standard MISOF model are shown in table 20. The probabilities get their contributions from the sources in table 17 and 18. The same results with its contributions are shown graphically with HyRAM's results in figure 39. Note that the plot is made using the data without detectors. The data with and without detection lies so close it is meaningless to include plots. The effect of the detectors are discussed in section 6.2.2.

Detect.	With \leq IP44 equipment				Detect	With \leq IP44 equipment		
	kg/s	P_T	P_C	P_D		P_T	P_C	P_D
Off	0.1	$1.7 \cdot 10^{-2}$	$7.1 \cdot 10^{-3}$	$7.4 \cdot 10^{-3}$	On	$1.7 \cdot 10^{-2}$	$7.6 \cdot 10^{-3}$	$7.4 \cdot 10^{-3}$
	1	$1.2 \cdot 10^{-1}$	$8.2 \cdot 10^{-2}$	$3.4 \cdot 10^{-2}$		$1.2 \cdot 10^{-1}$	$8.6 \cdot 10^{-2}$	$3.5 \cdot 10^{-2}$
	10	$8.4 \cdot 10^{-2}$	$6.9 \cdot 10^{-2}$	$1.5 \cdot 10^{-2}$		$8.7 \cdot 10^{-2}$	$7.1 \cdot 10^{-2}$	$1.5 \cdot 10^{-2}$
Detect.	With \geq IP64 equipment				Detect.	With \geq IP64 equipment		
	kg/s	P_T	P_C	P_D		P_T	P_C	P_D
Off	0.1	$2.8 \cdot 10^{-3}$	$4.2 \cdot 10^{-4}$	$5.3 \cdot 10^{-5}$	On	$2.9 \cdot 10^{-3}$	$5.1 \cdot 10^{-4}$	$4.8 \cdot 10^{-5}$
	1	$7.5 \cdot 10^{-3}$	$2.9 \cdot 10^{-3}$	$2.3 \cdot 10^{-3}$		$7.8 \cdot 10^{-3}$	$3.2 \cdot 10^{-3}$	$2.3 \cdot 10^{-3}$
	10	$8.5 \cdot 10^{-3}$	$2.8 \cdot 10^{-3}$	$3.4 \cdot 10^{-3}$		$8.7 \cdot 10^{-3}$	$2.9 \cdot 10^{-3}$	$3.5 \cdot 10^{-3}$

Table 20: Total ignition probability results for the standard MISOF model

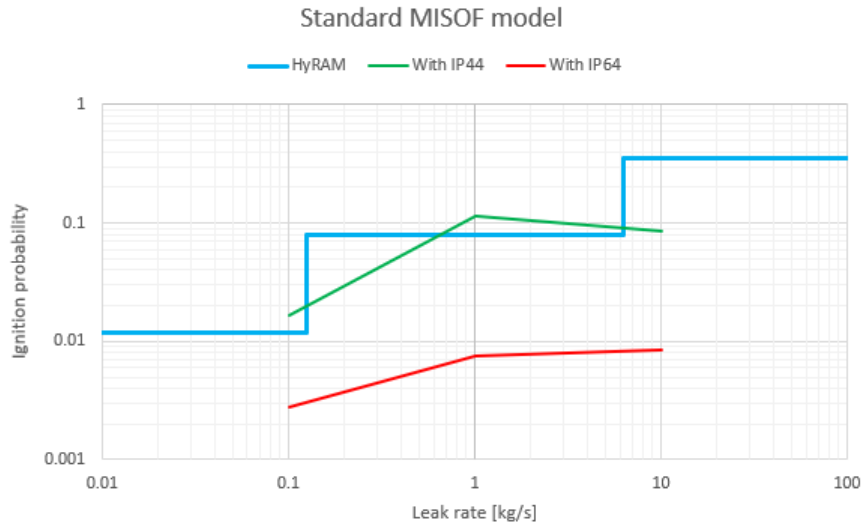


Figure 39: Total ignition probability for the standard MISOF model

Figure 40 shows the ignition probabilities in terms of release direction for 1 kg/s releases with IP44 equipment.

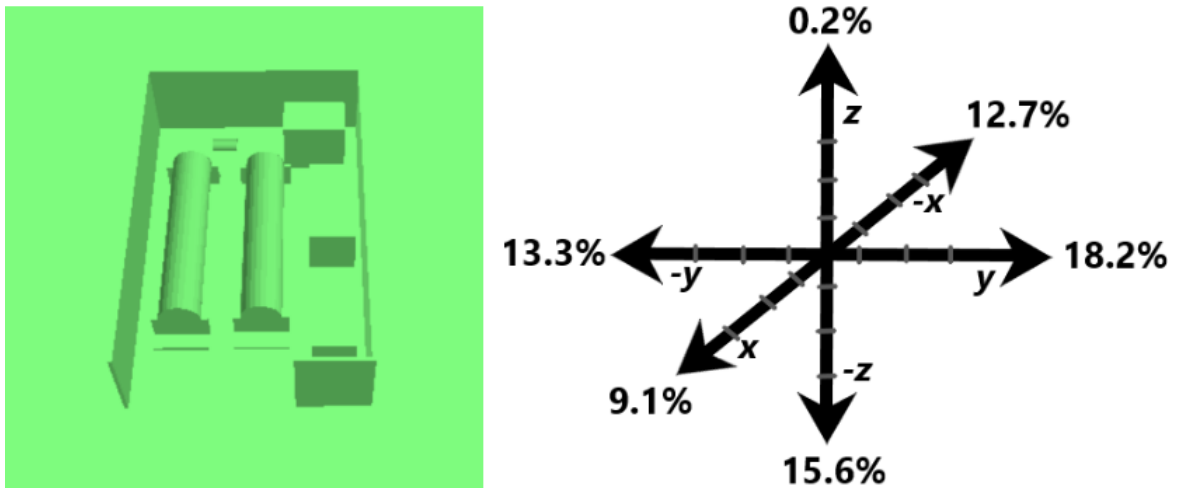


Figure 40: Ignition probabilities for 1 kg/s release in different directions

4.2.4 Offshore MISOF model

The volumetric ignition source in the offshore MISOF model has only one component, thus it is not divided into electrical, rotating and other like the standard MISOF model. The probability of this total, volumetric source is shown in table 21.

Detection	kg/s	P_T	P_C	P_D
Off	0.1	$2.5 \cdot 10^{-4}$	$1.9 \cdot 10^{-4}$	$5.2 \cdot 10^{-5}$
	1	$1.1 \cdot 10^{-3}$	$1.0 \cdot 10^{-3}$	$1.0 \cdot 10^{-4}$
	10	$1.0 \cdot 10^{-3}$	$9.6 \cdot 10^{-4}$	$8.6 \cdot 10^{-5}$
On	0.1	$2.6 \cdot 10^{-4}$	$2.1 \cdot 10^{-4}$	$4.7 \cdot 10^{-5}$
	1	$1.2 \cdot 10^{-3}$	$1.1 \cdot 10^{-3}$	$1.2 \cdot 10^{-4}$
	10	$1.1 \cdot 10^{-3}$	$9.8 \cdot 10^{-4}$	$1.4 \cdot 10^{-4}$

Table 21: Ignition probability contribution from the volumetric source

The total, continuous and discrete ignition probabilities for the offshore MISOF model are shown in table 22. The probabilities get their contributions from the sources in table 17 and 21. The offshore MISOF results are plotted with HyRAM in figure 41. Note that the obtained ignition probabilities are very close to the results of the standard MISOF model above.

Detect.	With \leq IP44 equipment				Detect.	With \leq IP44 equipment		
	kg/s	P_T	P_C	P_D		P_T	P_C	P_D
Off	0.1	$1.7 \cdot 10^{-2}$	$7.0 \cdot 10^{-3}$	$7.4 \cdot 10^{-3}$	On	$1.7 \cdot 10^{-2}$	$7.4 \cdot 10^{-3}$	$7.4 \cdot 10^{-3}$
	1	$1.1 \cdot 10^{-1}$	$8.2 \cdot 10^{-2}$	$3.4 \cdot 10^{-2}$		$1.2 \cdot 10^{-1}$	$8.5 \cdot 10^{-2}$	$3.5 \cdot 10^{-2}$
	10	$8.3 \cdot 10^{-2}$	$6.8 \cdot 10^{-2}$	$1.5 \cdot 10^{-2}$		$8.6 \cdot 10^{-2}$	$7.0 \cdot 10^{-2}$	$1.5 \cdot 10^{-2}$
Detect.	With \geq IP64 equipment				Detect.	With \geq IP64 equipment		
	kg/s	P_T	P_C	P_D		P_T	P_C	P_D
Off	0.1	$2.7 \cdot 10^{-3}$	$2.6 \cdot 10^{-4}$	$5.3 \cdot 10^{-5}$	On	$2.7 \cdot 10^{-3}$	$2.8 \cdot 10^{-4}$	$4.8 \cdot 10^{-5}$
	1	$6.5 \cdot 10^{-3}$	$1.9 \cdot 10^{-3}$	$2.3 \cdot 10^{-3}$		$6.6 \cdot 10^{-3}$	$2.0 \cdot 10^{-3}$	$2.3 \cdot 10^{-3}$
	10	$7.4 \cdot 10^{-3}$	$1.7 \cdot 10^{-3}$	$3.4 \cdot 10^{-3}$		$7.5 \cdot 10^{-3}$	$1.7 \cdot 10^{-3}$	$3.5 \cdot 10^{-3}$

Table 22: Total ignition probability results for the offshore MISOF model

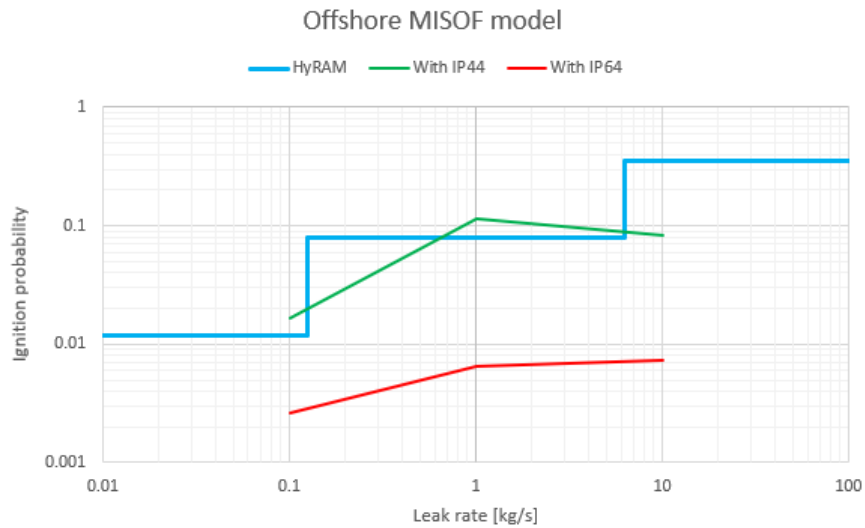


Figure 41: Total ignition probability for the offshore MISOF model

4.2.5 Onshore MISOF model

The onshore MISOF model only differs from the offshore MISOF model in p_{iso} . Therefore, the results with no detection using either onshore or offshore MISOF are identical, and are presented in the previous table. The results with detection from the onshore MISOF model are presented in table 23, 24 and figure 42.

Detection	kg/s	P_T	P_C	P_D
On	0.1	$2.8 \cdot 10^{-4}$	$2.2 \cdot 10^{-4}$	$6.0 \cdot 10^{-5}$
	1	$1.3 \cdot 10^{-3}$	$1.1 \cdot 10^{-3}$	$1.5 \cdot 10^{-4}$
	10	$1.1 \cdot 10^{-3}$	$9.8 \cdot 10^{-4}$	$1.4 \cdot 10^{-4}$

Table 23: Ignition probability contribution from the volumetric source

Detect.	With \leq IP44 equipment			
	kg/s	P_T	P_C	P_D
On	0.1	$1.7 \cdot 10^{-2}$	$7.4 \cdot 10^{-3}$	$7.4 \cdot 10^{-3}$
	1	$1.2 \cdot 10^{-1}$	$8.5 \cdot 10^{-2}$	$3.5 \cdot 10^{-2}$
	10	$8.6 \cdot 10^{-2}$	$6.7 \cdot 10^{-2}$	$1.5 \cdot 10^{-2}$
Detect.	With \geq IP64 equipment			
	kg/s	P_T	P_C	P_D
On	0.1	$2.7 \cdot 10^{-3}$	$2.9 \cdot 10^{-4}$	$6.1 \cdot 10^{-5}$
	1	$6.6 \cdot 10^{-3}$	$2.0 \cdot 10^{-3}$	$2.3 \cdot 10^{-3}$
	10	$7.5 \cdot 10^{-3}$	$1.7 \cdot 10^{-3}$	$3.5 \cdot 10^{-3}$

Table 24: Total ignition probability results for the onshore MISOF model

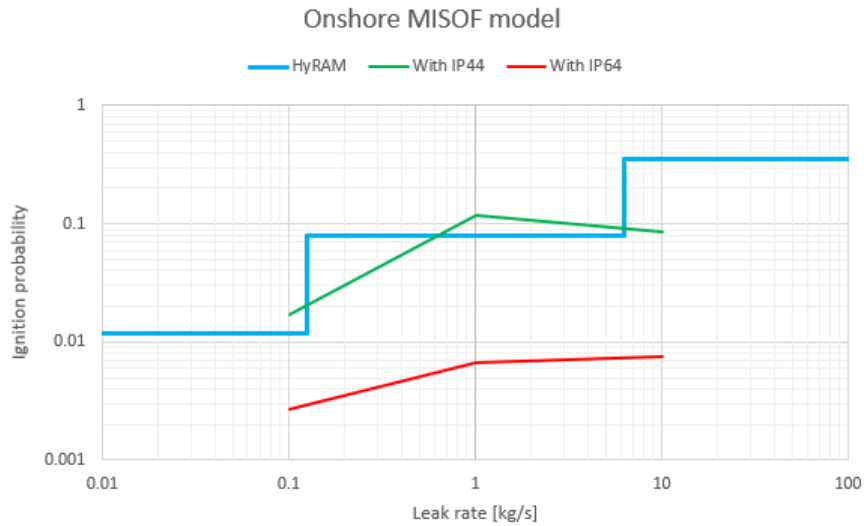


Figure 42: Total ignition probability for the onshore MISOF model

4.2.6 SAFEN₁₀ model

The volumetric ignition source in the two following SAFEN models also have only one component. The results from the SAFEN₁₀ model are presented in table 25, 26 and figure 43.

Detection	kg/s	P_T	P_C	P_D
Off	0.1	$2.4 \cdot 10^{-3}$	$1.7 \cdot 10^{-3}$	$5.2 \cdot 10^{-4}$
	1	$1.1 \cdot 10^{-2}$	$1.0 \cdot 10^{-2}$	$1.0 \cdot 10^{-3}$
	10	$1.0 \cdot 10^{-2}$	$9.6 \cdot 10^{-3}$	$8.6 \cdot 10^{-4}$
On	0.1	$2.5 \cdot 10^{-3}$	$2.0 \cdot 10^{-3}$	$4.7 \cdot 10^{-4}$
	1	$1.2 \cdot 10^{-2}$	$1.1 \cdot 10^{-2}$	$1.2 \cdot 10^{-3}$
	10	$1.1 \cdot 10^{-2}$	$9.8 \cdot 10^{-3}$	$1.4 \cdot 10^{-3}$

Table 25: Ignition probability contribution from the volumetric source

Detect.	With \leq IP44 equipment				Detect.	With \leq IP44 equipment		
	kg/s	P_T	P_C	P_D		P_T	P_C	P_D
Off	0.1	$1.7 \cdot 10^{-2}$	$8.6 \cdot 10^{-3}$	$7.7 \cdot 10^{-3}$	On	$1.9 \cdot 10^{-2}$	$9.2 \cdot 10^{-3}$	$7.8 \cdot 10^{-3}$
	1	$1.2 \cdot 10^{-1}$	$9.0 \cdot 10^{-2}$	$3.5 \cdot 10^{-2}$		$1.3 \cdot 10^{-1}$	$9.3 \cdot 10^{-2}$	$3.6 \cdot 10^{-2}$
	10	$9.2 \cdot 10^{-2}$	$7.6 \cdot 10^{-2}$	$1.5 \cdot 10^{-2}$		$9.4 \cdot 10^{-2}$	$7.8 \cdot 10^{-2}$	$1.6 \cdot 10^{-2}$
Detect.	With \geq IP64 equipment				Detect.	With \geq IP64 equipment		
	kg/s	P_T	P_C	P_D		P_T	P_C	P_D
Off	0.1	$4.8 \cdot 10^{-3}$	$2.0 \cdot 10^{-3}$	$5.2 \cdot 10^{-4}$	On	$4.9 \cdot 10^{-3}$	$2.1 \cdot 10^{-3}$	$4.7 \cdot 10^{-4}$
	1	$1.7 \cdot 10^{-2}$	$1.1 \cdot 10^{-2}$	$3.2 \cdot 10^{-3}$		$1.7 \cdot 10^{-2}$	$1.2 \cdot 10^{-2}$	$3.4 \cdot 10^{-3}$
	10	$1.7 \cdot 10^{-2}$	$1.0 \cdot 10^{-2}$	$4.2 \cdot 10^{-3}$		$1.7 \cdot 10^{-2}$	$1.0 \cdot 10^{-2}$	$4.7 \cdot 10^{-3}$

Table 26: Total ignition probability results for the SAFEN₁₀ model

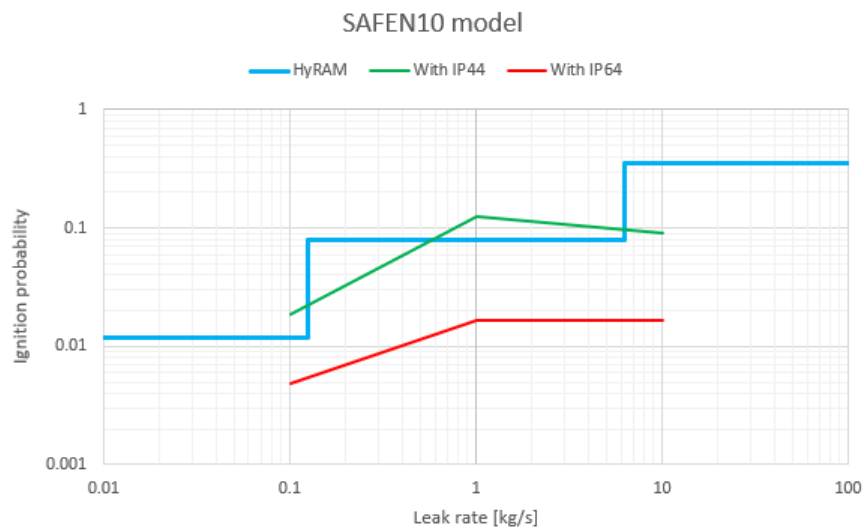


Figure 43: Total ignition probability for the SAFEN₁₀ model

4.2.7 SAFEN₁₀₀ model

The results from the SAFEN₁₀₀ model are presented in table 27, 28 and figure 44. The only difference compared to SAFEN₁₀ is that the lambdas are ten times higher, as seen in table 15.

Detection	kg/s	P_T	P_C	P_D
Off	0.1	$2.3 \cdot 10^{-2}$	$1.8 \cdot 10^{-2}$	$5.2 \cdot 10^{-3}$
	1	$1.1 \cdot 10^{-1}$	$9.6 \cdot 10^{-2}$	$1.0 \cdot 10^{-2}$
	10	$9.8 \cdot 10^{-2}$	$9.0 \cdot 10^{-2}$	$8.5 \cdot 10^{-3}$
On	0.1	$2.5 \cdot 10^{-2}$	$2.0 \cdot 10^{-2}$	$4.7 \cdot 10^{-3}$
	1	$1.1 \cdot 10^{-1}$	$1.0 \cdot 10^{-1}$	$1.2 \cdot 10^{-2}$
	10	$1.0 \cdot 10^{-1}$	$9.1 \cdot 10^{-2}$	$1.3 \cdot 10^{-2}$

Table 27: Ignition probability contribution from the volumetric source

Detect.	With \leq IP44 equipment				Detect.	With \leq IP44 equipment		
	kg/s	P_T	P_C	P_D		P_T	P_C	P_D
Off	0.1	$3.9 \cdot 10^{-2}$	$2.5 \cdot 10^{-2}$	$1.2 \cdot 10^{-2}$	On	$4.1 \cdot 10^{-2}$	$2.7 \cdot 10^{-2}$	$1.2 \cdot 10^{-2}$
	1	$2.0 \cdot 10^{-1}$	$1.7 \cdot 10^{-1}$	$4.5 \cdot 10^{-2}$		$2.1 \cdot 10^{-1}$	$1.7 \cdot 10^{-1}$	$4.6 \cdot 10^{-2}$
	10	$1.7 \cdot 10^{-1}$	$1.5 \cdot 10^{-1}$	$2.3 \cdot 10^{-2}$		$1.8 \cdot 10^{-1}$	$1.5 \cdot 10^{-1}$	$2.8 \cdot 10^{-2}$
Detect.	With \geq IP64 equipment				Detect.	With \geq IP64 equipment		
	kg/s	P_T	P_C	P_D		P_T	P_C	P_D
Off	0.1	$2.6 \cdot 10^{-2}$	$1.8 \cdot 10^{-2}$	$5.2 \cdot 10^{-3}$	On	$2.7 \cdot 10^{-2}$	$2.0 \cdot 10^{-2}$	$4.7 \cdot 10^{-3}$
	1	$1.1 \cdot 10^{-1}$	$9.7 \cdot 10^{-2}$	$1.3 \cdot 10^{-2}$		$1.2 \cdot 10^{-1}$	$1.0 \cdot 10^{-1}$	$1.4 \cdot 10^{-2}$
	10	$1.0 \cdot 10^{-1}$	$9.0 \cdot 10^{-2}$	$1.2 \cdot 10^{-2}$		$1.1 \cdot 10^{-1}$	$9.2 \cdot 10^{-2}$	$1.7 \cdot 10^{-2}$

Table 28: Total ignition probability results for the SAFEN₁₀₀ model

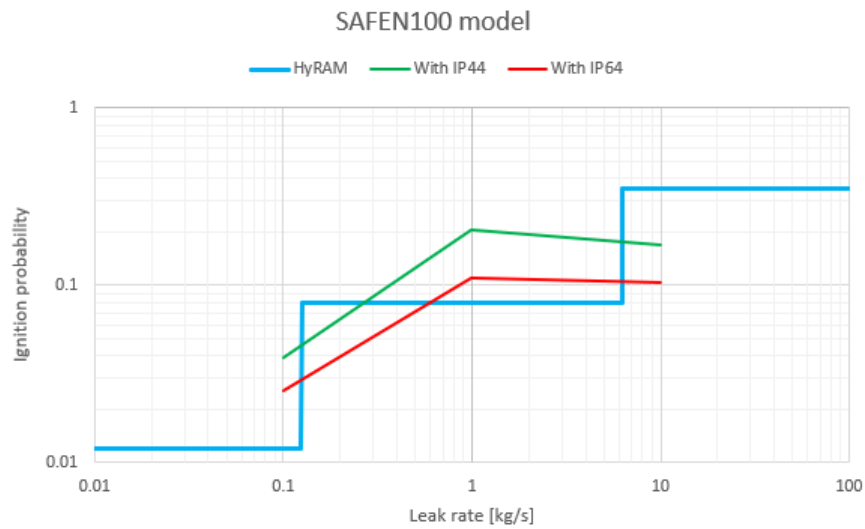


Figure 44: Total ignition probability for the SAFEN₁₀₀ model

4.2.8 Ignition probability summary

Leak rate [kg/s]	Without detection			With detection		
	0.1	1	10	0.1	1	10
Standard MISOF	$1.7 \cdot 10^{-2}$	$1.2 \cdot 10^{-1}$	$8.4 \cdot 10^{-2}$	$1.7 \cdot 10^{-2}$	$1.2 \cdot 10^{-1}$	$8.7 \cdot 10^{-2}$
Offshore MISOF	$1.7 \cdot 10^{-2}$	$1.1 \cdot 10^{-1}$	$8.3 \cdot 10^{-2}$	$1.7 \cdot 10^{-2}$	$1.2 \cdot 10^{-2}$	$8.6 \cdot 10^{-2}$
Onshore MISOF	Same as offshore			$1.7 \cdot 10^{-2}$	$1.2 \cdot 10^{-1}$	$8.6 \cdot 10^{-2}$
SAFEN ₁₀	$1.9 \cdot 10^{-2}$	$1.2 \cdot 10^{-2}$	$9.1 \cdot 10^{-2}$	$1.9 \cdot 10^{-2}$	$1.3 \cdot 10^{-1}$	$9.4 \cdot 10^{-2}$
SAFEN ₁₀₀	$3.9 \cdot 10^{-2}$	$2.0 \cdot 10^{-1}$	$1.7 \cdot 10^{-1}$	$4.1 \cdot 10^{-2}$	$2.1 \cdot 10^{-1}$	$1.8 \cdot 10^{-1}$

Table 29: Total ignition probability results for IP44 equipment summarized

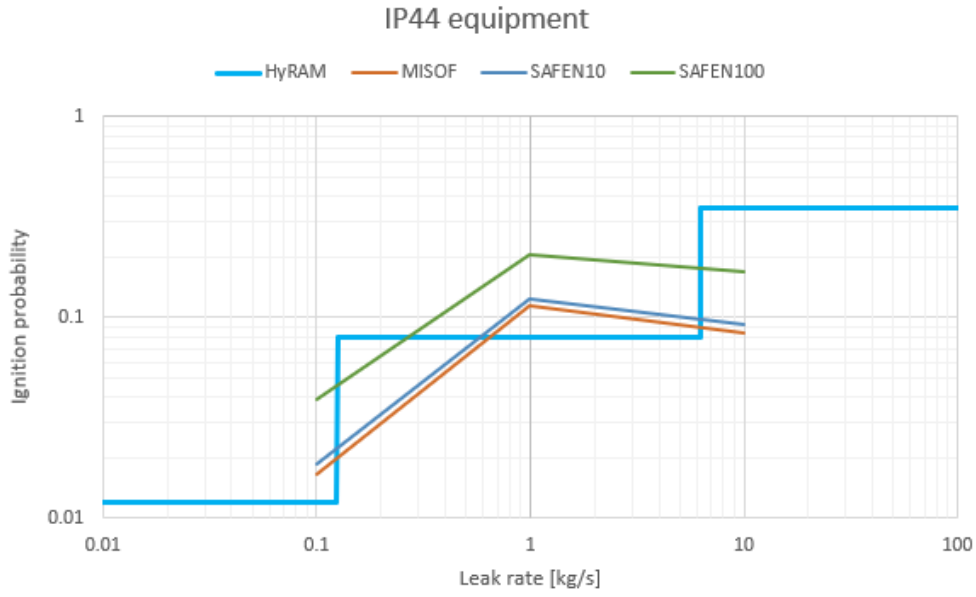


Figure 45: Plot of total ignition probability for the refueling station with IP44 equipment

Leak rate [kg/s]	Without detection			With detection		
	0.1	1	10	0.1	1	10
Standard MISOF	$2.8 \cdot 10^{-3}$	$7.5 \cdot 10^{-3}$	$8.5 \cdot 10^{-3}$	$2.9 \cdot 10^{-3}$	$7.8 \cdot 10^{-3}$	$8.7 \cdot 10^{-3}$
Offshore MISOF	$2.7 \cdot 10^{-3}$	$6.5 \cdot 10^{-3}$	$7.4 \cdot 10^{-3}$	$2.7 \cdot 10^{-3}$	$6.6 \cdot 10^{-3}$	$7.5 \cdot 10^{-3}$
Onshore MISOF	Same as offshore			$2.7 \cdot 10^{-3}$	$6.6 \cdot 10^{-3}$	$7.5 \cdot 10^{-3}$
SAFEN ₁₀	$4.8 \cdot 10^{-3}$	$1.7 \cdot 10^{-2}$	$1.7 \cdot 10^{-2}$	$4.9 \cdot 10^{-3}$	$1.7 \cdot 10^{-2}$	$1.7 \cdot 10^{-2}$
SAFEN ₁₀₀	$2.6 \cdot 10^{-2}$	$1.1 \cdot 10^{-1}$	$1.0 \cdot 10^{-1}$	$2.7 \cdot 10^{-2}$	$1.2 \cdot 10^{-1}$	$1.0 \cdot 10^{-1}$

Table 30: Total ignition probability results for IP64 equipment summarized

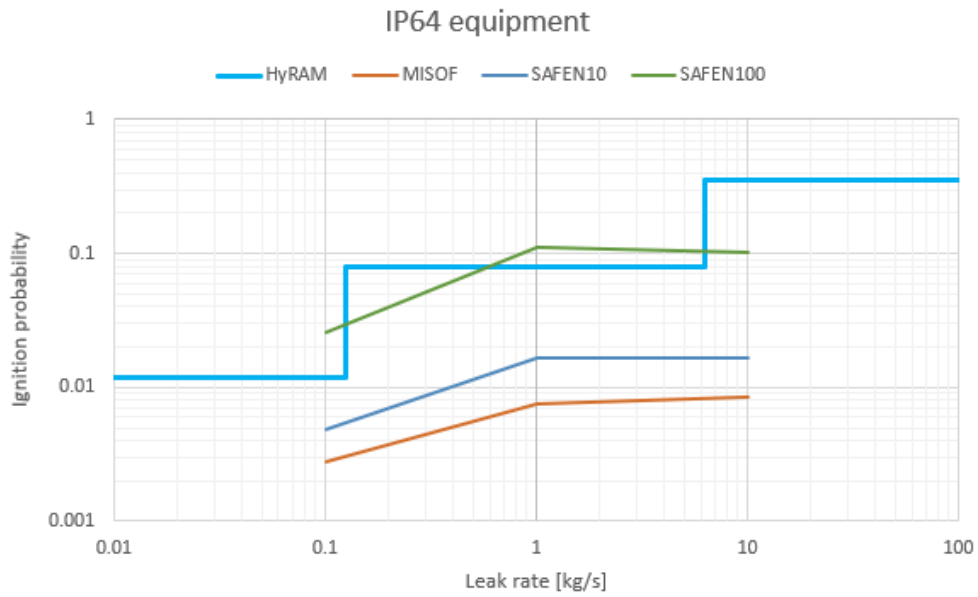


Figure 46: Plot of total ignition probability for the refueling station with IP64 equipment

4.2.9 Comparison with methane

The gas cloud dispersion for a 1 kg/s downward, CH₄ release is shown in figure 47. The surface plot is done at 4% volumetric concentration.

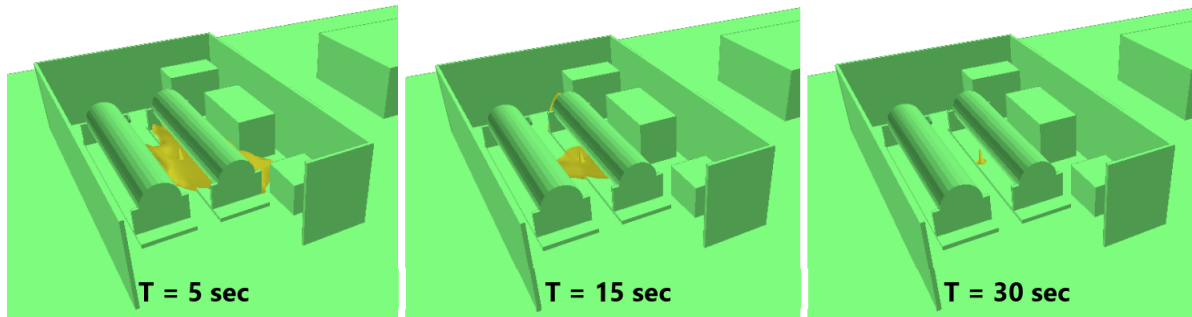


Figure 47: Surface plot of 4% CH₄ concentration for 1 kg/s downward release

Figure 48 shows the cloud volume within the flammable range for hydrogen and methane. Referring to section 2.1, the flammable range of hydrogen and methane is 4-75% and 5.4-17% respectively. Figure 49 shows the transient development of the ignition probability for the same cases. The ignition probabilities for different release directions are averaged based on leak rate and shown in table 31.

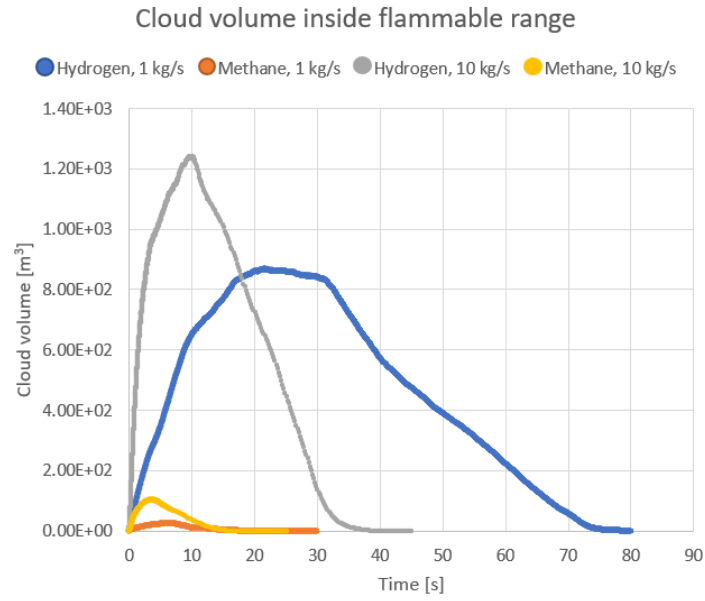


Figure 48: Transient flammable cloud volume for downward releases with methane and hydrogen

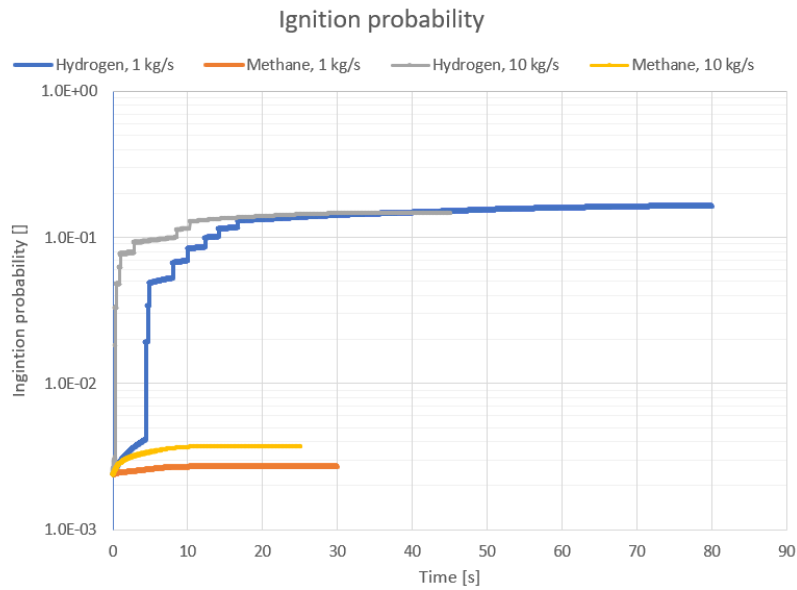


Figure 49: Transient ignition probability for downward releases with methane and hydrogen

Detection	kg/s	Hydrogen	Methane
On	1	$1.2 \cdot 10^{-1}$	$2.5 \cdot 10^{-3}$
	10	$8.7 \cdot 10^{-2}$	$1.5 \cdot 10^{-2}$

Table 31: Total ignition probability for hydrogen and methane with standard MISOF model and IP44 equipment

4.2.10 The final SAFEN parameters

The total ignition probabilities of the simulations with the final SAFEN parameters are shown in table 32.

Leak rate [kg/s]	<IP44	>IP64
1	$8.4 \cdot 10^{-1}$	$1.2 \cdot 10^{-1}$
10	$7.3 \cdot 10^{-1}$	$1.3 \cdot 10^{-1}$

Table 32: Total ignition probabilities in the final SAFEN model

4.2.11 Grid sensitivity

The results from the grid sensitivity using a 0.1, 1 and 10 kg/s initial leak rate are shown below. Figure 50 to 52 shows the volume of gas within the flammable range throughout the simulation.

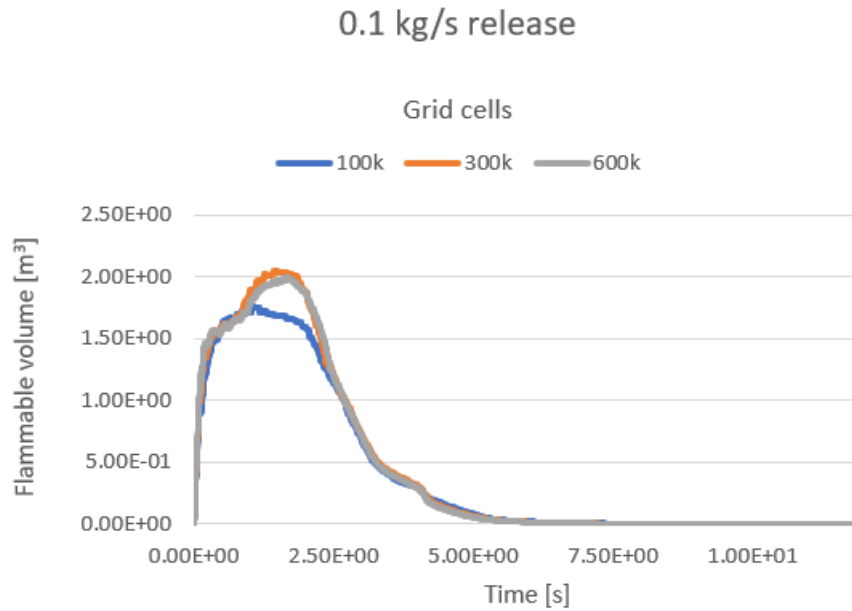


Figure 50: Grid sensitivity for 0.1 kg/s leak rate

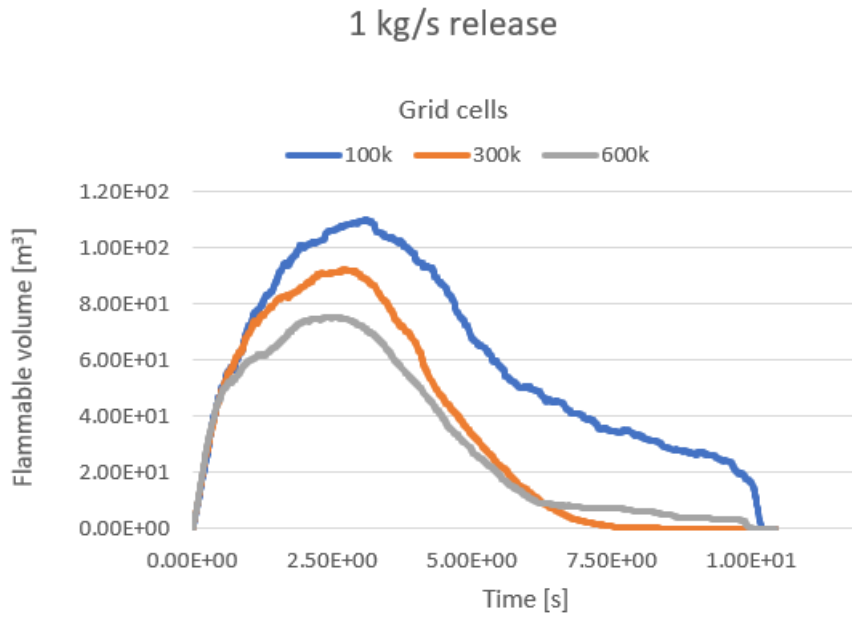


Figure 51: Grid sensitivity for 1 kg/s leak rate

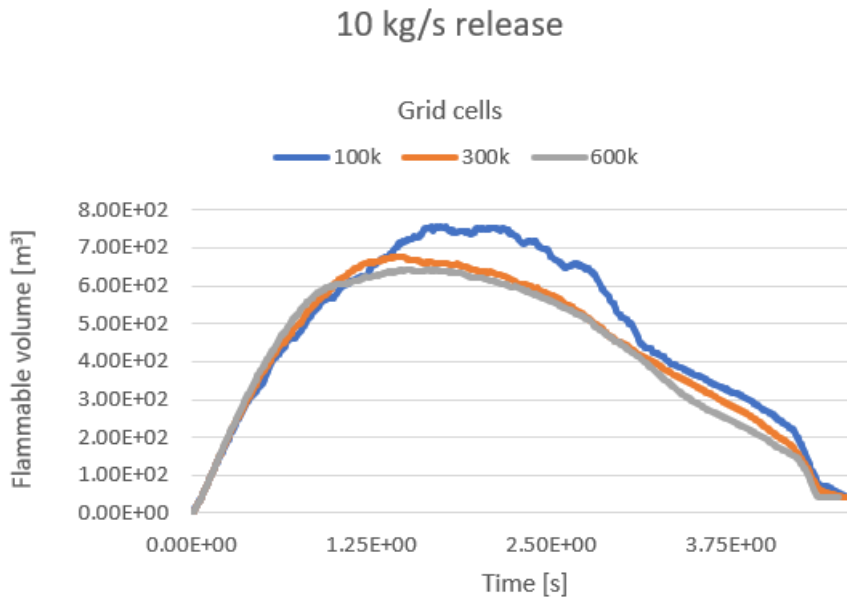


Figure 52: Grid sensitivity for 10 kg/s leak rate

The total, continuous and discrete ignition probability for the same grid sensitivities are shown in table 33 to 35.

Cells	100k	300k	600k
Total	$2.4 \cdot 10^{-3}$	$2.4 \cdot 10^{-3}$	$2.4 \cdot 10^{-3}$
Continuous	$2.2 \cdot 10^{-5}$	$3.7 \cdot 10^{-5}$	$5.2 \cdot 10^{-5}$
Discrete	$4.67 \cdot 10^{-8}$	$5.1 \cdot 10^{-8}$	$5.0 \cdot 10^{-8}$

Table 33: Grid sensitivity ignition probability for 0.1 kg/s release

Cells	100k	300k	600k
Total	$4.7 \cdot 10^{-2}$	$6.2 \cdot 10^{-2}$	$1.9 \cdot 10^{-2}$
Continuous	$4.4 \cdot 10^{-2}$	$5.8 \cdot 10^{-1}$	$1.6 \cdot 10^{-2}$
Discrete	$7.6 \cdot 10^{-3}$	$2.1 \cdot 10^{-3}$	$8.3 \cdot 10^{-3}$

Table 34: Grid sensitivity ignition probability for 1 kg/s release

Cells	100k	300k	600k
Total	$9.6 \cdot 10^{-2}$	$1.1 \cdot 10^{-1}$	$9.5 \cdot 10^{-2}$
Continuous	$8.8 \cdot 10^{-2}$	$1.0 \cdot 10^{-1}$	$8.7 \cdot 10^{-2}$
Discrete	$6.9 \cdot 10^{-3}$	$7.2 \cdot 10^{-3}$	$5.7 \cdot 10^{-3}$

Table 35: Grid sensitivity ignition probability for 10 kg/s release

4.3 The container storage

4.3.1 Gas dispersion

The release profiles for the container storage releases are identical to the ones in figure 28, 30 and 32. The gas cloud for the downward releases at some time steps is shown in figure 53, 54 and 55. The container roof is removed for visual inspection.

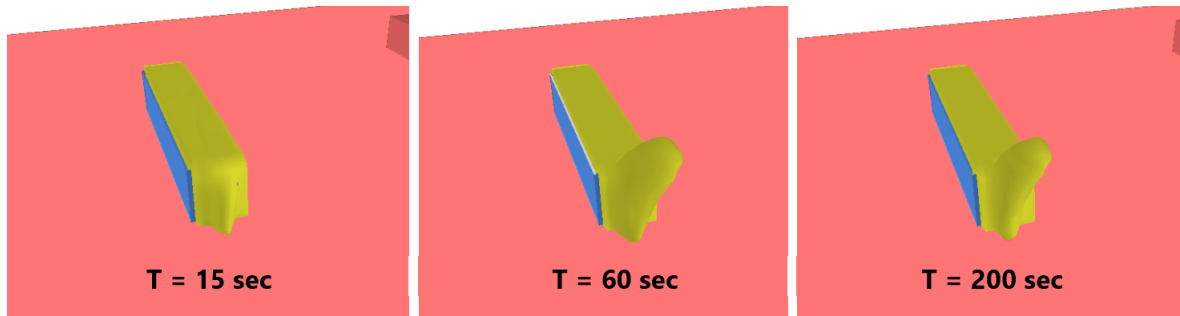


Figure 53: Surface plot of 4% H_2 concentration for 0.1 kg/s downward release

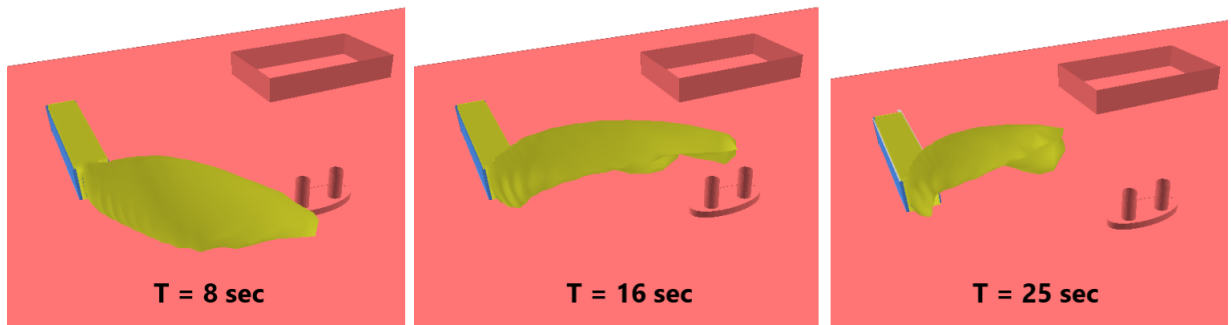


Figure 54: Surface plot of 4% H_2 concentration for 1 kg/s downward release

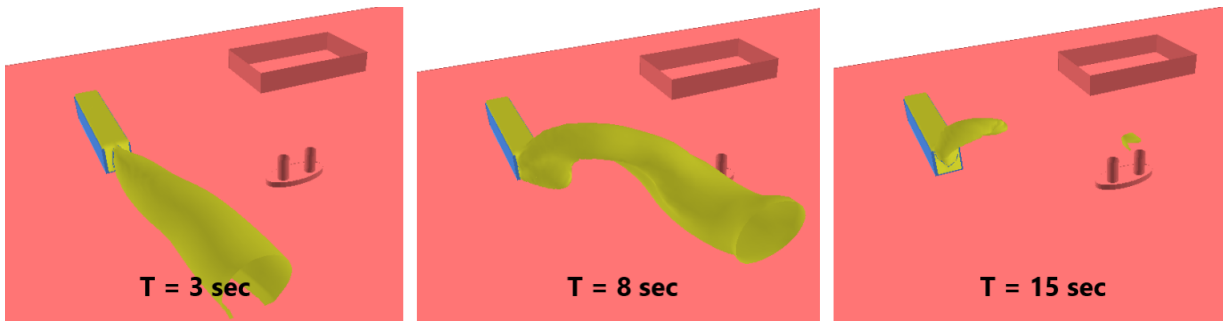


Figure 55: Surface plot of 4% H₂ concentration for 10 kg/s downward release

A comparison between the release directions for 1 kg/s releases is shown in figure 56. The only direction which differs from the others is the x-direction, where gas is blasted straight out the slit in the door of the container. The gas concentration inside the container is shown in figure 59. Figure 58 shows the flammable cloud volume for different downward releases. Figure 57 shows a velocity distribution inside the container for a 0.1 kg/s and 10 kg/s downward release at 3 seconds.

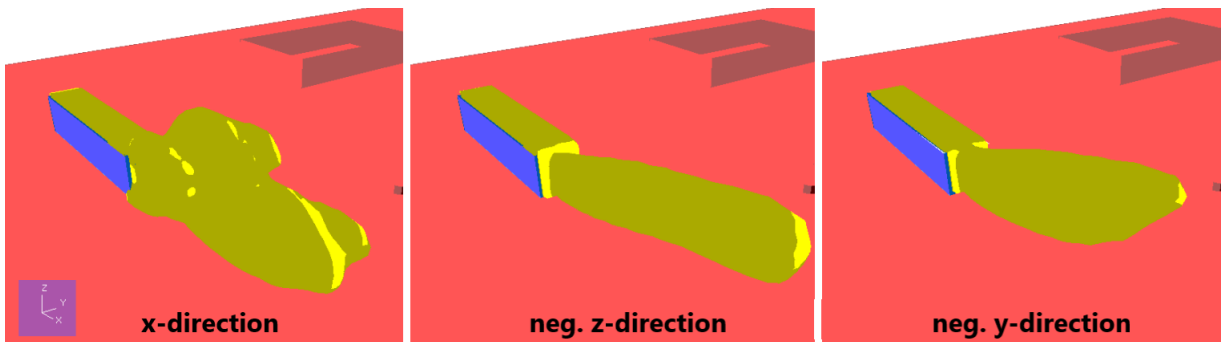


Figure 56: Surface plot of 4% H₂ concentration for 1 kg/s releases at 5 seconds

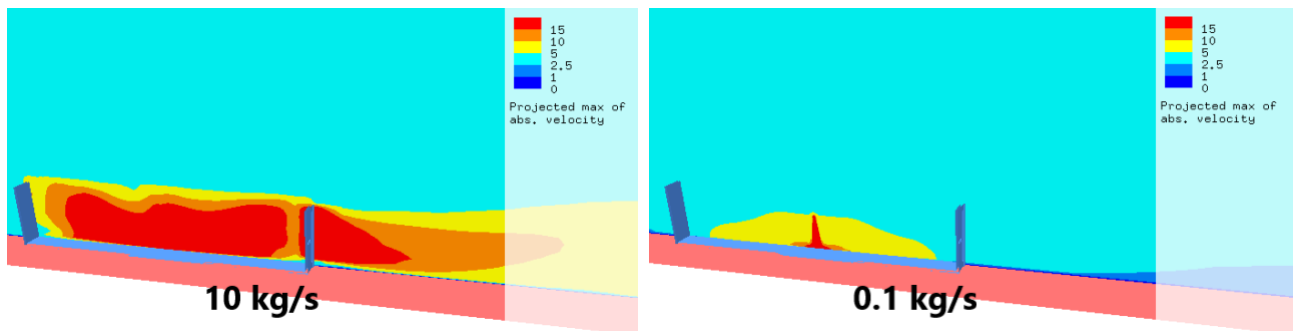


Figure 57: Absolute velocity inside the container for downward releases at 3 seconds

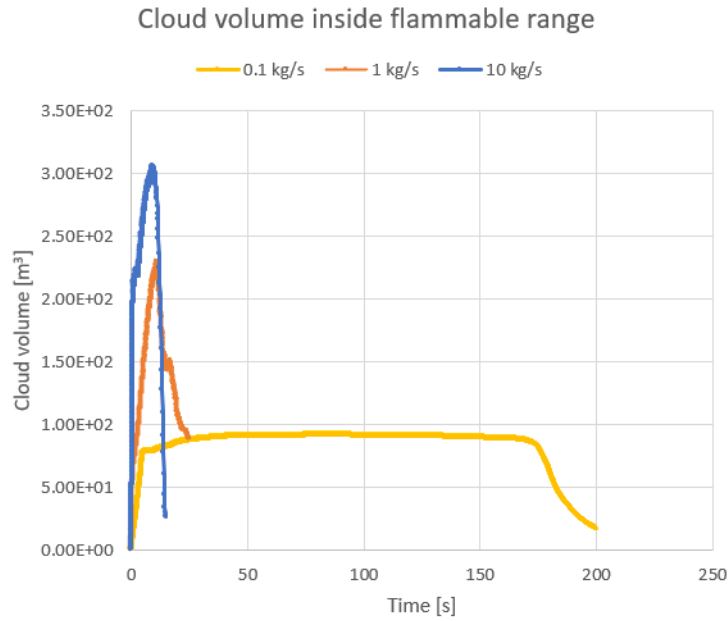


Figure 58: Transient volume of flammable cloud for downward releases

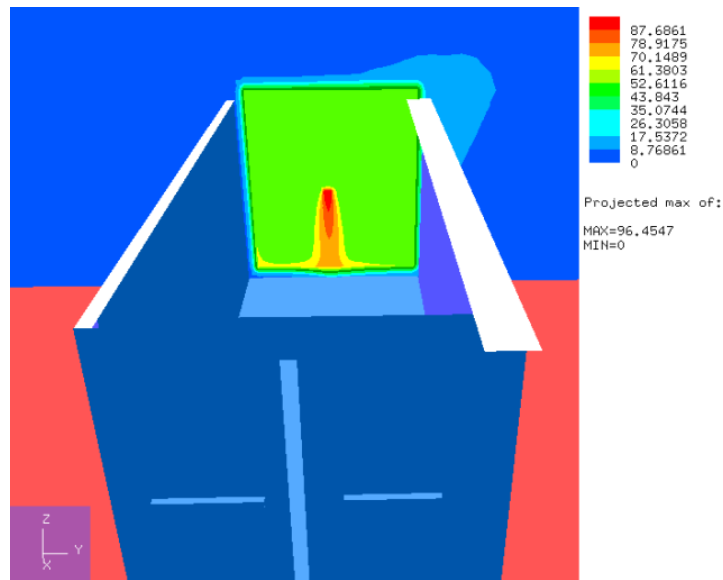


Figure 59: Concentration of H₂ inside the container

4.3.2 Ignition probability

The contribution from non-ATEX equipment is shown in table 36. The total ignition probabilities for the standard MISOF model is tabulated in table 37. Other tables similar to those in section 4.2 are found in appendix A.

Detection	kg/s	$P_{T,IP44}$	$P_{C,IP44}$	$P_{D,IP44}$	$P_{T,IP64}$	$P_{C,IP64}$	$P_{D,IP64}$	$P_{D,Car}$
On	0.1	$3.5 \cdot 10^{-1}$	$1.3 \cdot 10^{-1}$	$2.6 \cdot 10^{-1}$	$3.9 \cdot 10^{-3}$	$1.5 \cdot 10^{-3}$	$3.2 \cdot 10^{-5}$	0
	1	$1.6 \cdot 10^{-1}$	$1.4 \cdot 10^{-1}$	$2.5 \cdot 10^{-2}$	$1.4 \cdot 10^{-2}$	$1.5 \cdot 10^{-3}$	$1.0 \cdot 10^{-2}$	$1.0 \cdot 10^{-2}$
	10	$1.2 \cdot 10^{-1}$	$1.1 \cdot 10^{-1}$	$2.5 \cdot 10^{-2}$	$1.0 \cdot 10^{-2}$	$1.2 \cdot 10^{-3}$	$6.8 \cdot 10^{-3}$	$6.8 \cdot 10^{-3}$

Table 36: Ignition probability results constant for all models

Detect.	With \leq IP44 equipment			
	kg/s	P_T	P_C	P_D
On	0.1	$3.6 \cdot 10^{-1}$	$1.3 \cdot 10^{-1}$	$2.6 \cdot 10^{-1}$
	1	$1.7 \cdot 10^{-1}$	$1.4 \cdot 10^{-1}$	$3.5 \cdot 10^{-2}$
	10	$1.2 \cdot 10^{-1}$	$1.1 \cdot 10^{-1}$	$9.5 \cdot 10^{-3}$
Detect.	With \geq IP64 equipment			
	kg/s	P_T	P_C	P_D
On	0.1	$4.7 \cdot 10^{-3}$	$2.2 \cdot 10^{-3}$	$2.0 \cdot 10^{-4}$
	1	$1.5 \cdot 10^{-2}$	$2.0 \cdot 10^{-3}$	$1.0 \cdot 10^{-2}$
	10	$1.1 \cdot 10^{-2}$	$1.7 \cdot 10^{-3}$	$6.8 \cdot 10^{-3}$

Table 37: Total ignition probability results for the standard MISOF model

The total ignition probabilities for the container storage plotted against HyRAM are shown in figure 60 and 61. The SAFEN₁₀ model curve lies on top of the standard MISOF curve.

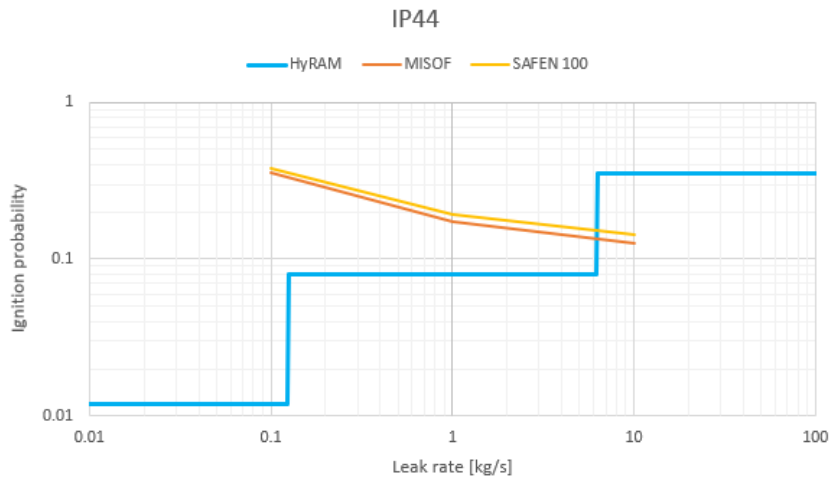


Figure 60: Total ignition probability for the container storage with IP44 equipment

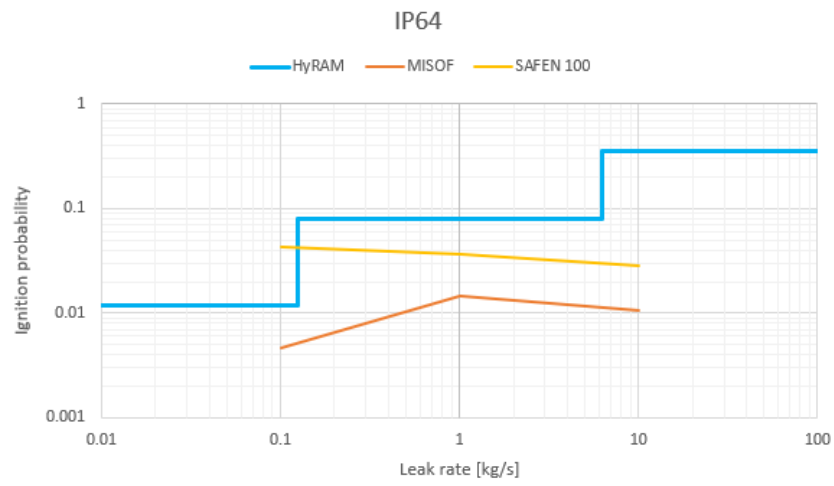


Figure 61: Total ignition probability for the container storage with IP64 equipment

5 Verification and validation

In this section, a discussion of the trustworthiness of the results will be done. This will consist of verification and validation. In the verification part, it is checked that the simulation gives the right result. This will be done mainly with a grid sensitivity and hand calculations. In the validation part, a discussion about the software's ability to model a real world system is carried out.

5.1 Verification

5.1.1 Grid sensitivity

In this subsection, a grid sensitivity will be used to argue what number of grid cells are adequate for the purpose of this study. The purpose of the study is not to find an exact ignition probability for a facility. There will be large variations from facility to facility, and there are also uncertainty in the parameters given as input. However, uncertainty due to a poor grid is unwanted, as it adds yet more uncertainty to the results. The grid sensitivity results are presented in figure 50 to 52, and table 33 to 35. It is important to note that the ignition probabilities for the grid sensitivity does not correspond with any of the other results for the refueling station. The reason for this is a bug discovered later. However, this bug does not interfere with the validity of the grid sensitivity. The result of interest is the difference in ignition probabilities between grid cell numbers, not the values themselves.

For releases of 0.1 kg/s and 10 kg/s shown in figure 50 and 52, using 100 000 grid cells will give results which deviates significantly from 300 000 cells and 500 000 cells. For the 0.1 kg/s release with 100 000 cells, the flammable cloud volume is approximately 33% larger when using 300 000 or 500 000 grid cells instead. For the 10 kg/s release with 100 000 cells, the flammable cloud volume is approximately 25% smaller when using 300 000 or 500 000 cells instead. Notice that the trend of what number of grid cells give the largest volume is reversed. The reason behind this is uncertain.

The difference in results between 300 000 cells and 500 000 cells is small for the 0.1 kg/s and 10 kg/s release. This is seen in figure 50 and 52, and also supported by the corresponding ignition probabilities in table 33 and 35. The difference in cloud volume for 1 kg/s between 300 000 and 500 000 cells is larger. However, for the purpose of this study where shorter simulation time is valued above extreme precision by using a large number of grid cells, 300 000 grid cells is considered to be adequate.

5.1.2 Hand calculations

The purpose of the hand calculations is to find a rough ignition probability based on the following parameters.

- Volume of the cloud
- Duration of the cloud
- Number of ignition sources
- Lambda values of the ignition sources

The hand calculation will mirror the 1 kg/s downward release with the standard MISOF model. The results of this case are found in section 4.2.3. The theory of the procedure is given in section 2.9. The formulas will still be shown here to make it easy to follow.

The simulations showed that the downward 1 kg/s release with the standard MISOF model and \leq IP44 rated equipment had an ignition probability of 15.6%, shown in figure 40. In the calculations in this section, there are three components to the total ignition probability of interest;

the volumetric sources, the non-ATEX equipment and the immediate ignition probability. The contribution from the car area proved to be so small, it is neglected for this section.

The starting point for this calculation is the volume inside the fenced area. In section 3.2.1 this was shown to be 1170 m³. To find the volumetric contribution, the volumetric lambdas are needed. The lambdas for the onshore and offshore MISOF model are actually the totals of the electric, rotating and other equipment in the standard MISOF model. The values of λ_C and λ_D for the total volumetric source are given below. An average exposure duration of the entire segment is also needed. An exact value of this is not possible to gather from KFX, so visual inspection is required. Based on the surface plots in figure 30, the transient cloud volume plot in figure 48 and the transient ignition probability plot in figure 49, the average duration is set to 25 seconds. There are uncertainty in this estimate, but the goal of this section is only to get a rough estimate of the ignition probability. Nine of the ten ignition sources are exposed according to output files from KFX. It is also possible to observe this visually by counting the number of steps on the blue line in figure 49. The parameters used for the calculations are shown in table 38.

V	1170 m ³
$\lambda_{C,vol}$	$2.8 \cdot 10^{-6}$ (1/m ³)
$\lambda_{D,vol}$	$1.2 \cdot 10^{-8}$ (1/s · m ³)
$\lambda_{C,IP44}$	$1.5 \cdot 10^{-2}$ (1/m ³)
$\lambda_{D,IP44}$	$1.8 \cdot 10^{-4}$ (1/s · m ³)
$P_{immediate}$	$2.4 \cdot 10^{-3}$
t	25 s
Non-ATEX units exposed	9

Table 38: Parameters used for hand calculations

The volumetric continuous ignition probability is found by using equation 3.

$$P_{C,vol} = 1 - e^{\lambda_{C,vol} \cdot V} = 1 - e^{2.8 \cdot 10^{-6} \cdot 1170} = 3.2 \cdot 10^{-3}$$

The volumetric discrete ignition probability is found by using equation 6.

$$P_{D,vol} = 1 - e^{\lambda_{D,vol} \cdot V \cdot t} = 1 - e^{1.2 \cdot 10^{-8} \cdot 1170 \cdot 25} = 4.4 \cdot 10^{-4}$$

The total volumetric ignition probability is found by using equation 8.

$$P_{T,vol} = 1 - ((1 - P_{C,vol})(1 - P_{D,vol})) = 1 - ((1 - 3.2 \cdot 10^{-3})(1 - 4.4 \cdot 10^{-4})) = 3.7 \cdot 10^{-3}$$

The next step is to calculate the contribution from non-ATEX sources. They use almost the same equations as the volumetric source. However, they are point sources and independent of the volume, thus the volume is left out of the equations. The contribution from one source is found first.

$$P_{C,IP44,single\ unit} = 1 - e^{\lambda_{C,IP44}} = 1 - e^{1.5 \cdot 10^{-2}} = 1.5 \cdot 10^{-2}$$

$$P_{D,IP44,single\ unit} = 1 - e^{\lambda_{D,IP44} \cdot t} = 1 - e^{1.8 \cdot 10^{-4} \cdot 25} = 4.5 \cdot 10^{-3}$$

$$P_{T,IP44,single\ unit} = 1 - ((1 - P_{C,IP44})(1 - P_{D,IP44})) = 1 - ((1 - 1.5 \cdot 10^{-2})(1 - 4.5 \cdot 10^{-3})) = 1.9 \cdot 10^{-2}$$

The total contribution for all nine non-ATEX sources is found by again using equation 8.

$$P_{T,IP44,all\ units} = 1 - ((1 - P_{C,vol})^{units\ exposed}) = 1 - ((1 - 1.9 \cdot 10^{-2})^9) = 1.6 \cdot 10^{-1}$$

Finally, the immediate ignition probability is used in equation 8 to find the total ignition probability for the scenario.

$$P_T = 1 - ((1 - P_{T,vol})(1 - P_{T,IP44})(1 - P_{immediate})) =$$
$$1 - ((1 - 3.7 \cdot 10^{-3})(1 - 1.6 \cdot 10^{-1})(1 - 3.4 \cdot 10^{-3})) = 1.7 \cdot 10^{-1}$$

Compared to the 15.6% obtained in the simulations, the 17.0% obtained in the hand calculations suggest that the ignition probability obtained by KFX is roughly correct based on the input given to the software.

5.2 Validation

In this subsection, whether or not the simulations are able to simulate the real world will be discussed. The topic is specifically if the simulations used in this thesis actually provides a correct picture of the likelihood that a hydrogen leak ignites.

First and foremost, it is worth discussing if KFX is able to simulate the dispersion of a gas cloud correctly. It is hard to investigate this in this thesis. However, KFX is made especially to simulate gas leaks. Not a lot of freedom is left to the user when it comes to CFD parameters not found in the setup shown in figure 6. Therefore, few things can go wrong, and one would expect KFX to simulate gas clouds accurately. This is as long as the grid is sufficient, which it was concluded to be the case.

SAFEN aims to develop a model that mirrors the real world. Of course, this is extremely difficult, reflected by the scale of the SAFEN project. The input parameters provided by Safetec is based on experiments and empirical data. Thus, the model will never be more accurate than the data of which the parameters inherit their values. The model will never get to the point where it is a replica of reality, but it can get close, and most likely more accurate than HyRAM.

6 Discussion

6.1 Basic hydrogen leak

The simulations of basic hydrogen releases in a geometry with and without terrain was conducted to map the behaviour of hydrogen in the CFD software. In this subsection, this behaviour will be discussed. The characteristics of the gas are important when designing hydrogen infrastructure, finding safety distances etc. According to the simulations, one common misconception of hydrogen releases, is that the gas will quickly rise out of harms way due to its low density. However, when high pressure hydrogen expands to atmospheric pressure, the gas cools, and its density will be higher than hydrogen at standard conditions. Another reason why the gas doesn't rise immediately, is the high impulse of the gas due to its velocity. Safetec experts also suggested this could create low pressure zones near ground level, preventing the gas from rising. In figure 18 and 19 one can see high concentrations of hydrogen is present at ground level. In the model with terrain, the gas cloud also climbs the hill at ground level. This means eliminating ignition sources at ground level is important when designing future hydrogen facilities. In cases where the release is liquid, LH_2 pools will be formed if the mass flow rate is significantly large. This pool will evaporate gradually, but means high concentration hydrogen cloud will be found at ground level as long as the pool is present. For releases onto water, there is also a significant risk for ignition due to sparking between rising ice crystals, as discussed in section, 2.1.

In figure 20 and 21 the max dispersion plots for the wind sensitivity are displayed. It is evident that the most dangerous scenarios will occur in low winds. This is probably due to the diffusing effect of the turbulence in the wind. One may imagine high wind could carry the cloud far downstream before it has time to diffuse to lower concentrations, but this does not appear to be the case. It is unclear why there is such a difference between the flat geometry and model with terrain. One explanation of why gas at the LFL is found 40 seconds after release in the terrain model, is that small blobs of gas ends up in locations where the wind is blocked by terrain or buildings. Through detailed conversations with Safetec, it was discovered that similar results have been observed in simulations of ammonia leaks.

For the pressure sensitivity in figure 22 and figure 23, only minor differences between the gas dispersion results can be observed. However, the pressure sensitivity was only conducted with a downward release direction. When the gas jet hits the ground, it will spread evenly in all directions. For a release in any other direction, the jet can travel much further if undisturbed. Therefore, it is expected that high release pressures would mean the cloud disperses further than for low pressure releases, if the release direction is any other direction than downwards. The mass flow sensitivity in figure 24 and 25 shows results which corresponds well with what is predictable. As all releases last for 20 seconds, and larger release rate will result in a larger total quantity of gas released. Therefore, large releases gives the furthest dispersion.

The release direction sensitivity is shown in figure 26. Releases upwards will not disperse far, because the dispersion is measured in the xy-plane. The dispersion might be tall, but this is generally not a problem from a risk consultant perspective. Horizontal releases and downward releases are the most dangerous according to the simulations.

6.2 The hydrogen refueling station

6.2.1 Gas dispersion

The first thing one may notice from the figures in section 4.2.1, is the fencing's ability to contain the gas. This was also the case in the Sandvika accident. In case of ignition, the fencing will make sure most of the blast energy will be directed upwards, and not sideways where bystanders and cars are likely to be situated. In the geometry used, the area in the front is open so trucks can easily deliver hydrogen to the refueling station. In reality, it is unlikely there would be such an opening facing the filling area. In the simulations, gas is free to escape towards the car area. However, with proper fencing it is unlikely the car area would see any gas at all, as long as the fence is tall

enough. For the car area, it is more important that the fence ensures the blast pressure is low enough to not cause severe damage. Just like for the basic hydrogen leak, the gas spends some time at ground level before rising. One can see the temperature of the hydrogen is significantly colder than the surrounding temperature in figure 35, giving the gas a slightly higher density than at room temperature. In addition, the high impulse of the gas prevents it from rising. This means ignition sources will be exposed for longer. This problem will increase if LH₂ is used. The simulations were only conducted with GH₂ at 350 bar, but according to the pressure sensitivity done for the basic hydrogen leak discussed in section 6.1, the gas dispersion would most likely not have been much different for higher pressures. However, the gas jet would hit obstacles with more momentum and cause the cloud volume to grow somewhat faster.

One may also notice the released amount of gas is not 13 kg as described in section 3.2.2. This can be seen in figure 27, 29 and 31. The plots only show the mass of H₂ present in the domain, as some of it leaves the boundaries. However, one can observe that the area under the leak rate line is greater than 13 kg, or simply consider the fact that the total mass of H₂ in figure 31 peaks at approximately 16 kg. This fact is due to a bug in the KFX RBM software during the initial thermodynamic calculations. This will have some effect on the results, as the flammable cloud would be larger compared to an actual 13 kg leak. However, the bug is not of importance, as 13 kg is somewhat arbitrary. It was chosen based on what is presented in section 2.2, but will be different for every station.

6.2.2 Ignition probability

First, it is worth investigating what sources contribute the most to the ignition probability. In most of the sources, the continuous contribution will be largest, simply because of the size of the input parameters described in section 2.7. By source, the largest contributor is by far IP44 equipment. Without detection, the IP44 equipment with a release rate of 1 kg/s has an ignition probability of 11% alone, which would likely be considered unacceptable. In a design analysis, the ignition probability would be multiplied with the leak frequency to obtain a fire frequency. This fire frequency would be used to obtain a risk of casualty for the plant, which is what is used in safety regulations from safety authorities. However, any discussion about this matter is outside the scope of the thesis.

Simply using IP64 equipment or higher reduces the contribution from non-ATEX equipment by a factor of approximately 10. Using non-ATEX equipment will still result in a high ignition probability, easily avoided by using ATEX equipment. Other than the non-ATEX equipment, the car area also makes a minor contribution to the total ignition probability. Notice that the 0.1 kg/s leak is not sufficient to reach the car area, and the ignition probability is zero. For the 1 kg/s and 10 kg/s releases, the ignition probability is in the order of 10⁻³, approximately equal to the contribution from IP64 equipment. If the car area was closer to the release and a larger part of it exposed, the ignition probability would be much larger than it currently is. However, in reality it is easy to avoid exposure to cars by using proper fencing and placement of the hydrogen process equipment. In a spacious area, process equipment and hydrogen storages will most likely be placed further away than what is done in the model. However, for urban refueling station, it is important to set a large enough safety distance. Land area is expensive in urban areas, and refueling station companies will likely choose the minimum allowed safety distances to save investment costs. Also note the procedure for determining λ_D for the car area in section 3.2.3 has a great deal of uncertainty, and will vary greatly with the location and demand of the refueling station.

The contribution from the volumetric sources are small compared to that of non-ATEX equipment, especially IP44. The contribution in the MISOF models are in the order of 10⁻³. The exception is for small releases in the offshore MISOF model, which is 10 times smaller. The SAFEN₁₀ model sees probabilities about 10 times larger than the standard MISOF model. Not surprisingly, the volumetric equipment in the SAFEN₁₀₀ model sees an ignition probability 10 times larger than the SAFEN₁₀ model. The total ignition probabilities between the different models lie close to one another. This is because the volume of the process area is quite small when compared to large, industrial plants. Thus, the volumetric contribution is small. In the total ignition probability,

the volumetric contribution is nearly invisible because of the large contribution from non-ATEX sources. What the ignition probabilities of the volumetric sources mean compared to one another is outside the scope of the thesis. However, given the small contribution compared to IP44 equipment, especially in the MISOF models, it highlights the importance of using ATEX equipment.

When comparing the the ignition probabilities with and without detectors, the results with detectors seem questionable. Hydrogen detectors are slow, and there are only five detectors. For the small release rates of 0.1 kg/s, the cloud surface plots in figure 28 show that there is a possibility that no detectors are exposed in some release directions. This is especially true for a vertical release. For the large release rates of 10 kg/s, the large release rate will give a quick burst of hydrogen. There will be a large cloud initially, but rising hydrogen won't be replaced by more hydrogen leaking from the vessel, as the volume is quickly emptied. This can be seen in figure 32. As the detectors are slow, the danger will be close to over when they have detected H₂ and shut off ignition sources. The major issue with the detectors, is that it was later suggested by Safetec experts they were contributing to the ignition probability. Therefore, the ignition probability that is avoided by early detection, might be cancelled by the contribution from the detectors. However, it is not possible to see the size of the contribution from detectors in KFX, neither the input lambdas for the detectors. Therefore, comparison between detectors either enabled or disabled is invalid.

The gas cloud formed and the resulting ignition probability has a major dependence on the release direction. The differences in the gas dispersion are best visualized in figure 33, 37 and 38. The resulting ignition probabilities are best visualized by figure 40. First and foremost, one may note the negligible ignition probability of 0.2% in the z-direction. This is because the jet does not expose many ignition sources, and the cloud rises as the jet diffuses. Next, notice the ignition probability in the x-direction is significantly lower than the other x and y-directions. This is because the gas jet is directed towards the opening of the fence. More gas can expose the car area, but less gas expose the many ignition sources inside the fence. The y, negative y and negative x-direction ignition probability suggests that how quickly the jet hits an object will have an effect. This is because the jet diffuses quicker, and therefore resulting in a faster growing gas cloud. A jet hitting the ground and diffusing is shown in figure 36. The y-direction release hits one of the trailer tubes right away. The distance between the release and this tube is approximately 20 cm. The negative z-direction has the second largest ignition probability, where the cloud growth is sped up by the jet hitting the ground. The jet in the negative y and negative x-direction releases meet obstructions further away from the release, and also has lower ignition probabilities. From these results, it is clear release direction and geometry is important. This highlights the power of combining ignition probability calculations and CFD. Which and how many ignition sources get exposed is dependent on the gas cloud. This is one of the big advantages KFX RBM has compared to HyRAM.

To propose what is the worst leak rate, there are multiple topics to consider. The simulations show that 1 kg/s is in some cases worse than 10 kg/s. The reason for this lies in the gas dispersion. As suggested earlier, the 10 kg/s release rate will result in a burst of hydrogen which quickly rises out of harm's way. Such a high release rate is more than what is required to fill the process area with gas. The 1 kg/s release rate cases also seem to fill most of the process area. The difference is that rising gas is replaced by more gas from the leaking vessel, meaning the process area is exposed to gas for longer. Therefore, the simulations suggest 1 kg/s release rate is the worst case. However, if the process area was larger, the story might have been different. If 1 kg/s can't fill the process area with gas, but 10 kg/s can, 10 kg/s might be the worst leak rate.

It is also worth mentioning that the released mass of H₂ has an impact on the ignition probability, another variable not captured by HyRAM. For a given leak rate, a greater mass inside the leaking vessel will mean the release will last longer. Although this is not investigated in the simulations, it is plausible a greater released mass will always give a higher ignition probability. It is again worth mentioning the importance of considering the geometry when investigating the ignition probability. If the leak happens inside a volume with a roof, such as inside a building or an underground parking lot, the amount of released gas is probably more important than the leak rate. If the gas can't escape, the mass of gas will determine how much volume is exposed to a flammable cloud. This underlines the importance of also considering the mass of gas released when making an ignition probability model.

In terms of what is the most dangerous direction, there are more things to consider than what is shown through the simulations. In this case, a release in the y-direction gave the highest ignition probability. However, there are phenomena that is not considered by KFX RBM relevant for hydrogen in particular. The jet has a very high velocity due to the pressure levels hydrogen is typically stored at. If this jet hits debris such as gravel or sand on the ground, the internal collision between those particles can cause ignition. This was explained in section 2.1. These ignition mechanisms are considered in the final SAFEN model. This makes a downward release direction worse than what is shown through the ignition probabilities from the simulations. The industry should therefore focus on keeping surroundings tidy, especially keeping floors clean. To make proper cleaning possible, process equipment must be placed in a way which makes it possible to access the surrounding floor with cleaning equipment.

6.2.3 Comparison with methane

First, one may notice the gas cloud is a lot smaller when methane is used. The gas cloud also diffuses fast. This is seen in figure 47. Nearly no gas is left after 30 seconds. Methane also has a much narrower flammability range than hydrogen, which means the flammable volume will be small even if the cloud was larger. This explains the large differences between flammable cloud volume between hydrogen and methane in figure 48.

The ignition probability for methane is less than what of hydrogen. Put simply, the flammable parts of the methane cloud hardly exposes any ignition sources. The non-ATEX equipment is placed too high for the cloud to expose it. This is especially true for the 1 kg/s average ignition probability in table 31 of 0.0025. The largest contributor there, is the immediate ignition probability. In general, the simulations suggest the average ignition probability for methane is approximately ten times less than for hydrogen. As a final point, it is worth mentioning 13 kg of methane is a small amount of gas compared to 13 kg of hydrogen when it comes to storage and usage.

Whether or not non-ATEX equipment exposed to methane should have such a lower ignition probability compared to non-ATEX equipment exposed to hydrogen is debatable. Although the minimum ignition energy of hydrogen is much smaller than methane's, a powerful discharge would ignite any flammable mixture. Therefore, the number of ignitions that occurs due to an ignition energy somewhere between hydrogen's MIE and methane's MIE should be further investigated. Given gas cloud exposure, this range of ignitions must be able to explain the much larger ignition probability of hydrogen compared to methane.

6.2.4 The final SAFEN parameters

The total ignition probabilities in the final SAFEN model are substantially greater than what of any other model. The highest ignition probability occurs for IP44 equipment with a leak rate og 1 kg/s, and is 84%. While the immediate ignition probability is larger in the final SAFEN model, most of the total ignition probability's value comes from the non-ATEX equipment. The input lambdas for the non-ATEX equipment are significantly higher than for the MISOF model. This is the reason the ignition probabilities are so much higher. The final SAFEN simulations were conducted at the very end of the semester, and results are therefore not as detailed.

6.3 The container storage

The container is an almost enclosed volume. This means the amount of gas that can escape, is small. Most of the gas escaping the container, comes out the opening in the door at the front of the container. The gas coming through this opening then exposes the car area around the dispenser. In figure 53, 54 and 55 the roof of the container is removed for visual inspection, and one can see the entire volume of the container is filled with gas. Figure 59 shows that the concentration inside is high. It is unknown for how long it takes for the hydrogen to leave the container, as the simulations had to be stopped due to limited time. However, these facts mean the ignition sources

inside the container are exposed for a significant amount of time. As the opening of the container is directed towards the car area, cars will be exposed. This is especially true if the leak happens in the x-direction shown in figure 56. In such a case, the jet travels straight towards the opening. All other release direction produced similar gas clouds outside the container.

The ignition probability of the container storage is higher than the refueling station discussed earlier. This is mainly due the fact that the container contains the gas for a significant amount of time. Consider a case where the door was not open, and only small amounts of gas could escape through cracks and small openings in the container. Even with fewer ignition sources, the ignition probability would converge towards 100%, because the ignition sources would be exposed for a long duration. In general, an ignition source with even a low lambda value will result in 100% ignition probability when exposure time goes towards infinity. The container does not contain the hydrogen for infinity, but significantly longer than the open fencing used at the refueling station.

An interesting result for the container storage, is that the smallest leak rate of 0.1 kg/s gives the highest ignition probability. This is especially true for IP44 equipment shown in figure 60. This is mainly because a leak rate of 0.1 kg/s can sustain a flammable cloud inside the container for longer, seen by the curves in figure 58. The 10 kg/s leaks are more violent in terms of velocities inside the container as seen in figure 57, so more gas will be forced out the opening. This result contradicts HyRAM directly, and highlights the importance of considering the geometry when determining an ignition probability.

As an end to the discussion, one must understand that there are uncertainties in the input parameters. When it comes to the release itself, which was 13 kg H₂, it is somewhat arbitrary. It was chosen because literature in section 2.2 presented a design where a cascade storage of three 13 kg vessels of H₂ was used. The size of the storage will vary greatly with the demand the refueling station must meet, and storage tanks can be much larger or smaller. It is also possible leaks can happen in parts of the plant which is not directly coupled to the volume of the tanks. This can be parts of pipe containing only small amounts of H₂, isolated from the tank by valves. There are also uncertainty in the number of ignition sources placed. Ten non-ATEX sources were placed inside the process area, and all station designs are likely different. The non-ATEX equipment was placed there mainly to demonstrate the increase in ignition probability, and the importance of using ATEX equipment. The volumetric ignition probability lambdas inherit their value partly from the equipment density of oil and gas facilities onshore and offshore. If this equipment density is representative for hydrogen facilities is outside the scope of the thesis, but should be investigated further.

7 Conclusion

The goal of this master thesis was mainly to find an ignition probability for different hydrogen facilities. The facilities which were investigated were a hydrogen refueling station and a hydrogen container storage. This was done with three different release rates, 0.1, 1 and 10 kg/s, releasing a total of 13 kg of hydrogen. Multiple different input ignition parameters were tested. The standard MISOF model is an ignition model from the petroleum industry, a good baseline for the study. Using this model when doing simulations on the refueling station with IP44 equipment, the leak rates of 0.1, 1 and 10 kg/s resulted in ignition probabilities of 1.7%, 12.0% and 8.4% respectively. The hydrogen container storage obtained ignition probabilities of 36%, 17% and 12% using the same leak rates. Using IP64 rated equipment resulted in ignition probabilities about ten times smaller. The final SAFEN parameters resulted in ignition probabilities as high as 84% for a 1 kg/s release with IP44 equipment at the refueling station. This underlines the importance of using ATEX-equipment, which is rated for use in explosive atmospheres.

The simulations also showed the importance of considering the geometry and release direction when determining an ignition probability. In the simplified HyRAM, the ignition probability increases with leak rate. When there is no geometry and the terrain is flat, this is true. In such a case, a large leak rate will result in a larger cloud, and thus exposing more ignition sources. However, in cases with a geometry, KFX RBM generated different results compared to what HyRAM would predict. Of the three release rates of 0.1, 1 and 10 kg/s, the refueling station obtained the highest ignition probabilities with 1 kg/s leaks, and the container storage with 0.1 kg/s leaks. This occurred because even small leaks was enough to produce cloud concentrations above the LFL. When the released gas gets trapped and can't rise to the atmosphere, the mass of released gas might be more important than the release rate. The release direction also played a key role. Releases straight up give a negligible ignition probability. If the jet hits a surrounding object, especially walls, it will affect the development of the gas cloud. This highlights the importance of considering both the release direction, the released amount of gas and the geometry when determining an ignition probability.

Another goal of the master thesis was to study the behaviour of hydrogen leaks using CFD software, and formulate relevant design points for hydrogen facilities. The simulations showed that released hydrogen does stay around ground level for a significant amount of time after being released, partly due to the high impulse of the released gas. This meant ignition sources at ground level were exposed. Hydrogen also has wide flammability limits and produce large clouds when leaking compared to light hydrocarbons. Therefore, it is crucial to be aware of ignition sources when designing a facility, and not make the common misconception that hydrogen will rise harmlessly into the atmosphere. The exception is if the leak is directed straight upwards, which proved to be no problem in terms of ignition probability. Therefore, facilities should aim to make releases travel upwards if a leak were to happen. This could for example be placing pressure relief valves in a direction which results in an upward release. Another way of reducing the risk of gas exposing the areas where humans are, is proper use of fences. However, this is no new piece of technology, and reduced the consequences of the accident at the refueling station in Sandvika. The simulations also showed proper fencing contained most of the gas, and the lack of fences can be disastrous.

8 Additional content

8.1 Workflow and complications

Much of the time during the master semester was spent figuring out how KFX RBM works. It is an experimental software made many years ago, and no manual exists. When one problem was solved, multiple new hurdles appeared. However, through time consuming trial and error, the meaning of each of the parameters that goes into a simulation was understood. A major part of the time was also spent understanding how the ignition probability is calculated, to then recreate a Python tool to give more freedom afterwards.

8.2 Further work

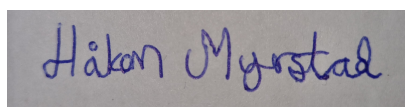
Parts of the work conducted in this master thesis will live on in the SAFEN project. A new phase of the project will start in autumn 2023. The engineers at Safetec and the project partners will continue to develop their improved hydrogen ignition probability model.

It is possible to improve the ignition probability model in several ways, both with simulations and experiments. Simulations using other hydrogen facilities could be done, using an accurate layout of an actual plant. It is also possible to conduct experiments. For example, this could be done to map the ignition probability of cars. Various cars, both internal combustion engine cars, EV's and FCEV's can be investigated. This could be done by releasing hydrogen in various locations around the car, and find an ignition probability based on how often the hydrogen ignites.

8.3 Acknowledgement

The outline of this master thesis is made by Chief Advisor Ingar Fossan at Safetec. He has provided the input required to do the simulations, and created a scope that benefits the SAFEN project. Professor Nicola Paltrinieri has participated in the startup phase, and provided useful feedback. Nils Inge Lilleheie at DNV, one of the creators of KFX RBM, has provided guidance when progress had stopped due to software problems. Rune Kleiveland at Safetec has been a mentor throughout the entire 5th year at NTNU. A big thanks goes out to everyone who participated in the work for this master thesis.

Håkon Engan Myrstad
Energy & Environmental Engineering
Department of Process Engineering



Trondheim, 8th June 2023

Bibliography

- [1] International organization for standardization (ISO). *Gaseous hydrogen refueling stations, general requirements (ISO 19880-1)*. URL: <https://www.iso.org/obp/ui/#iso:std:iso:19880:-1> (visited on 31st May 2023).
- [2] M. Ang A. Cox F. Lees. ‘Classification of hazardous locations’. In: (1990).
- [3] R. Ono A. Kumamoto H. Iseki. ‘Measurement of minimum ignition energy in hydrogen/oxygen-nitrogen premixed gas by spark discharge’. In: 1 (2011).
- [4] M. Majkut A. Witkowski A. Rusin. ‘Comprehensive analysis of hydrogen compression and pipeline transportation from thermodynamics and safety aspects’. In: (2017).
- [5] E. Hecht B. Ehrhart. ‘Hydrogen plus other alternative fuels risk assesment models (HyRAM+) version 5.0 technical reference manual’. In: (2022).
- [6] International Electrotechnical Comission. *IP code*. URL: <https://www.iec.ch/ip-ratings> (visited on 2nd June 2023).
- [7] C. La Conca. ‘Risk Based Maintenance in hydrogen refuelling stations: Focus on Safety and Business Interruption risk’. In: (2020).
- [8] Dahl. ‘Risk of oil and gas blowout on the Norwegian continental shelf’. In: (1983).
- [9] L.M. Das. *Compendium in hydrogen energy*. URL: <https://www.sciencedirect.com/topics/engineering/lower-flammability-limit> (visited on 19th Feb. 2023).
- [10] DNV. *Kameleon FireEx*. URL: <https://www.dnv.com/services/fire-simulation-software-cfd-simulation-kfx-110598> (visited on 18th Jan. 2023).
- [11] World Energy. *Engie EPS Unveils Hydrogen Storage System*. URL: <https://www.world-energy.org/article/13181> (visited on 7th Apr. 2023).
- [12] I. Fossan. ‘Modelling of ignition sources on land-based oil and gas facilities’. In: Report No. ST-16542-1 (2022).
- [13] glpautogas. *How to refuel hydrogen car*. URL: <https://www.glpautogas.info/documentos/HOW-REFUEL-HYDROGEN-CAR.pdf> (visited on 5th Mar. 2023).
- [14] H2.LIVE. *Toyota Mirai*. URL: <https://h2.live/en/fuelcell-cars/toyota-mirai> (visited on 18th Feb. 2023).
- [15] European Agency for Health and Safety at Work. *Guidelines to Directive 2014/34 EU - ATEX ‘Product’ Directive*. URL: <https://osha.europa.eu/en/legislation/guidelines/guidelines-directive-201434-eu-atex-product-directive> (visited on 29th May 2023).
- [16] HIAD. URL: <https://hysafe.info/> (visited on 19th Jan. 2023).
- [17] Palmisano Hübert Boon-Brett. ‘Trends in gas sensor development for hydrogen safety’. In: (2019).
- [18] A. Sæbø I. Fossan. ‘Process leak for offshore installations frequency assessment model’. In: Report No. 107566/R1 (2018).
- [19] M. Vanierschot J. Berghmans. ‘Safety aspects of CNG cars’. In: (2014).
- [20] A. Elgowainy J. Pratt D. Terlip. ‘H2first reference station design task’. In: NREL/TP-5400-64107 (2015).
- [21] P. Kofstad. *Hydrogen*. URL: <https://snl.no/hydrogen> (visited on 18th Feb. 2023).
- [22] D. Lancaster. *What could cause a capacitor to explode*. URL: <https://electronicguidebook.com/what-would-cause-a-capacitor-to-explode> (visited on 17th Apr. 2023).
- [23] J. Løkke. ‘The Kjørbo incident’. In: (2019).
- [24] H. Myrstad. ‘Risk assessment of gas leaks in urban areas’. In: 1 (2022).
- [25] Offshore Norge. *MISOF report*. URL: <https://offshorenorge.no/rapporter/hms-drift/hms-og-drift/misof-report/> (visited on 28th May 2023).
- [26] NPROXX. *Why high pressure gas storage beats liquid hydrogen*. URL: <https://www.nproxx.com/why-high-pressure-gas-storage-beats-liquid-hydrogen/> (visited on 5th May 2023).

-
- [27] M. Eleryan Ø. Knudsen. ‘SAFEN: Ignition source literature study’. In: (2023).
- [28] British Petroleum. ‘Deepwater Horizon Accident Investigation Report’. In: (2010).
- [29] PortabeSpaceUK. *40ft shipping container blue*. URL: <https://www.portablespace.co.uk/product/40ft-x-8ft-one-trip-shipping-container-blue> (visited on 7th Apr. 2023).
- [30] J. Pratt. *H2 Liquid Gas Storage*. URL: <https://zeroemissionadvisors.com/blogs/news/h2-liquid-gas-storage> (visited on 19th Feb. 2023).
- [31] Safetec. *Proud initiator of SAFEN*. URL: <https://www.safetec.no/en/news/proud-initiator-of-safen-safe-energy-carriers-jip> (visited on 28th May 2023).
- [32] Erik Tandberg. *Hindenburg*. URL: <https://snl.no/Hindenburg> (visited on 31st May 2023).
- [33] CMB TECH. *Hydrogen system mass calculator*. URL: <https://cmb.tech/hydrogen-tools> (visited on 14th Mar. 2023).
- [34] The Engineering Toolbox. *Gases - Explosion and flammability concentration limits*. URL: https://www.engineeringtoolbox.com/explosive-concentration-limits-d_423.html (visited on 15th May 2023).
- [35] G. Vislie. ‘Key learning points hydrogen indicent’. In: (2019).

Appendix

A Container storage detailed ignition probabilities

A.1 Standard MISOF model

Detection	kg/s	P_T	P_C	P_D
On	0.1	$3.2 \cdot 10^{-3}$	$6.8 \cdot 10^{-4}$	$1.6 \cdot 10^{-4}$
	1	$2.9 \cdot 10^{-3}$	$5.0 \cdot 10^{-4}$	$1.4 \cdot 10^{-5}$
	10	$2.8 \cdot 10^{-3}$	$4.0 \cdot 10^{-4}$	$2.2 \cdot 10^{-6}$

Table 39: Total ignition probability contribution from the volumetric sources in the standard MISOF model

A.2 SAFEN₁₀ model

Detection	kg/s	P_T	P_C	P_D
On	0.1	$4.1 \cdot 10^{-3}$	$2.4 \cdot 10^{-3}$	$1.6 \cdot 10^{-3}$
	1	$2.3 \cdot 10^{-3}$	$2.1 \cdot 10^{-3}$	$1.4 \cdot 10^{-4}$
	10	$1.8 \cdot 10^{-3}$	$1.8 \cdot 10^{-3}$	$2.2 \cdot 10^{-5}$

Table 40: Total ignition probability contribution from the volumetric sources in the SAFEN₁₀ model

Detect.	With \leq IP44 equipment			
On	kg/s	P_T	P_C	P_D
	0.1	$3.6 \cdot 10^{-1}$	$1.3 \cdot 10^{-1}$	$2.6 \cdot 10^{-1}$
	1	$1.7 \cdot 10^{-1}$	$1.4 \cdot 10^{-1}$	$3.5 \cdot 10^{-2}$
10	$1.3 \cdot 10^{-1}$	$1.2 \cdot 10^{-1}$	$9.5 \cdot 10^{-3}$	
Detect.	With \geq IP64 equipment			
On	kg/s	P_T	P_C	P_D
	0.1	$7.9 \cdot 10^{-3}$	$3.9 \cdot 10^{-3}$	$1.7 \cdot 10^{-3}$
	1	$1.6 \cdot 10^{-2}$	$3.6 \cdot 10^{-3}$	$1.0 \cdot 10^{-2}$
10	$1.2 \cdot 10^{-2}$	$3.1 \cdot 10^{-3}$	$6.8 \cdot 10^{-3}$	

Table 41: Total ignition probability results for the SAFEN₁₀ model

A.3 SAFEN₁₀₀ model

Detection	kg/s	P_T	P_C	P_D
On	0.1	$4.0 \cdot 10^{-2}$	$2.4 \cdot 10^{-2}$	$1.6 \cdot 10^{-2}$
	1	$2.3 \cdot 10^{-2}$	$2.1 \cdot 10^{-2}$	$1.4 \cdot 10^{-3}$
	10	$1.8 \cdot 10^{-2}$	$1.8 \cdot 10^{-2}$	$2.2 \cdot 10^{-4}$

Table 42: Total ignition probability contribution from the volumetric sources in the SAFEN₁₀₀ model

Detect.	With \leq IP44 equipment			
On	kg/s	P_T	P_C	P_D
	0.1	$3.8 \cdot 10^{-1}$	$1.5 \cdot 10^{-1}$	$2.7 \cdot 10^{-1}$
	1	$1.9 \cdot 10^{-1}$	$1.6 \cdot 10^{-1}$	$3.6 \cdot 10^{-2}$
	10	$1.4 \cdot 10^{-1}$	$1.3 \cdot 10^{-1}$	$9.7 \cdot 10^{-3}$
Detect.	With \geq IP64 equipment			
On	kg/s	P_T	P_C	P_D
	0.1	$4.4 \cdot 10^{-2}$	$2.5 \cdot 10^{-2}$	$1.6 \cdot 10^{-2}$
	1	$3.6 \cdot 10^{-2}$	$2.3 \cdot 10^{-2}$	$1.2 \cdot 10^{-2}$
	10	$2.8 \cdot 10^{-2}$	$1.9 \cdot 10^{-2}$	$7.0 \cdot 10^{-3}$

Table 43: Total ignition probability results for the SAFEN₁₀₀ model

B Sandvika accident description from HIAD [16]

Explosion in a HRS

Major leak (est. 1.5 to 3 kg) of hydrogen from high-pressure storage, resulting in detonation, from hydrogen refuelling station.

Causes were two untightened bolts securing the gasket between the high-pressure tank and the pipeline. Gasket held for over 2 years against 900 bar pressure before eventually giving way due to fatigue induced by pressure oscillations during refuelling.

Specific tank was the one closest to the ground; after breaching the high-pressure gasket, hydrogen quickly broke through the low-pressure gasket and rapidly leaked to atmosphere, forming an explosive cloud.

The untightened bolts were blamed on faulty assembly by manufacturer NEL, who took responsibility. They enacted new procedures, similar to the aviation industry, to ensure such a mistake would not occur again.

Damage to surrounding buildings (65 m away) indicate that a detonation occurred. The HRS was by a busy roundabout at the outskirts of Oslo on a day when Norwegians were driving home from holidays. Two car drivers were checked in at hospitals after their airbags opened due to the shockwave, but there were no direct damages to people; injuries were light.

Neighbourhood was alarmed by the loudness of the blast, which was heard in a large area; one dog panicked and jumped from a balcony at the fourth floor of a neighbouring building.

NEL shut down immediately all similar plants worldwide pending inspection on bolts. Station operator Uno-X has after 10 months not yet reopened their hydrogen stations, and may have been permanently swayed against the technology.

C Radar Python code

```

import matplotlib.pyplot as plt
import sys
sys.path.append('/proj/P10475_RA/STUDENTS/2022/Hakon/PYTHON/kfxutils')
from kfxutils import r3d
from safeutils.cfd import utils
import tmp_safen_utils
import numpy as np
num_sec = 100

center = (-34., 45.) #Release center
LFL = 0.27
folder_Path =
'/proj/P10475_RA/STUDENTS/2022/Hakon/Sommerjobb/Ammonia_semi_complex_geometry/Liquid_spray/2_nh3liq_drop_semi/case_safen_std_00150125.r3d'

r = r3d.read(folder_Path)
concentration = r.fielddata[4]

# Compute cell centers
if r.r3d_type == 4:
    xc = r3d.estimate_center_from_staggered(r.xs)
    yc = r3d.estimate_center_from_staggered(r.ys)
    zc = r3d.estimate_center_from_staggered(r.zs) # Not really needed
else: # R3d type 1 (e.g. made from bullet monitors) or 2
    xc = r.xc
    yc = r.yc
    zc = r.zc

radar = tmp_safen_utils.radar(center, concentration, (xc, yc, zc), LFL, num_sectors=num_sec, zrange=[0, 20])
print(radar)

all_angles = np.linspace(0, 2 * np.pi, num_sec + 1)
# Repeat all angles but the first and last
low_angles = all_angles[:-1]
high_angles = all_angles[1:]
plot_angles = np.vstack((low_angles, high_angles)).ravel(order='F')
# Duplicate the radar values for matching with duplicated angles
plot_radar = np.vstack((radar, radar)).ravel(order='F')
# Set up the plot
fig = plt.figure()
ax = fig.add_subplot(111, polar=True)
ax.set_theta_offset(np.pi / 2)
ax.set_theta_direction(-1)
ax.fill(plot_angles, plot_radar)
plt.show()

```

D Unignite Python code


```

        if setToZero[(3 * i) + 2] == 1:
            other_prob[:, i] = np.zeros(len(_total_prob))
        else:
            other_prob[:, i] = df['Prob_D_' + sourceName].to_numpy()

for i in range(0, len(_total_prob)):
    for j in range(len(other_prob[1])):
        if other_prob[i, j] != 0 and _total_prob[i] == 0:
            _total_prob[i] = (1 - other_prob[i, j])
        elif other_prob[i, j] != 0 and _total_prob[i] != 0:
            _total_prob[i] *= (1 - other_prob[i, j])

        if j == len(other_prob[1]) - 1 and _total_prob[i] != 0:
            temp = _total_prob[i]
            _total_prob[i] = 1 - temp

return _total_prob

#Print total probability
def printProb(_Prob, _Prob_C, _Prob_D):
    for i in range(len(_Prob)):
        print('Iteration: ' + str(i) + '      Prob: ' + str(round(_Prob[i], 5)) + '      Prob_C: '
              + str(round(_Prob_C[i], 5))
              + '      Prob_D: ' + str(round(_Prob_D[i], 5)))
    print('Total prob: ' + str(_Prob[-1]))
    print('Total continuous: ' + str(_Prob_C[-1]))
    print('Total discrete: ' + str(_Prob_D[-1]))

def ReadFirstLine(_filename):
    with open(_filename, 'r') as csvfile:
        reader = csv.reader(csvfile)
        first_line = next(reader)
    return first_line

def ReadLastLine(_filename):
    with open(_filename, 'r') as csvfile:
        reader = csv.reader(csvfile)
        last_line = deque(reader, 1)[0]
    return last_line

def WriteLineExcel(_workbook, _sheet, _line):
    wb = load_workbook(_workbook)
    sheet = wb[_sheet]
    rows = sheet.max_row

    for c in range(len(_line)):
        sheet.cell(rows + 1, c + 2).value = _line[c]
    wb.save(_workbook)

def ReadColumnToArray(_column, _startRow, _sheet, _wb):
    wb = load_workbook(_wb)
    sheet = wb[_sheet]
    rows = sheet.max_row
    result = []

    for i in range(_startRow, rows + 1):
        cell = sheet.cell(i, _column)
        result.append(cell.value)
    return result

ignprob_filename = 'case_ignprob.log'
pathToSimulations =
r'/proj/P10475_RA/STUDENTS/2022/Hakon/Masterprosjekt/Fuelling_Station/SAFEN_final'
saveToFolder =
r'/proj/P10475_RA/STUDENTS/2022/Hakon/Masterprosjekt/Fuelling_Station/python_test'

```

```
files = os.listdir(pathToSimulations)
workbook = r'/proj/P10475_RA/STUDENTS/2022/Hakon/PYTHON/Pool/Ignprobdata_final.xlsx'
sheet = 'Test'
```

```
numSources = 24
```

```
casesFound = 1
```

```
setToZero = [0, 0, 0 #1 Electric
             ,0, 0, 0 #2 Rotating
             ,0, 0, 0 #3 Other
             ,0, 0, 0 #4 Offshore
             ,0, 0, 0 #5 Onshore
             ,0, 0, 0 #6 Safen_10
             ,0, 0, 0 #7 Safen_100
             ,0, 0, 0 #8 Safen_iso
             ,0, 0, 0 #9
             ,0, 0, 0 #10
             ,0, 0, 0 #11
             ,0, 0, 0 #12
             ,0, 0, 0 #13
             ,1, 1, 1 #14
             ,1, 1, 1 #15
             ,1, 1, 1 #16
             ,1, 1, 1 #17
             ,1, 1, 1 #18
             ,1, 1, 1 #19
             ,1, 1, 1 #20
             ,1, 1, 1 #21
             ,1, 1, 1 #22
             ,1, 1, 1 #23
             ,0, 0, 0 #24
             ,1, 1, 1 #25
             ,1, 1, 1 #26
             ,1, 1, 1 #27
             ,1, 1, 1 #28
             ,1, 1, 1 #29
             ,1, 1, 1 #30
             ,1, 1, 1 #31
             ,1, 1, 1 #32
             ,1, 1, 1 #33
             ,1, 1, 1 #34
             ,1, 1, 1 #35
             ,1, 1, 1 #36
             ,1, 1, 1 #37
             ,1, 1, 1 #38
             ,1, 1, 1 #39
             ]
```

```
oneCaseFound = False
```

```
for i in range(len(files)):
```

```
    if (pathToSimulations + '/' + files[i] + '/' + ignprob_filename).count('ignprob'):
```

```
        try:
```

```
            df = pd.read_csv(pathToSimulations + '/' + files[i] + '/' + ignprob_filename)
```

```
        except: continue
```

```
    else: continue
```

```
print('Calculating ignprob for ' + files[i])
```

```
df.columns = [c.strip() for c in df.columns]
```

```
# Calculate total probabilities
```

```
Prob = total_ign_prob('T', setToZero, df)
```

```
Prob_C = total_ign_prob('C', setToZero, df)
```

```
Prob_D = total_ign_prob('D', setToZero, df)
```

```
newColumns = fillColumns(setToZero, len(Prob))
```

```
# Make new dataframe with new values
```

```
modified_ignprob = pd.DataFrame({'time': df['time'].to_numpy(),
```

```

# 'DetIndex': df['DetIndex'].to_numpy(),
# 'VolEqStCl': df['VolEqStCl'].to_numpy(),
# 'VolUel2Lel': df['VolUel2Lel'].to_numpy(),

'Prob': Prob, 'Prob_I': df['Prob_I'].to_numpy(),

'Prob_C': Prob_C,

'Prob_D': Prob_D

, 'Prob_001': newColumns[:, 0], 'Prob_C_001':
newColumns[:, 1],
'Prob_D_001': newColumns[:, 2]
, 'Prob_002': newColumns[:, 3], 'Prob_C_002':
newColumns[:, 4],
'Prob_D_002': newColumns[:, 5]
, 'Prob_003': newColumns[:, 6], 'Prob_C_003':
newColumns[:, 7],
'Prob_D_003': newColumns[:, 8]
, 'Prob_004' : newColumns[:, 9], 'Prob_C_004' :
newColumns[:, 10],
'Prob_D_004' : newColumns[:, 11]
, 'Prob_005' : newColumns[:, 12], 'Prob_C_005' :
newColumns[:, 13],
'Prob_D_005' : newColumns[:, 14]
, 'Prob_006' : newColumns[:, 15], 'Prob_C_006' :
newColumns[:, 16],
'Prob_D_006' : newColumns[:, 17]
, 'Prob_007' : newColumns[:, 18], 'Prob_C_007' :
newColumns[:, 19],
'Prob_D_007' : newColumns[:, 20]
, 'Prob_008' : newColumns[:, 21], 'Prob_C_008' :
newColumns[:, 22],
'Prob_D_008' : newColumns[:, 23]
, 'Prob_009' : newColumns[:, 24], 'Prob_C_009' :
newColumns[:, 25],
'Prob_D_009' : newColumns[:, 26]
, 'Prob_010' : newColumns[:, 27], 'Prob_C_010' :
newColumns[:, 28],
'Prob_D_010' : newColumns[:, 29]
, 'Prob_011' : newColumns[:, 30], 'Prob_C_011' :
newColumns[:, 31],
'Prob_D_011' : newColumns[:, 32]
, 'Prob_012' : newColumns[:, 33], 'Prob_C_012' :
newColumns[:, 34],
'Prob_D_012' : newColumns[:, 35]
, 'Prob_013' : newColumns[:, 36], 'Prob_C_013' :
newColumns[:, 37],
'Prob_D_013' : newColumns[:, 38]
, 'Prob_014' : newColumns[:, 39], 'Prob_C_014' :
newColumns[:, 40],
'Prob_D_014' : newColumns[:, 41]
, 'Prob_015' : newColumns[:, 42], 'Prob_C_015' :
newColumns[:, 43],
'Prob_D_015' : newColumns[:, 44]
, 'Prob_016' : newColumns[:, 45], 'Prob_C_016' :
newColumns[:, 46],
'Prob_D_016' : newColumns[:, 47]
, 'Prob_017' : newColumns[:, 48], 'Prob_C_017' :
newColumns[:, 49],
'Prob_D_017' : newColumns[:, 50]
, 'Prob_018' : newColumns[:, 51], 'Prob_C_018' :
newColumns[:, 52],
'Prob_D_018' : newColumns[:, 53]
, 'Prob_019' : newColumns[:, 54], 'Prob_C_019' :
newColumns[:, 55],
'Prob_D_019' : newColumns[:, 56]
, 'Prob_020' : newColumns[:, 57], 'Prob_C_020' :
newColumns[:, 58],

```

```

        'Prob_D_020' : newColumns[:, 59]
            , 'Prob_021' : newColumns[:, 60], 'Prob_C_021' :
newColumns[:, 61],
        'Prob_D_021' : newColumns[:, 62]
            , 'Prob_022' : newColumns[:, 63], 'Prob_C_022' :
newColumns[:, 64],
        'Prob_D_022' : newColumns[:, 65]
            , 'Prob_023' : newColumns[:, 66], 'Prob_C_023' :
newColumns[:, 67],
        'Prob_D_023' : newColumns[:, 68]
            , 'Prob_024' : newColumns[:, 69], 'Prob_C_024' :
newColumns[:, 70],
        'Prob_D_024' : newColumns[:, 71]
            , 'Prob_025' : newColumns[:, 72], 'Prob_C_025' :
newColumns[:, 73],
        'Prob_D_025' : newColumns[:, 74]
            , 'Prob_026' : newColumns[:, 75], 'Prob_C_026' :
newColumns[:, 76],
        'Prob_D_026' : newColumns[:, 77]
            , 'Prob_027' : newColumns[:, 78], 'Prob_C_027' :
newColumns[:, 79],
        'Prob_D_027' : newColumns[:, 80]
            , 'Prob_028' : newColumns[:, 81], 'Prob_C_028' :
newColumns[:, 82],
        'Prob_D_028' : newColumns[:, 83]
            , 'Prob_029' : newColumns[:, 84], 'Prob_C_029' :
newColumns[:, 85],
        'Prob_D_029' : newColumns[:, 86]
            , 'Prob_030' : newColumns[:, 87], 'Prob_C_030' :
newColumns[:, 88],
        'Prob_D_030' : newColumns[:, 89]
            , 'Prob_031' : newColumns[:, 90], 'Prob_C_031' :
newColumns[:, 91],
        'Prob_D_031' : newColumns[:, 92]
            , 'Prob_032' : newColumns[:, 93], 'Prob_C_032' :
newColumns[:, 94],
        'Prob_D_032' : newColumns[:, 95]
            , 'Prob_033' : newColumns[:, 96], 'Prob_C_033' :
newColumns[:, 97],
        'Prob_D_033' : newColumns[:, 98]
            , 'Prob_034' : newColumns[:, 99], 'Prob_C_034' :
newColumns[:, 100],
        'Prob_D_034' : newColumns[:, 101]
            , 'Prob_035' : newColumns[:, 102], 'Prob_C_035' :
newColumns[:, 103],
        'Prob_D_035' : newColumns[:, 104]
            , 'Prob_036' : newColumns[:, 105], 'Prob_C_036' :
newColumns[:, 106],
        'Prob_D_036' : newColumns[:, 107]
            , 'Prob_037' : newColumns[:, 108], 'Prob_C_037' :
newColumns[:, 109],
        'Prob_D_037' : newColumns[:, 110]
            , 'Prob_038' : newColumns[:, 111], 'Prob_C_038' :
newColumns[:, 112],
        'Prob_D_038' : newColumns[:, 113]
            , 'Prob_039' : newColumns[:, 114], 'Prob_C_039' :
newColumns[:, 115],
        'Prob_D_039' : newColumns[:, 116]

        #'ftf_vol': df['ftf_vol'].to_numpy(),
        #'LeL_vol': df['LeL_vol'].to_numpy(),
        #'LeakRate': df['LeakRate'].to_numpy()
    })

    modified_ignprob.to_csv(saveToFolder + '/' + files[i] + '_' + ignprob_filename,
encoding='utf-8', sep=',')

```

```

#Write last line to excel
if oneCaseFound == False:
    oneCaseFound = True
    first_line = ReadFirstLine(saveToFolder + '/' + files[i] + '_' + ignprob_filename)
    first_line[0] = 'Folder'
    WriteLineExcel(workbook, sheet, first_line)
last_line = ReadLastLine(saveToFolder + '/' + files[i] + '_' + ignprob_filename)
last_line[0] = files[i]
WriteLineExcel(workbook, sheet, last_line)

```

```

#Calculate averages based on flow rate
print('Calculating averages...')
average = []
names = np.zeros(casesFound - 1)
excelMatrix = np.zeros(shape=(casesFound, 7 + (3 * numSources)))
for j in range(7 + (3 * numSources)):
    if j == 0:
        names = ReadColumnToArray(j + 2, 3, sheet, workbook)
    else:
        excelMatrix[:, j] = ReadColumnToArray(j + 2, 3, sheet, workbook)

```

```

_01_avg = np.zeros(7 + (3 * numSources))
_1_avg = np.zeros(7 + (3 * numSources))
_10_avg = np.zeros(7 + (3 * numSources))
for j in range(casesFound):
    name = names[j][-5:-3]
    if name == '01':
        _01_avg += excelMatrix[j, :]
    elif name == '_1':
        _1_avg += excelMatrix[j, :]
    elif name == '10':
        _10_avg += excelMatrix[j, :]

```

```

_01_avg = _01_avg / 6
_1_avg = _1_avg / 6
_10_avg = _10_avg / 6

```

```

WriteLineExcel(workbook, sheet, _01_avg)
WriteLineExcel(workbook, sheet, _1_avg)
WriteLineExcel(workbook, sheet, _10_avg)

```

